Conceptual Design Studies of a Passively Safe Thorium Breeder Pebble Bed Reactor

TUDelft Faculty of
Applied Sciences

**Conceptual Design Studies
of a Passively Safe Thorium
Breeder Pebble Bed Reactor**

Frank Wols

Department of Radiation Science and Technology

Frank Wols

Invitation

For the public defence
of my PhD thesis

**Conceptual Design
Studies of a Passively
Safe Thorium Breeder
Pebble Bed Reactor**

Wednesday 1st april, 2015

Senaatszaal, Aula of TU Delft,
Mekelweg 5, Delft

12:00 Introductory talk
12:30 Thesis defence

Frank Wols

Propositions

accompanying the dissertation

CONCEPTUAL DESIGN STUDIES OF A PASSIVELY SAFE THORIUM BREEDER PEBBLE BED REACTOR

by

Frank WOLS

1. There is no fundamental limitation that prohibits the achievement of both breeding and passive safety inside a Pebble Bed Reactor that employs a thorium fuel cycle. *(This thesis)*

2. It is impossible to achieve breeding inside a pebble bed nuclear reactor with only a single moderation ratio. *(Ch. 2, this thesis)*

3. A short doubling time is not a relevant design objective for breeder reactors anymore. *(Ch. 6, this thesis, and C.R. Adkins, The breeding ratio with correlation to doubling time and fuel cycle reactivity variation. Nuclear Technology 13.1 (1972): pp. 114-130.)*

4. After release of radioactive isotopes into the environment, more harm is caused to the health of people by the fear of ionizing radiation than by its physical effects. *(M.C. Hatch, S. Wallenstein, J. Beyea, J.W. Nieves, M. Susser, Cancer Rates after the Three Mile Island Nuclear Accident and Proximity of Residence to the Plant. American Journal of Public Health, June 1991, Vol. 81, No. 6, pp. 719-724)*

5. The development of programming skills deserves equal attention in the physics curriculum as the acquirement of theoretical knowledge. *(R. Landau. Computational physics: A better model for physics education?. Computing in science and engineering 8.5 (2006): pp. 22-30.)*

6. All scientific journals should facilitate an interactive discussion of draft articles before peer review. *(U. Pöschl. Interactive journal concept for improved scientific publishing and quality assurance. Learned publishing 17.2 (2004): 105-113.)*

7. Opinion polls have become a too decisive factor in the outcome of Dutch parliamentary elections, in view of the positive feedback of polls and the stimulation of strategic voting. *(W. Tiemeijer, Wat 93,7 procent van de Nederlanders moet weten over opiniepeilingen / English: What 93.7 percent of the Dutch people should know about voting polls, Amsterdam University Press, 2008)*

8. The large-scale exploitation of shale gas is disastrous for reducing climate change. *(R.W. Howarth, R. Santoro, and A. Ingraffea. Methane and the greenhouse-gas footprint of natural gas from shale formations. Climatic Change 106.4 (2011): pp. 679-690)*

9. Not the height of an income as such, but the lack of objective standards to justify a very high salary in the Dutch (semi-)public sector justifies a maximum wage. *(Het debat over topinkomens mist echte argumenten / E: Real arguments are missing in top income debate, opinion article by T.J. Dekker in Dutch newspaper Trouw, 4-2-2013)*

10. Since people have the possibility to avoid entering small cafes, while they don't have the possibility to evade hazardous exhaust gases from two-stroke scooters, the Dutch government could better ban the use of two-stroke scooters than smoking in small cafes. *(S.M. Platt et al., Two-stroke scooters are a dominant source of air pollution in many cities, Nature Communications, doi: 10.1038/ncomms4749, 2014)*

These propositions are regarded as opposable and defendable, and have been approved as such by the supervisor prof. dr. ir. T.H.J.J. Van der Hagen.

Stellingen

behorende bij het proefschrift

CONCEPTUAL DESIGN STUDIES OF A PASSIVELY SAFE THORIUM BREEDER PEBBLE BED REACTOR

door

Frank WOLS

1. Er is geen fundamentele beperking die het bereiken van zowel een conversiefactor groter dan één als passieve veiligheid in een kogelbedreactor met een thorium splijtstofcyclus onmogelijk maakt. *(Dit proefschrift)*

2. Het is onmogelijk om een conversiefactor groter dan één te bereiken in een nucleaire reactor van het kogelbedtype met één enkele moderator fractie. *(H. 2, dit proefschrift)*

3. Een korte verdubbelingstijd is geen relevante ontwerpdoelstelling voor kweekreactoren meer. *(H6, dit proefschrift, en C.R. Adkins, The breeding ratio with correlation to doubling time and fuel cycle reactivity variation. Nuclear Technology 13.1 (1972): pp. 114-130.)*

4. De angst voor ioniserende straling levert meer schade op voor de gezondheid van de bevolking dan haar fysieke gevolgen na een vrijgave van radioactieve isotopen aan de omgeving. *(M.C. Hatch, S. Wallenstein, J. Beyea, J.W. Nieves, M. Susser, Cancer Rates after the Three Mile Island Nuclear Accident and Proximity of Residence to the Plant. American Journal of Public Health, June 1991, Vol. 81, No. 6, pp. 719-724)*

5. De ontwikkeling van programmeervaardigheden verdient evenveel aandacht als het verkrijgen van theoretische kennis tijdens de opleiding tot natuurkundige. *(R. Landau, Computational physics: A better model for physics education?. Computing in science and engineering 8.5 (2006), pp. 22-30.)*

6. Alle wetenschappelijke journals dienen, voorafgaande aan peer review, een interactieve discussie van conceptartikelen te faciliteren. *(U. Pöschl. Interactive journal concept for improved scientific publishing and quality assurance. Learned publishing 17.2 (2004): pp. 105-113.)*

7. Opiniepeilingen zijn een te bepalende factor in de uitslag van Nederlandse parlementsverkiezingen geworden, met het oog op het zelfversterkende effect van peilingen en de bevordering van strategisch stemgedrag. *(W. Tiemeijer, Wat 93,7 procent van de Nederlanders moet weten over opiniepeilingen, Amsterdam University Press, 2008)*

8. De grootschalige exploitatie van schaliegas is desastreus voor het tegengaan van klimaatverandering. *(R.W. Howarth, R. Santoro, and A. Ingraffea. Methane and the greenhouse-gas footprint of natural gas from shale formations. Climatic Change 106.4 (2011): pp. 679-690)*

9. Niet de hoogte van het inkomen als zodanig, maar het gebrek aan objectieve maatstaven om een zeer hoog inkomen te rechtvaardigen, rechtvaardigt de invoering van een maximaal inkomen in de (semi-)publieke sector. *(Het debat over topinkomens mist echte argumenten, opiniestuk T.J. Dekker in dagblad Trouw, 4-2-2013)*

10. Gezien het feit dat mensen de keuzevrijheid hebben kleine cafe's te mijden, maar niet de mogelijkheid hebben om schadelijke uitlaatgassen van twee-takt scooters te ontlopen, zou de Nederlandse overheid eerder twee-takt scooters moeten verbieden dan roken in kleine cafe's. *(S.M. Platt et al., Two-stroke scooters are a dominant source of air pollution in many cities, Nature Communications, doi: 10.1038/ncomms4749, 2014).*

Deze stellingen worden opponeerbaar en verdedigbaar geacht en zijn als zodanig goedgekeurd door de promotor prof. dr. ir. T.H.J.J. Van der Hagen.

Conceptual Design Studies of a Passively Safe Thorium Breeder Pebble Bed Reactor

Conceptual Design Studies of a Passively Safe Thorium Breeder Pebble Bed Reactor

Proefschrift

ter verkrijging van de graad van doctor
aan de Technische Universiteit Delft,
op gezag van de Rector Magnificus prof. ir. K. C. A. M. Luyben,
voorzitter van het College voor Promoties,
in het openbaar te verdedigen op
woensdag 1 april 2015 om 12:30 uur

door

Frank Jozef Wols

natuurkundig ingenieur
geboren te Rotterdam

This dissertation has been approved by the

promotor: Prof. dr. ir. T. H. J. J. Van der Hagen and
copromotor: Dr. ir. J. L. Kloosterman

Composition of the doctoral committee:

Rector Magnificus
Prof. dr. ir. T. H. J. J. Van der Hagen,   promotor
Dr. ir. J. L. Kloosterman,   copromotor

Independent members:
Prof. dr. H. T. Wolterbeek,   Fac. of Applied Sciences, TU Delft
Prof. dr. ir. P. M. Herder,   Fac. of Technology, Policy and Management, TU Delft
Prof. T. J. Abram,   University of Manchester, United Kingdom
Prof. dr. C. Demaziere,   Chalmers University, Sweden
Dr. ir. A. I. Van Heek,   Nuclear Research Group Petten

CONTENTS

1

INTRODUCTION

1

WITH an ever increasing world population and industrialization of developing countries, a further increase in worldwide energy and electricity demand can be anticipated in the coming decades. The International Energy Agency (IEA) expects the world's primary energy demand to rise by 1.2% each year between 2012 and 2035, while the global electricity demand increases on average by 2.2% per year [1]. Nuclear energy production is expected to rise by 2.4% each year [1] and to account for 11.6% of the total world-wide electricity production in 2035. In the coming decades, nuclear power plants provide a very competitive, low-carbon, secure, stable and reliable source of electricity [2]. The required natural resources are still widely available at low costs for (at least) the coming decades and nuclear power plants can make countries without significant fossil fuel resources more independent in terms of electricity production [3, 4]. For these reasons, it is easy to understand why nuclear energy is also expected to play an important role in the electricity production in 2035. However, the design of nuclear reactors, currently in operation or being built, can be improved significantly in terms of safety and sustainability.

Safety is one of the most important design aspects of a nuclear reactor. If an incident occurs during reactor operation, such as an unexpected increase of reactor power or a loss of offsite electric power supply, a rapid insertion of neutron absorbing control rods is initiated, which is called a reactor scram. After the fission chain reaction is stopped by a reactor scram, the decay of short-lived isotopes still produces a significant amount of heat, e.g. around 6% of the nominal power production shortly after reactor shutdown and still more than 1% after 1 hour. Most nuclear power plants currently in operation, or being constructed, are large-sized light water reactors, which rely on active systems to remove this decay heat from the core. The nuclear incident at the Fukushima power plant in 2011 has shown that such active systems, especially in older reactors, can fail under extreme circumstances. Though several improvements have been made in newer reactor designs over the years to improve the reliability of these systems, e.g. four independent safety buildings can provide emergency cooling in the new built European Pressurized Reactor (EPR) [5], the design of reactors with fully passive emergency cooling systems, e.g. High Temperature Reactors, would be preferable from a safety perspective.

Two other important issues of current nuclear reactors are the inefficient use of natural resources and the production of long-lived nuclear waste. Current light water reactors only use around 1% of the natural uranium ore mined for the production of electricity [6], i.e. the greatest part of the U-238 remains unused. Furthermore, without reprocessing, the depleted fuel extracted from current reactors needs to be stored for a few hundred thousand years before the radiotoxicity becomes smaller than the radiotoxicity of the original uranium ore [7].

These three issues of current nuclear reactors could be considerably improved by applying a thorium breeder fuel cycle within a passively safe Pebble Bed High Temperature Reactor, as will be explained in the following. However, it may not be easy to combine both breeding, which is considered as a greater production rate than consumption rate of U-233 in this thesis, and passive safety in a Pebble Bed Reactor design. The main research question of this thesis is if, and under which conditions, such a passively safe thorium breeder Pebble Bed Reactor can be achieved within a practical operating regime, in terms of reactor power, fuel pebble handling speed and limited length of the reactor start-up phase.

1.1. PEBBLE BED REACTORS

HIGH Temperature Reactors (HTRs) are the most mature nuclear reactor designs with fully passive cooling mechanisms. The HTR's fuel is contained within tiny fuel kernels, surrounded by several protective TRISO layers, which effectively retain the radioactive fission products produced by the fission chain reaction within the fuel particle for temperatures up to 1600 °C [8]. These TRISO particles are either contained in a graphite matrix within fuel pellets, called compacts, inside prismatic fuel blocks forming the reactor core of the so-called prismatic block type HTR, or they are contained within a graphite matrix within spherical graphite pebbles that are randomly stacked to form the reactor core of a so-called Pebble Bed Reactor (PBR). A schematic view of a fuel pebble and a TRISO particle is shown in figure 1.1.

PEBBLE

TRISO particle

Graphite

0.5 cm

Graphite

Graphite
matrix
containing
TRISO particles

0.5 cm

Graphite

6 cm

Fuel
kernel

D = 0.5
mm

Pyrolytic carbon (35 μm)
Silicon carbide (35 μm)
Pyrolytic carbon (40 μm)
Porous carbon (90 μm)
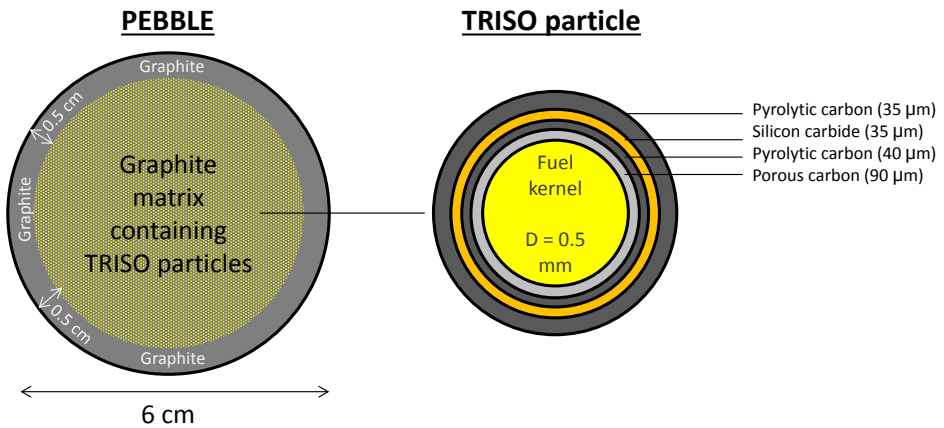
Figure 1.1: Schematic view of a fuel pebble and a TRISO particle (not to scale).

For both HTR types, high pressure helium is pumped through the fuel blocks or around the pebbles to extract the heat produced. HTRs can be constructed in such a way that decay heat can be removed by passive means during a Loss of Forced Cooling (LOFC), so purely by conduction, radiation and natural convection, even in case of a depressurization of the primary circuit. Other advantages of HTRs are the possibility to achieve high fuel burnups and the high outlet temperature of the coolant, which allows for efficient electricity production and offers opportunities for industrial process heat applications and hydrogen production [9].

Only Pebble Bed Reactors will be investigated in this thesis work. A very specific advantage of Pebble Bed Reactors is the capability of online refueling: pebbles can be inserted at the top of the reactor core and extracted at the bottom during operation and pebbles can be recycled multiple times in the core to flatten the power profile. Online refueling gives more flexibility in the fuel management of the core and limits the amount of excess reactivity and improves the fuel economy. This makes the Pebble Bed Reactor design more promising to achieve a breeder fuel cycle with thorium.

In the 20th century, Pebble Bed Reactors have been operated in Germany in the form of the experimental 46 MW$_{th}$ Arbeitsgemeinschaft Versuchsreaktor (AVR) [10], operating

between 1967 and 1988, and the commercial scale 300 MW_e Thorium High Temperature Reactor (THTR-300) [11, 12], operating between 1983 and 1989, where a lot of experience was gained with PBR operation and fuel performance and fabrication.

The concept of a passively safe PBR was first introduced by Reutler and Lohnert [13] with the so-called HTR-module. The HTR-module design combines a relatively large surface to volume ratio, i.e. the core height (9.6 m) is large compared to the core radius of 1.5 m, with a relatively low core power (200 MW_{th}) to ensure sufficient decay heat removal to avoid fuel temperatures from exceeding 1600 °C. Another advantage of the relatively small core radius is that control rods and absorber balls inside the side reflector are sufficient to achieve long-term reactor shutdown, while in-core safety rods are required for larger core diameters. By combining multiple reactor modules, a power plant with a significant power output can be constructed. The safety philosophy of the HTR-module is also applied in more recent PBR designs, such as the Chinese 10 MW_{th} prototype HTR-10 reactor [14] and the High Temperature Reactor-Pebble Bed Module (HTR-PM) [15], which is currently being constructed at Shidaowan in China's Shandong province. The HTR-PM demonstration plant design comprises two passively safe 250 MW_{th} Pebble Bed cores that will be connected to one turbine building to generate 210 MW of electricity [15]. The two HTR-PM units are expected to start operation around 2017 [16]. If these units are proven to be economically competitive, up to 18 additional core units may be constructed on the same site. The design of the HTR-PM is considered as a starting point for the neutronic and thermal-hydraulic studies performed in this thesis.

1.2. THORIUM FUEL CYCLE

T HE use of thorium inside nuclear reactors was initially investigated in and around the 1960s because thorium was seen as an interesting resource to supplement the known uranium reserves. In the fifties and sixties of the 20th century, these were thought to be limited, while the nuclear industry was expanding rapidly. The interest in the thorium fuel cycle strongly declined later on, as new resources of natural uranium were found and the growth of the nuclear industry slowed down [17]. Thorium fuel cycles have been considered both for Pebble Bed Reactors as well as for most other reactor types, for which an overview is given by Lung and Gremm [17] and by the IAEA [18]. The next section will discuss the utilization of thorium inside Pebble Bed Reactors.

The use of thorium in a nuclear reactor is more complicated than the use of uranium, because natural thorium (100 w% Th-232) does not contain a fissile isotope, like the 0.72 w% of U-235 contained in natural uranium. Thorium has to be converted into the fissile U-233 in a nuclear reactor first. Neutron capture by Th-232 leads to the formation of Th-233 ($t_{1/2}$=22.3 m), which forms Pa-233 via β-decay. After a second β-decay step, Pa-233 ($t_{1/2}$=26.967 d) forms the fissile isotope U-233. However, Pa-233 is a strong neutron absorber and a neutron captured in Pa-233 implies both the loss of a neutron as well as the loss of a potential fissile atom, as it cannot decay to U-233 anymore. So, restricting the Pa-233 concentration can improve the neutron economy and breeding potential of a system.

Besides an increased resource availability, i.e. thorium is three to four times more abundant in the earth's crust than uranium, thorium fuel cycles also offer several other interesting advantages over uranium fuel cycles. The use of thorium in a closed fuel cycle can reduce the radiotoxicity and required storage time of the nuclear waste, since the

production of long-lived minor actinides requires many additional neutron capture reactions for Th-232, as compared to U-238. Furthermore, ThO_2-fuels are chemically more stable, have a higher radiation resistance and favourable thermophysical properties over UO_2-based fuels. ThO_2 is also relatively inert making the long term storage and permanent disposal of spent fuel simpler as oxidation is no problem. On the other hand, the inertness can complicate the fuel fabrication. [17, 18]
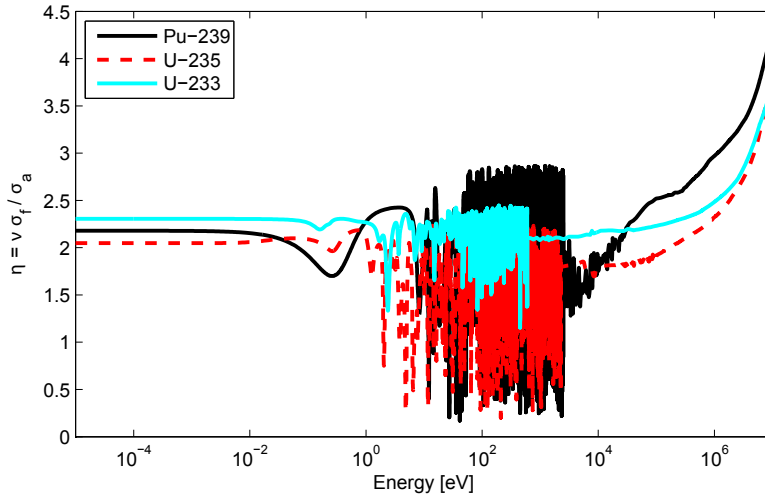
Figure 1.2: Neutron reproduction factor ($= \frac{\nu \sigma_f}{\sigma_a}$) as a function of neutron energy for U-233, U-235 and Pu-239 using data from the ENDF-VII library included in the JANIS-database [19].

In view of this thesis work, a very important advantage of the U-233/Th fuel cycle in comparison with the U-238/Pu-cycle, are its favourable nuclear properties for use in thermal breeder reactors. The neutron capture cross section for thermal neutrons in Th-232 is 7.4 barns compared to 2.7 barns for U-238 leading to higher fertile to fissile conversion ratios for Th-232. Secondly, the number of neutrons produced per neutron absorbed in U-233 is substantially greater than two over a wide energy range of the thermal neutron spectrum, as shown in figure 1.2. One of these neutrons is required to sustain the fission chain reaction, while theoretically more than one neutron remains to convert Th-232 into U-233. In practice, neutrons are also lost by parasitic neutron capture and neutron leakage and these losses have to be minimized to achieve breeding. Overall, the Th/U-233 fuel cycle is the most promising candidate to achieve breeding with thermal neutron spectra, like in a PBR. [18, 20]

1.3. THORIUM UTILIZATION IN PEBBLE BED REACTORS

THE use of thorium inside a PBR has been investigated, both on paper and in practice, in order to reduce uranium resource usage and to reduce the amount of higher actinides produced in or fed to the reactor, especially in combination with plutonium [21–23]. Simulations based upon the HTR-module design showed that burning plutonium in

combination with thorium produces only negligible amounts of second-generation plutonium [21] and that a large fraction of the plutonium could be fissioned [22]. Xia and Li quite recently performed studies on the use of thorium in the HTR-PM in order to reduce the U-235 consumption [24].

Thorium fuel was also used in the previously mentioned THTR-300, which reached criticality for the first time in September 1983. The pebble bed consisted of $675,000$ pebbles and the cylindrical core was 5.6 m in diameter and around 6 m high. A THTR fuel element contained 0.96 g of highly enriched U-235 and 10.2 g of Th-232. On average, a pebble would make six passes through the core up till a final burnup of around 110 GWd/t_{hm}. The THTR was shut down in August 1989 for economic reasons. Contrary to the HTR-module and HTR-PM designs, the THTR still had to rely on active cooling systems due to the combination of a relatively large core power and a small surface to volume ratio. [11]

More interesting for this thesis is the research related to PBR designs with a high conversion ratio (> 0.9). In the seventies, Teuchert and Rütten [25] investigated thorium based fuel cycles in the PBR with the conversion of thorium into U-233 as the main interest. Teuchert and Rütten investigated a PBR design with a maximum mass discharge rate of U-233, at the price of a somewhat lower conversion ratio (CR=0.76), and a near breeder PBR design (CR=0.97). The first reactor type could be used to supply the make-up fuel of over 10 near breeder PBRs. The average conversion ratio of this combined system is mentioned to be 0.95. The design and operation of the two reactor types are identical. This allows to alternate between the near breeder and maximum discharge design during full power operation. Teuchert and Rütten [25] also state that the reactor concept even allows for a conversion ratio above unity when parasitic neutron losses are reduced rigorously, e.g. by minimizing neutron capture in fission products and control poison and minimizing neutron leakage.

In another paper from 1975, Teuchert and Rütten also investigated several fuel cycles in the PBR, among which the recycling variant of the thorium fuel cycle [26]. According to Teuchert and Rütten, a conversion ratio in the range of 0.9 and 1.0 could be reached. In their calculations, a conversion ratio of 0.958 was found by a minimization of the average burnup to 24 GWd/t_{hm}, a reduced power density and an increase of the heavy metal loading to 33 grams per pebble.

Finally, in 1986, Teuchert [27] describes the concept of a net-breeder thorium PBR. To achieve breeding, the U-233 fraction in the fuel and the heavy metal loading per fuel pebble should be as large as possible. On the other hand, neutron losses due to capture by fission products and leakage should be minimized. For heavy metal loadings of 32 and 45 g/pebble, which is rather high from a fuel fabrication perspective, and for low burnups, around 20 GWd/t$_{hm}$, conversion ratios around unity are possible. By introducing a 30 cm radial blanket zone, the conversion ratio could even be increased to 1.05. However, with a core radius of almost 6 m, emergency cooling is unlikely to be achieved solely by passive means.

Historically, another great challenge of using a closed thorium fuel cycle inside a PBR is the technical difficulty of reprocessing the fuel, especially the cracking of the pebbles and coating layers of the kernels. Using methods relying on a combination of mechanical and chemical separation methods, the processing of carbide-coated fuel was even literally considered 'a headache' in a report by Lung in 1997 [28]. Fortunately, in recent years Füt-

terer et al. [29] made very interesting progress in fragmenting coated particle fuels. The method uses high voltage discharges inside a water vessel, which cause shock waves that disintegrate the fuel pebble and/or protective TRISO layers of the fuel kernel. The applicability of this technique is still to be demonstrated on an industrial scale.

1.4. OBJECTIVE AND OUTLINE OF THE THESIS

THE objective of this thesis work is the conceptual design of a passively safe thorium breeder Pebble Bed Reactor within a practical operating regime, in terms of reactor power, fuel pebble handling speed and limited length of the reactor start-up phase. In order to achieve breeding, neutron losses should be reduced strongly. The greatest reduction of neutron leakage can be achieved by reducing the surface to volume ratio of the core, e.g. by increasing the core diameter. However, this reduces the decay heat removal capability of the design, which could compromise passive safety. Furthermore, the temperature feedback of U-233/Th fueled cores is less negative, as compared to U-235/U-238 fueled cores, which could also affect passive safety. So, one of the main challenges of this thesis work is to discover if, and under which conditions, both breeding and passive safety can be achieved within a practical operating regime. If breeding is not possible, a conversion ratio as high as possible within passive safety and practical constraints is pursued.

The relevant research steps undertaken to achieve the objective of this thesis work are described in chapters two till six. Chapter 2 describes neutronic studies performed to determine the optimal fuel design to enhance conversion of Th-232 into U-233 or to maximize neutron multiplication, i.e. k_∞. Chapter 3 investigates whether it is possible to achieve breeding in the equilibrium core configuration of a thorium PBR, consisting of a central driver zone surrounded by a breeder zone, and whether this can also be achieved without reprocessing of the fuel extracted from the core.

In chapter 4, these basic equilibrium core design and fuel management studies for a two-zone thorium PBR, with reprocessing of the uranium content from the discharged fuel pebbles, are extended by including the spectral influence of the surrounding zones (driver, breeder and reflector) into the depletion calculations. Furthermore, the temperature feedback is included in the equilibrium core calculation scheme and a safety analysis of the different core configurations is performed, which includes the response to a Depressurized Loss of Forced Cooling (DLOFC) with and without scram and the maximum reactivity insertion due to water ingress, which should be small enough to be compensated by the temperature feedback without fuel temperatures exceeding 1600 °C. With the models developed in this chapter, it is investigated under which conditions a passively safe thorium breeder equilibrium core can be achieved within a practical operating regime.

The passively safe breeder design that will be proposed in chapter 4 has a driver zone of 100 cm radius, surrounded by a low power breeder zone of 200 cm thickness. Therefore, the neutron flux is very low in the radial reflector region, where the control rods are located in the HTR-module and HTR-PM design. Chapter 5 investigates whether the control rod worth can still be sufficient within the radial reflector to achieve long-term reactor shutdown or, if not, which alternative in-core positions provide a sufficient reactivity worth. Additionally, the use of a neutron absorber gas as an additional emergency shutdown mechanism is also investigated in chapter 5. The applicability of first order perturbation theory for both the control rod positioning problem, as well as the more homoge-

1

neous problem of the absorber gas insertion into the primary circuit, is also evaluated.

Since U-233 is not available in nature, an alternative fuel is required to start the passively safe thorium breeder PBR. The transition phase from the start-up core to the equilibrium core configuration, also called the running-in phase, was analysed using a simplified core depletion model in chapter 6, using enriched uranium (U-235/U-238) as a start-up fuel. The model is used to gain insight in the time-scale involved before the reactor starts to breed U-233 and before the equilibrium core composition is reached, especially the build up of U-234, U-235 and U-236 to their equilibrium concentrations takes quite some time. The adjustment of the enrichment or U-233 weight fraction of the feed driver fuel over time is investigated in order to limit excess reactivity and to achieve a net U-233 production more rapidly. Furthermore, a basic safety analysis, involving water ingress, reactivity coefficients, maximum power density and maximum fuel temperature during a DLOFC with scram, is performed for various stages of the running-in phase to demonstrate that the passive safety features of the equilibrium core also apply to the various stages of the running-in phase.

Finally, an overview of the conclusions and recommendations of this thesis is given in chapter 7.

REFERENCES

[1] International Energy Agency, *World energy investment outlook*, Tech. Rep. (2014).

[2] W. D'haeseleer, *Synthesis on the Economics of Nuclear Energy*, Tech. Rep. (2013).

[3] A. Corner, D. Venables, A. Spence, W. Poortinga, C. Demski, and N. Pidgeon, *Nuclear power, climate change and energy security: Exploring british public attitudes,* Energy Policy **39**, 4823–4833 (2011).

[4] V. H. Visschers, C. Keller, and M. Siegrist, *Climate change benefits and energy supply benefits as determinants of acceptance of nuclear power stations: Investigating an explanatory model,* Energy Policy **39**, 3621–3629 (2011).

[5] R. Leverenz, *The EPR - a safe and competitive solution for future energy needs,* in *Nuclear Energy for New Europe 2006* (Porotož, Slovenia, 2006).

[6] P. Wilson, *The nuclear fuel cycle: from ore to waste* (Oxford University Press, 1996).

[7] D. Westlén, *Reducing radiotoxicity in the long run,* Progress in Nuclear Energy **49**, 597–605 (2007).

[8] W. Schenk, G. Pott, and H. Nabielek, *Fuel accident performance testing for small HTRs,* Journal of Nuclear Materials **171**, 19–30 (1990).

[9] B. Yildiz and M. S. Kazimi, *Efficiency of hydrogen production systems using alternative nuclear energy technologies,* International Journal of Hydrogen Energy **31**, 77–92 (2006).

[10] E. Ziermann, *Review of 21 years of power operation at the AVR experimental nuclear power station in Jülich,* Nuclear Engineering and Design **121**, 135–142 (1990).

[11] R. Bäumer, I. Kalinowski, E. Röhler, J. Schöning, and W. Wachholz, *Construction and operating experience with the 300-MW THTR nuclear power plant,* Nuclear Engineering and Design **121**, 155–166 (1990).

[12] R. Bäumer and I. Kalinowski, *THTR commissioning and operating experience,* Energy **16**, 59–70 (1991).

[13] H. Reutler and G. H. Lohnert, *Advantages of going modular in HTRs,* Nuclear Engineering and Design **78**, 129–136 (1984).

[14] Z. Wu, D. Lin, and D. Zhong, *The design features of the HTR-10,* Nuclear Engineering and Design **218**, 25–32 (2002).

[15] Z. Zhang, Z. Wu, D. Wang, Y. Xu, Y. Sun, F. Li, and Y. Dong, *Current status and technical description of Chinese 2 x 250 MW$_{th}$ HTR-PM demonstration plant,* Nuclear Engineering and Design **239**, 1212–1219 (2009).

[16] World Nuclear News, *Helium fan produced for chinese htr-pm,* news article published on August 19 (2014) on `http://www.world-nuclear-news.org/NN-Helium-fan-produced-for-Chinese-HTR-PM-1908144.html`, (2014).

[17] M. Lung and O. Gremm, *Perspectives of the thorium fuel cycle,* Nuclear Engineering and Design **180**, 133–146 (1998).

[18] International Atomic Energy Agency (IAEA), *Thorium fuel cycle - Potential benefits and challenges,* Tech. Rep. IAEA-TECDOC-1450 (Vienna, 2005).

[19] Organization for Economic Co-operation and Development - Nuclear Energy Agency, *JANIS 4.0, User's Guide - Rev. 1* (2013).

[20] J. J. Duderstadt and L. J. Hamilton, *Nuclear Reactor Analysis* (John Wiley and Sons Inc., 1976).

[21] H. J. Rütten and K. A. Haas, *Research on the incineration of plutonium in a modular HTR using thorium-based fuel,* Nuclear Engineering and Design **195**, 353–360 (2000).

[22] H. Chang, Y. Yang, X. Jing, and Y. Xu, *Thorium-based fuel cycles in the modular high temperature reactor,* Tsinghua Science and Technology **11**, 731–738 (2006).

[23] E. Mulder, D. Serfontein, W. van der Merwe, and E. Teuchert, *Thorium and uranium fuel cycle symbiosis in a pebble bed high temperature reactor,* in *High temperature Reactor Conference 2010* (Prague, Czech Republic, 2010).

[24] B. Xia and F. Li, *Preliminary study on the feasibility of utilizing the thermal fissile breeding capability of the Th-U fuel cycle in HTR-PM,* in *21st International Conference on Nuclear Engineering (ICONE-21)*.

[25] E. Teuchert and H. J. Rütten, *Near breeding thorium fuel cycle in pebble bed HTR,* in *Proceedings of IAEA-OECD Symposium on Gas Cooled Reactors* (Jülich, 1975).

1

1

[26] E. Teuchert and H. J. Rütten, *Core physics and fuel cycles of the pebble bed reactor,* Nuclear Engineering and Design **34**, 109–118 (1975).

[27] E. Teuchert, *Brennstoffzyklen des Kugelhaufen-Hochtemperaturreaktors in der Computersimulation* (Kernforschungsanlage Jülich GmbH., 1986).

[28] M. Lung, *EUR 17771: A present review of the thorium nuclear fuel cycles (European Commission),* Tech. Rep. ISSN 1018-5593 (1997).

[29] M. A. Fütterer, F. von der Weid, and P. Kilchmann, *A high voltage head-end process for waste minimization and reprocessing of coated particle fuel for high temperature reactors,* in *Proceedings of ICAPP'10* (San Diego, CA, USA, 2010).

2

FUEL DESIGN STUDIES

This chapter investigates the optimal fuel pebble design, in terms of maximising thorium to U-233 conversion or maximising the infinite multiplication factor, for a thorium PBR. Using deterministic modules from SCALE6, the infinite multiplication factor and nuclide concentrations are calculated during depletion. Pebbles with thorium and different initial U-233 weight fractions are studied for heavy metal loadings up to 30 g, a conservative estimate from a fuel fabrication perspective. Pebble cross sections with a middle-of-life burnup are used as a surrounding material in the depletion calculation scheme to provide a more realistic neutron spectrum, which is found to have a significant impact on the results.

Using larger, instead of more, fuel kernels only leads to a small increase of the multiplication factor during the depletion calculations, because the reduced resonance absorption also results in a significant decrease of thorium to U-233 conversion. Lower specific powers result in higher multiplication factors during burnup, while the U-233 concentration hardly changes. The conversion of thorium into U-233 can be maximized for thorium pebbles with a large heavy metal loading of 30 g, using the standard fuel kernel radius of 0.025 cm, preferably irradiated at low specific power to improve the multiplication factor. Without fuel reprocessing, the addition of moderator pebbles is required to raise the infinite multiplication factor of these pebbles above unity. As a starting point for the core design studies in chapter 3, it is recommended to insert fresh pebbles with 30 g thorium into one or multiple breeder zones, without moderator pebbles, while the irradiated pebbles are recycled into one or multiple driver zones with moderator pebbles.

M^ANY variables, including fuel design parameters, are involved in the core design problem of a thorium breeder PBR. As a first step, it is convenient to separately analyse the influence of several fuel design parameters. The optimal fuel pebble design, in terms of thorium to U-233 conversion or enhanced fission, is investigated in this chapter.

For these fuel design studies, the influence of several parameters on the multiplication factor of a single fuel pebble in an infinite lattice is studied, both for fresh Th/U-233 fueled pebbles and during burnup. For the fresh fuel pebbles, the influence of the number of TRISO particles per pebble, the fuel kernel radius and the U-233 weight fraction upon the infinite multiplication factor is investigated, as well as the influence of using a mixture of fuel and moderator pebbles. The fresh fuel pebble calculations and results are presented in section 2.1.

Section 2.2 presents the fuel pebble depletion calculation method, which uses middle-of-life burnup pebble cross sections as a surrounding material to provide a more realistic neutron spectrum for the depletion calculations. The parameter studies in section 2.3 investigate the influence of the number of TRISO particles per pebble, the fuel kernel radius and the initial U-233 weight fraction on k_∞ and the nuclide concentrations as a function of burnup. Furthermore, the effect of the specific power on k_∞ as a function of burnup is studied for a pebble with a high heavy metal loading. This chapter ends with some conclusions in section 2.4.

2.1. FRESH FUEL PEBBLE PARAMETER STUDIES

F^UEL pebbles consist of several thousands of TRISO coated fuel particles dispersed in a graphite matrix surrounded by a fuel free graphite shell, as depicted in figure 1.1. Each coated fuel particle consists of a fuel kernel surrounded by a porous carbon layer, an inner-pyrolitic carbon layer, a silicon-carbide layer and an outer-pyrolitic carbon layer. Possible variations in the fuel design are the fuel kernel size, the number of fuel particles and graphite matrix diameter.

Table 2.1: Pebble nuclide concentrations in atoms/(barn·cm)

Fuel design layer	Nuclide	Atom density [$\frac{atoms}{barn \cdot cm}$]
Carbon buffer	C	$5.2645 \cdot 10^{-2}$
Inner PyC layer	C	$9.5262 \cdot 10^{-2}$
SiC layer	C	$4.7760 \cdot 10^{-2}$
	Si	$4.7760 \cdot 10^{-2}$
Outer PyC layer	C	$9.5262 \cdot 10^{-2}$
Graphite matrix	C	$8.7741 \cdot 10^{-2}$
Pebble outer shell	C	$8.7741 \cdot 10^{-2}$
Coolant	He	$5.5740 \cdot 10^{-2}$

The nuclide concentrations in table 2.1 are used for the TRISO buffer layers and the pebble coating layers [1] during the calculations, in combination with the geometrical properties in table 2.2. A pebble temperature of 1300 K is used for the calculations in this chapter. A variation of the fuel kernel radius may require a change of the TRISO coating layer thicknesses to ensure the retention of all the fission products. However, it is not evident whether a simple (linear) relation exists between the fuel kernel radius and the

desirable coating thicknesses. However, the thickness of the coating layers has an almost negligible influence upon the neutronics. Therefore, constant TRISO coating layer thicknesses are used in all of the calculations. A mixture of UO_2 and ThO_2 is used in the fuel kernels, where for uranium the U-233 isotope is meant.

Table 2.2: Geometric properties of fuel pebble and TRISO coating layers

Pebble packing fraction	0.61
Pebble radius	3.0 cm
Fuel zone radius	2.5 cm
Material	Thickness (mm)
Porous carbon buffer layer	0.09
Inner PYC-layer	0.04
SiC-layer	0.035
Outer PYC-layer	0.035

The unit cell calculations of the fresh fuel pebble are performed using the CSASI sequence of the SCALE6 code package [2]. The DOUBLEHET-module is used inside the CSASI sequence to include the double-heterogeneity of the fuel into the calculation and it can handle all the TRISO buffer layers of the fuel particles and the whole pebble at once [2, 3]. The DOUBLEHET module uses CENTRM/PMC to perform the resolved resonance processing for multi-group cross sections. The ENDF-V5, V6 or V7 238-group libraries can be used in combination with the DOUBLEHET-module. A deterministic 1D XSDRN calculation is performed near the end of the CSASI sequence to calculate k_∞.

In the first and most elaborate parameter study, the infinite multiplication factor has been calculated for different U-233 weight fractions, between 2% and 20%, and for different heavy metal loadings, ranging from 0.5 g to 30 g HM per pebble. The heavy metal loading of a fuel pebble is given by

$$m_{hm} = \frac{4}{3}\pi \rho_{hm} n_{triso} r_{fk}^3,$$

(2.1)

where ρ_{hm} is the heavy metal density, n_{triso} the number of TRISO particles per pebble and r_{fk} the fuel kernel radius. During the calculations, the heavy metal loading is either increased by increasing the fuel kernel radius or by increasing the number of TRISO particles. So, the change of k_∞ can be compared for a large kernel size with respect to the standard size at the same heavy metal loading per pebble.

A second parameter study investigates the influence on k_∞ of adding moderator pebbles between the fuel pebbles. The addition of moderator pebbles changes the moderation ratio of the fuel without making changes to the fuel pebble design itself. Fuel pebbles with a high heavy metal loading are used for this parameter study, since they are strongly undermoderated without moderator pebbles. The results of these two parameter studies are discussed in the next two subsections.

2.1.1. Varying heavy metal loading
For the first parameter study, the k_∞ of the fresh Th/U-233 fueled pebble was calculated for heavy metal loadings varying between 0.5 g and 30 g. In one case, the heavy metal loading was varied by changing the fuel kernel radius in 21 steps between 0.1079 and 0.4224 mm
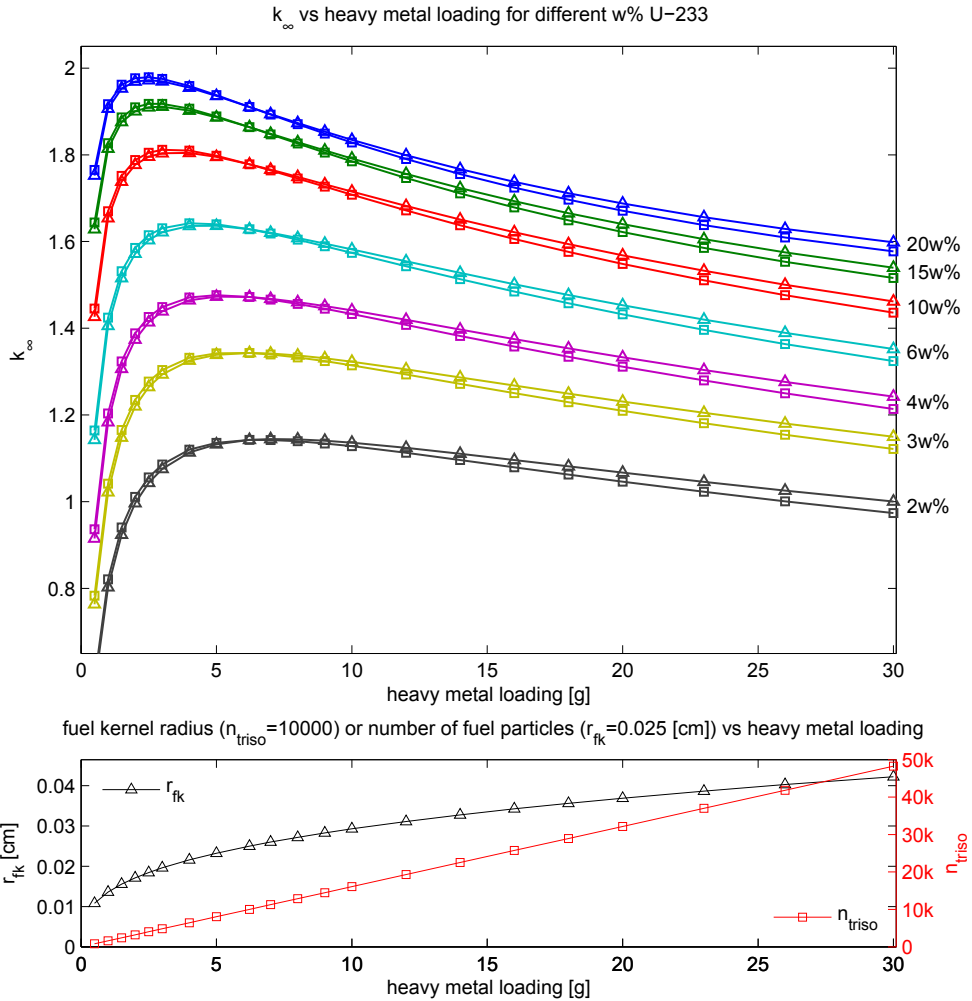
Figure 2.1: k_∞ of a fresh fuel pebble as a function of heavy metal loading for different U-233 weight fractions (*top*) and for two different methods used for varying the heavy metal loading, either by increasing fuel kernel size - triangles - or number of TRISO particles - squares (*bottom*)

using 10000 TRISO particles per pebble. In the second case, the heavy metal loading was also varied in 21 steps by changing the number of TRISO particles between 804 and 48249 using a fuel kernel radius of 0.25 mm. These calculations were performed for 14 U-233 weight fractions ranging from 2% till 20%. For this first parameter study, the DOUBLEHET module of the CSASI sequence and the ENDF-V5 238 group library were used.

The results in figure 2.1 clearly show that the magnitude of the heavy metal loading is of great importance for the pebble k_∞. The method to vary the metal loading, either by enlarging the fuel kernel or increasing the number of particles, is of smaller importance for thorium pebbles, since the resonances in the Th-232 capture cross section are relatively small. For U-238, this fuel lumping effect is much more significant. The largest relative difference between the two methods is found at the highest metal loading (30 g) for a thorium fueled pebble with 2 w-% U-233. For this thorium pebble, the k_∞ is 2.76% higher when an enlarged fuel kernel is used, while the relative difference in k_∞ is 5.90% for a pebble (30 g HM) containing 2% U-235 and 98% U-238.

The fuel pebble is overmoderated for low metal loadings and a slight increase of the heavy metal loading leads to an increase of k_∞. The fuel pebble is undermoderated for high metal loadings and adding more heavy metal leads to a decrease of k_∞. The maximum of k_∞ occurs at higher metal loadings as the U-233 weight fraction decreases. Since the ratio between carbon moderator and fissile material is already lower for a higher U-233 weight fraction, the pebble will already become undermoderated at a lower heavy metal loading.

With respect to the fuel design, it can be noted that an increase of fuel self shielding leads to an increase of k_∞. It also results in a decrease of neutron capture in thorium and conversion into U-233. Choices should be made between these two opposite effects for the fuel design of a thorium breeder PBR.

2.1.2. ADDING MODERATOR PEBBLES

The addition of moderator pebbles is the second parameter study performed for fresh fuel pebbles. The ratio between moderator and fuel pebbles, denoted by f, was varied between 0 and 10, for a fuel pebble with a 30 g heavy metal loading (n_{triso}=48249; r_{fk}=0.25 mm). Calculations were performed for a range of U-233 weight fractions between 2% and 20%. The 2REGION method [2] was used for the resonance self shielding calculation. The 2RE-GION method solves a slowing-down equation representing a system by an interior region containing the material mixture to be self shielded and an outer moderator region. A user specified Dancoff factor, depending on the amount of moderator pebbles present in the fuel, accounts for the double-heterogeneity of the fuel. These Dancoff factors were calculated by means of the analytical equations derived by Bende et al. [4]. The cross section generation procedure used for a mixture of fuel pebbles and moderator pebbles has been described in the thesis work of Boer [5]. Cross sections are obtained from the ENDF-V7 238-group library. The k_∞ is plotted as a function of f for 2, 2.5, 3 and 4 w% of U-233 in figure 2.2.

A fuel pebble (f=0) with a heavy metal loading of 30 grams is strongly undermoderated. For all U-233 weight fractions of U-233, the addition of moderator pebbles initially leads to an increase of k_∞ until the moment the fuel pebble becomes overmoderated as f increases. The transition from undermoderated to overmoderated occurs at increasing
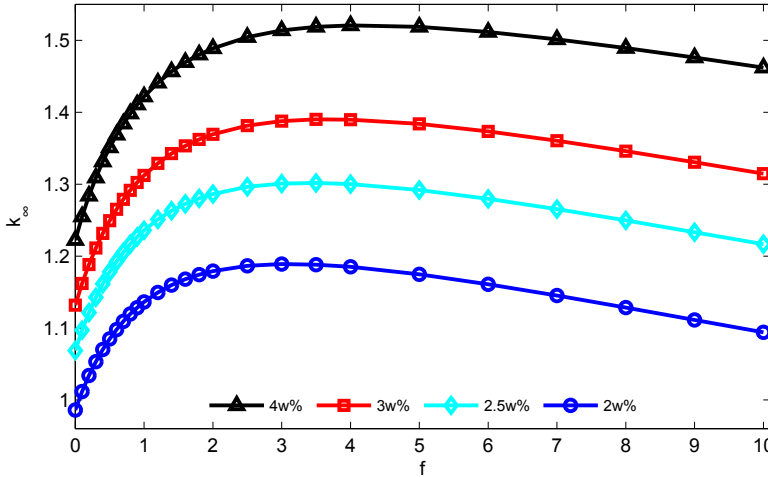
Figure 2.2: k_∞ as a function of moderator to fuel pebble ratio (f) for different U-233 w% (m_{hm}=30 g)

f-values as the U-233 weight fraction increases.

A significant increase of the pebble k_∞ can be achieved by the addition of moderator pebbles. Adding 3.5 moderator pebbles per fuel pebble increases k_∞ from 1.1319 to 1.3902 for a 3 w% U-233 fuel pebble (30 g HM). Moderator pebbles offer the opportunity to significantly raise the k_∞ of a pebble with a large heavy metal loading without changing the fuel pebble composition itself.

2.2. CALCULATION METHOD FOR FUEL DEPLETION

T HE change of the fuel composition due to depletion is an important aspect of the fuel design choice of a thorium PBR. An accurate determination of the fuel depletion inside a reactor requires knowledge of the configuration of the whole reactor core, since this determines the flux (and spectrum) inside the fuel during depletion. However, it is not feasible to work with core configurations, as the fuel design is still to be determined. For this reason, a simplified method has been developed to perform burnup calculations for a single fuel pebble. It is important that the method is relatively fast in order to perform extensive parameter studies of the fuel design with respect to burnup.

The average distance a neutron travels before absorption is much longer inside a PBR than the size of a single pebble. Therefore, the neutron spectrum inside a pebble is mainly determined by the composition of the surrounding pebbles. Usually, the fuel pebbles in a PBR are recirculated multiple times in the core and the equilibrium core composition is of main interest. In that case, according to Massimo [6], all burnup stages of the fuel are represented in any volume element of the core and, because of the small size of the fuel elements, the neutron spectrum is determined by the average nuclide composition.

Several modules of the SCALE6 code package were used for the burnup calculation scheme. As a first step, the fuel depletion is calculated for a single pebble in an infinite lattice. Therefore, an AMPX-library with zone weighted microscopic cross sections is gen-

erated by the CSASI-sequence for the nuclides in the fuel kernel of the pebble. For the unit cell calculation, the ENDF-V5 238-group library has been used in combination with NITAWL for the resonance self shielding calculation. First, COUPLE is used to create an updated ORIGEN working library with the neutron spectrum from the AMPX-library, followed by a fuel depletion calculation by ORIGEN-S with a constant specific power during one burnup step. ORIGEN-S divides the depletion calculation for each burnup step again into several subintervals. After each burnup step, new nuclide concentrations are calculated for the fuel kernel from the ORIGEN-S output and a new AMPX-library is generated by the CSASI-sequence to provide the neutron spectrum inside the fuel kernel for the next depletion calculation step by ORIGEN-S. This process is repeated until the final burnup is reached. The k_∞ of a fuel pebble before and after each burnup step is also extracted from the CSASI unit cell calculations.

As previously mentioned, the neutron spectrum inside a fuel pebble is mainly determined by the average composition of the surrounding pebbles. The spectral influence of these surrounding pebbles was not taken into account during the first part of the calculation. Using the first part of the calculation, a cell-weighted macroscopic cross section set of a fuel pebble at middle of life (MOL) burnup is generated to represent MOL burnup pebble bed material. It is assumed that a pebble at a MOL burnup level is representative for the average nuclide composition of the surrounding pebbles.

The second part of the calculation starts with generating an AMPX-library with zone weighted microscopic cross sections of a fuel kernel using the CSASI-sequence. A separate CSASI calculation is run to generate macroscopic cross sections using an inner-cell weighting over the fuel zone. These two AMPX libraries and the MOL burnup pebble bed material cross sections are then merged together into one library using WAX. Using the cross sections of the different material regions, a 1D transport calculation is performed with XSDRN for the pebble of interest surrounded by MOL burnup pebble material. The radius of the MOL pebble material is chosen to be large (200 cm) compared to the size of the pebble. In the center of the pebble of interest, one separate fuel kernel is modelled in order to obtain zone-weighted cross sections for the fuel kernel material. This way, the neutron spectrum inside the fuel kernel is obtained with a good estimate of the influence of the MOL burnup surrounding pebbles.

First, COUPLE converts the fuel kernel cross sections generated by XSDRN into an ORIGEN working library, followed by an ORIGEN-S depletion calculation over a single burnup step. New nuclide concentrations are read from the ORIGEN-S output and the procedure above is repeated to generate new fuel kernel cross sections and neutron spectrum for the next burnup step. A schematic view of the geometry used for the cross section generation in the first and second part of the calculation is given in figure 2.3.

2.2.1. EFFECT OF MOL PEBBLE ENVIRONMENT ON DEPLETION

Before discussing the complete set of results obtained by the burnup parameter studies of a fuel pebble, it is interesting to check the influence of using a single pebble spectrum or the inclusion of the MOL burnup material around the fuel pebble upon the results of the parameter studies. The relative difference in k_∞ or the nuclide concentrations has been defined by eq. 2.2 and eq. 2.3 in order to obtain a single quantitative parameter to describe the relative difference between the use of a single or a MOL environment spectrum for a
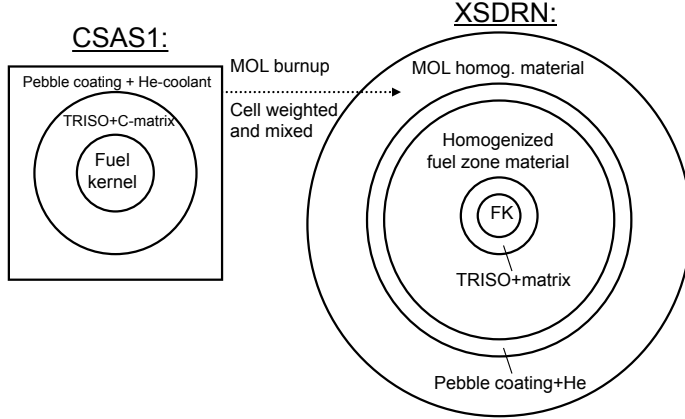
Figure 2.3: Schematic view of the burnup calculation method to include the influence of MOL burnup pebbles upon the fuel kernel spectrum. (not to scale)

whole parameter set

$$\delta k_\infty = \frac{\sum\limits_{n_j} \left| k_{\infty,MOL}\left(t_j\right) - k_{\infty,single}\left(t_j\right) \right|}{\sum\limits_{n_j} \left| k_{\infty,MOL}\left(t_j\right) \right|} \tag{2.2}$$

$$\delta N_i = \frac{\sum\limits_{n_j} \left| N_{i,\text{MOL}}\left(t_j\right) - N_{i,\text{single}}\left(t_j\right) \right|}{\sum\limits_{n_j} \left| N_{i,\text{MOL}}\left(t_j\right) \right|} \tag{2.3}$$

Here n_j stands for the total number of burnup steps and j represents the j-th burnup step. 2D plots of the relative differences in k_∞ and the U-233, Th-232 and Pa-233 nuclide concentrations, as defined by equations 2.2 and 2.3, as a function of heavy metal loading and initial U-233 weight fraction are shown in figure 2.4.

Including the spectral influence of a MOL environment into the burnup calculation, has a quite small impact upon k_∞ over the largest part of the computational domain for the Th/U-233 fueled pebbles, especially for higher U-233 weight fractions. However, the relative difference is greater than 1% for pebbles with a metal loading between 5 and 15 grams and U-233 weight fraction between 5% and 10%. For pebbles with a large metal loading and low initial U-233 weight fraction, the relative difference in k_∞ can even become greater than 3%.

The relative differences in the Th-232 concentration are small. This is mainly because the absolute differences are small compared to the large amount of thorium available in the fuel. The relative differences in the Pa-233 and U-233 concentrations can be significant. The largest relative difference in the Pa-233 concentration is 11.3%. The largest relative difference, with a value of 8.28%, in the U-233 concentration is also found at a large metal loading and low initial U-233 weight fraction.

However, it should also be mentioned that there are some geometrical differences, besides the MOL environment of the pebble, in the cross section generation geometries

18
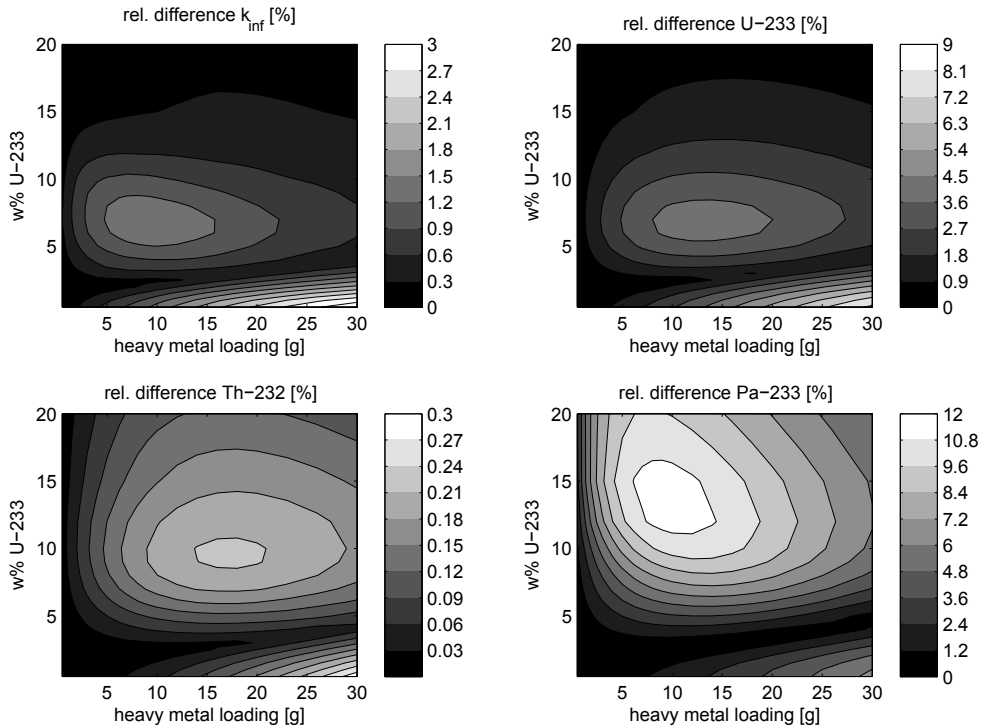
Figure 2.4: Relative difference - in % - in k_∞, U-233, Th-232 and Pa-233 concentrations between the use of a MOL environment and a single pebble spectrum as a function of heavy metal loading and initial U-233 weight fraction

shown in figure 2.3. During the first depletion calculation phase, without MOL environment, the spectrum and cross sections were generated using a single fuel kernel surrounded by two zones, i.e. a TRISO plus matrix layer and a pebble coating plus helium layer, with equivalent dimensions to the dimension of a single fuel kernel. While in the second depletion calculation phase of figure 2.3, the MOL environment surrounds an entire pebble, including an equivalent amount of helium.

Some additional calculations were performed with an adjusted scheme, see figure 2.5, to asses the effect of the MOL environment and to verify that the relative differences in figure 2.4 are indeed mainly caused by the spectral influence of the MOL environment. For the first depletion calculation phase, without MOL environment, the cross sections and neutron spectrum are now also calculated for a central fuel kernel within a whole pebble, similar to the approach in the second depletion calculation phase, with MOL environment, in figure 2.3.

A comparison between the two calculation methods, the original scheme from figure 2.3 and the adjusted scheme from figure 2.5, is made in table 2.3. For the original calculation scheme, a small part of the relative differences observed in figure 2.4 can indeed be attributed to other geometrical differences than the addition of the MOL environment. However, the largest part (> 90%) of the relative differences in table 2.3 can be attributed
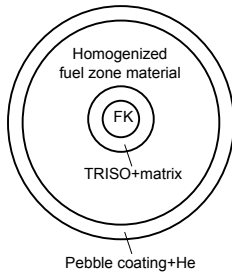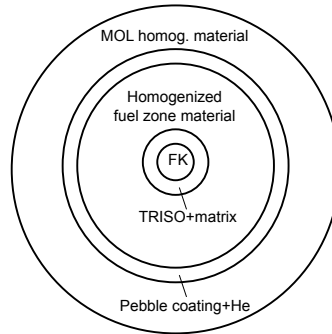
Figure 2.5: Adjusted cross section generation scheme for comparison of MOL environment effect. For the first depletion calculation phase, without MOL environment, the cross sections and neutron spectrum are now also generated for a central fuel kernel inside a whole pebble.

to the spectral influence of the MOL environment for most cases, which underlines the importance of including such effects during fuel pebble depletion calculations. For the 20 g HM and 30 g HM cases with an initial U-233 fraction of 10 w%, the difference due to the MOL environment is larger than for the original method, which also involved other geometrical differences. In these cases, the difference caused by the self-shielding effect of the graphite matrix appears to have a negative impact on the difference between the calculation with and without MOL environment by the original method. Still, also for these cases the spectral influence of the MOL environment is the most important effect for the original method.

Table 2.3: Comparison of relative differences due to MOL environment using the original scheme, shown in figure 2.3, and the adjusted scheme from figure 2.5, which purely involves the MOL environment effect.

Pebble configuration		Original scheme - rel. difference [%]				Adjusted scheme - rel. difference [%]			
HM [g]	w% U-233	k_∞	U-233	Th-232	Pa-233	k_∞	U-233	Th-232	Pa-233
3	0.5	0.420	0.686	0.0108	0.429	0.406	0.662	0.0106	0.418
3	10	0.773	1.45	0.0859	5.28	0.742	1.402	0.0833	5.12
10	0.5	1.32	2.62	0.0515	1.67	1.27	2.51	0.0497	1.599
10	10	0.934	2.80	0.189	10.1	0.922	2.74	0.185	9.89
20	0.5	2.46	5.67	0.152	3.82	2.35	5.36	0.142	3.63
20	10	0.676	2.69	0.213	8.86	0.700	2.757	0.214	8.94
30	0.5	3.23	8.28	0.291	6.32	3.08	7.85	0.267	5.94
30	10	0.508	1.98	0.175	5.75	0.596	2.26	0.194	6.11

As a conclusion, it can be stated that including the MOL spectrum into the calculations leads to small changes in k_∞ and U-233 concentration for high initial weight fractions of U-233. The relative difference between a MOL spectrum and a single pebble spectrum becomes larger for lower initial U-233 weight fractions. This is especially the case when fuel pebbles with a large heavy metal loading and very low initial U-233 weight fraction are used. The next subsection will show that this pebble type is actually the most interesting for use in a thorium high conversion pebble bed reactor.

2.3. PARAMETER STUDIES OF FUEL DEPLETION

2.3.1. IMPACT OF HEAVY METAL LOADING ON BURNUP

The depletion of U-233/Th pebbles was analysed for different heavy metal loadings, in a similar parameter study as for a fresh fuel pebble in section 2.1.1. This time also initial U-233 weight fractions of 0.5%, 1.0% and 1.5% were included in the calculation. A specific power of 80 MW/t_{hm} is used during the burnup calculation, which is divided into 16 burnup steps, consisting of 10 intervals per ORIGEN-S calculation. Each interval corresponds to a period of 10 days, which leads to a maximum burnup of 128 GWd/t_{hm} and a MOL burnup of 64 GWd/t_{hm}.

The burnup calculations were performed for 21 different metal loadings, achieved by either varying the fuel kernel radius or the number of TRISO particles, and 17 different U-233 weight fractions. The possible increase in U-233 concentration, the Pa-233 concentration and k_∞ are relevant indicators of the usefulness of a fuel inside a thorium PBR. From these parameter studies, it was found that a pebble with a high heavy metal loading (and obviously a low initial w% U-233) can achieve the largest increase of the U-233 concentration.

The infinite multiplication factor, the U-233 concentration and Pa-233 concentration are shown in figure 2.6 for a pebble with an initial U-233 weight fraction of 0.5% and three different metal loadings. The constant specific power used in ORIGEN-S and the low initial fissile content of the fuel pebble, lead to a high neutron flux in the first stages of the burnup calculation. The high neutron flux causes a high capture rate in the thorium, which leads to a peak in the Pa-233 concentration at low burnup. In reality, such a peak is not likely to occur as the conversion of fertile isotopes is driven by the flux inside the core, instead of the power.

The k_∞ remains below 1 for all pebble configurations with 0.5% initial U-233 weight fraction. This might be improved a bit by including decay intervals for Pa-233 during burnup, so that less neutrons are captured by Pa-233 before it has decayed into fissile U-233. For pebbles with a high metal loading, k_∞ can be increased by adding moderator pebbles. This enables the creation of an undermoderated breeding zone and an optimally moderated driver zone. The possible effect of adding moderator pebbles upon k_∞ has been demonstrated previously for a 30 g HM fresh fuel pebble.

Figure 2.7 shows k_∞ and the U-233 weight fraction at final burnup as a function of heavy metal loading and initial U-233 weight fraction using the standard fuel kernel radius (0.25 mm). In many cases, roughly the same U-233 concentration is found at final burnup for all the different U-233 initial weight fractions, except for high initial U-233 weight fractions and higher metal loadings. In these cases, the fuel has not depleted far enough yet to approach equilibrium conditions at the moment the maximum burnup is reached. As already demonstrated in figure 2.6, the U-233 weight fraction at final burnup increases with increasing heavy metal loading.

In general, the k_∞ at final burnup is smaller than unity, except for cases with relatively high metal loadings and high initial U-233 weight fraction (> 9 w%). Since the fuel has not depleted far enough to approach an equilibrium in these cases, it can be stated that it is not possible to achieve breeding in combination with criticality for a core consisting only of a single pebble type and moderation ratio.

For fresh fuel pebbles, the method by which the metal loading is varied (either by en-
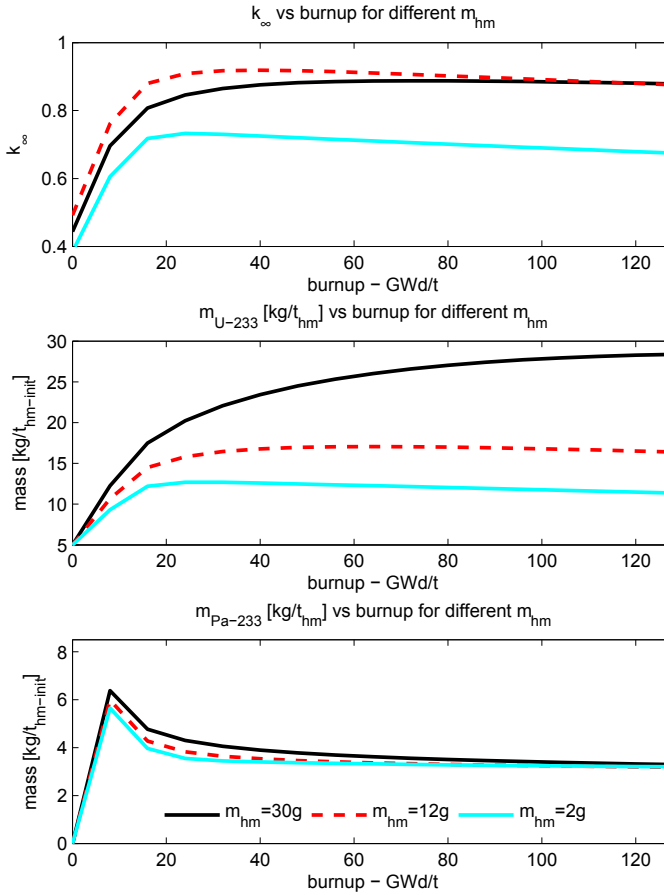
Figure 2.6: k_∞, U-233 and Pa-233 concentrations as a function of burnup for different metal loadings per pebble using an initial U-233 weight fraction of 0.5% and 80 MW/t_{hm} specific power

larging the fuel kernel or increasing the number of particles) was found to be of much smaller importance than the magnitude of the heavy metal loading itself. The fuel depletion studies indicate that the differences in k_∞ between either increasing kernel size or number of coated particles tend to become even smaller with increasing burnup.

At the maximum burnup, the difference in k_∞ between the two methods for a 30 g HM pebble with 0.5 initial w% U-233 is only 0.28%. However, the U-233 concentration at maximum burnup is 24.736 kg/t_{hm} (r_{fk}=0.4224 mm, n_{triso}=10000) compared to 26.598 kg/t_{hm} (r_{fk}=0.25 mm, n_{triso}=48249) for this case. This corresponds to a difference of 7.53%. The self shielding effect is smaller inside a fuel pebble with a larger amount of smaller fuel kernels. Consequently, the neutron capture rate by thorium is higher and therefore the U-233 concentration at final burnup is higher. The negative effect of the increased neutron capture is that less neutrons are available for new fission reactions. Apparently, the increased amount of fissile material and the lower availability of neutrons for fission almost balance
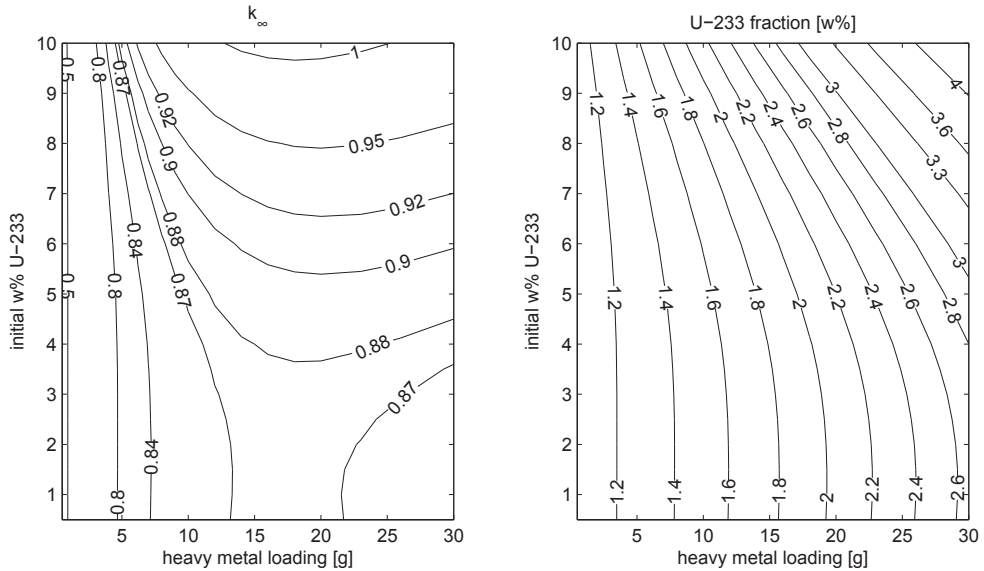
Figure 2.7: k_∞ (*left*) and U-233 weight fraction (*right*) at final burnup (128 GWd/t$_{hm}$) as a function of heavy metal loading and initial U-233 weight fraction using fuel kernels with a 0.25 mm radius.

each other out.

2.3.2. IMPACT OF SPECIFIC POWER ON BURNUP

A specific power of 80 MW/t_{hm} was used during the previous fuel depletion studies. The use of a higher or lower specific power can have a significant impact upon k_∞ and the U-233 and Pa-233 concentrations. It influences the rate of Pa-233 production by means of neutron capture in thorium and changes the time scale available for Pa-233 to decay into U-233. The specific power during fuel burnup could also be a relevant parameter to optimize with respect to the conversion from thorium into U-233.

Using a 30 g HM pebble with 0.5 initial w% U-233, the burnup calculation has been performed for eight specific power values between 5 MW/t_{hm} and 800 MW/t_{hm}. Figure 2.8 shows the k_∞ and the U-233 and Pa-233 concentrations for specific powers of 20, 80 and 400 MW/t_{hm} as a function of burnup. Again, the peak in the Pa-233 concentration is a result of the large flux required during the early burnup stages to obtain a constant power for the fuel pebble with a low initial fissile loading. A high specific power leads to a strong increase of the Pa-233 concentration, because more neutrons are captured by thorium. A much shorter time is required to reach a certain burnup level for a higher specific power. Consequently, Pa-233 has less time to decay to U-233, and the increase of k_∞ and the U-233 concentration is much slower as a function of burnup if a high specific power is used.

For specific powers below 80 MW/t_{hm}, the maximum concentration of U-233 during burnup is not significantly different from the 80 MW/t_{hm} case, but the Pa-233 concentration is lower and less neutrons are captured by Pa-233. As a consequence, the k_∞ of the pebble irradiated with a lower specific power is quite a bit higher. In conclusion, the dif-
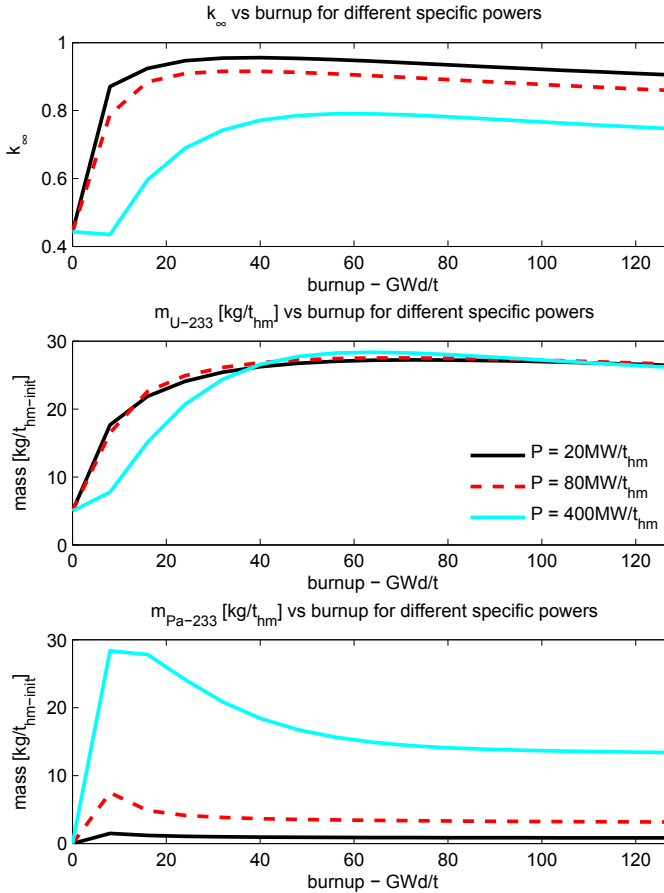
Figure 2.8: k_∞, U-233 and Pa-233 concentrations as a function of burnup for different specific powers for a 30 g heavy metal loaded pebble using an initial U-233 weight fraction of 0.5%

ferences in the U-233 concentration as a function of burnup are quite small for specific powers between 5 MW/t_{hm} and 160 MW/t_{hm}, but k_∞ becomes higher as a lower specific power is used.

2.4. CONCLUSION

FUEL design studies have been performed in this chapter for fresh thorium pebbles and during depletion. The calculation scheme included middle-of-life burnup pebble cross sections as a surrounding material to provide a more realistic neutron spectrum for the ORIGEN depletion calculation, which has a significant influence on k_∞ and the U-233 concentration in case of very low initial U-233 weight fractions and large heavy metal loadings.

The results of the fuel design studies presented in this chapter form a basis for the core

design and fuel management studies of a thorium PBR in the following chapter. Such a core should consist of one or multiple breeder zones and one or multiple driver zones, since breeding and criticality can not be achieved in a core with a single pebble type and moderation ratio. A breeder zone is loaded only with thorium pebbles with a large heavy metal loading (30 g), and its fuel particles have the standard fuel kernel radius of 0.025 cm. The highest possible thorium to U-233 conversion could be achieved for such pebbles during the depletion calculations in this chapter.

Following the irradiation in the breeder zone and a certain decay period for the Pa-233, the fuel pebbles can be recirculated, one or multiple times, into a driver zone. The driver zone consists of a mixture of fuel and moderator pebbles. The addition of moderator pebbles reduces resonance absorption and raises k_∞ above unity, without reprocessing of the fuel. Whether it is possible to achieve breeding without reprocessing or not, will be investigated in the next chapter.

REFERENCES

[1] G. Ilas, N. H. Hudson, F. Rahnema, A. M. Ougouag, and H. G. Gougar, *On a few-group cross-section generation methodology for PBR analysis,* Annals of Nuclear Energy **33**, 1058–1070 (2006).

[2] Radiation Safety Information Computational Center, Oak Ridge National Laboratory, *"SCALE: A Modular Code System for Performing Standardized Computer Analyses for Licensing Evaluations", Vols. I-III, Version 6, CCC-750; ORNL/TM-2005/39* (2009).

[3] G. Ilas, *On SCALE validation for PBR analysis,* in *PHYSOR-2010* (Pittsburgh, 2010).

[4] E. E. Bende, A. H. Hogenbirk, J. L. Kloosterman, and H. van Dam, *Analytical calculation of the average Dancoff factor for a fuel kernel in a pebble bed high-temperature reactor,* Nuclear Science and Engineering **133**, 147–162 (1999).

[5] B. Boer, *Optimized Core Design and Fuel Management of a Pebble-Bed Type Nuclear Reactor,* Ph.D. thesis, Delft University of Technology (2008).

[6] L. Massimo, *Physics of high-temperature reactors* (Pergamom Press, 1976).

3

FEASIBILITY STUDIES OF A THORIUM BREEDER

This chapter investigates whether breeding is feasible within a thorium pebble bed reactor (PBR), and if so, under which operating conditions and fuel recycling strategy. A method was developed to calculate the equilibrium core configuration of a thorium pebble bed reactor, consisting of a driver and a breeder zone. The SCALE system is used for cross section generation and fuel depletion, while a 2D(R,Z)-flux profile is obtained by the DALTON neutron diffusion code. With the code scheme, the influence of several geometrical, operational and fuel management parameters upon the breeding capability was studied.

Three fuel recycling schemes were investigated. The first scheme recycles breeder pebbles into the driver zone after some delay for additional Pa-233 decay. The second one reprocesses the discharged breeder pebbles, to make driver pebbles with higher U-233 contents. The third scheme also reprocesses the uranium isotopes from the discharged driver pebbles. Criticality, and thus breeding, can only be achieved in practice for this case.

One should take notice that the calculation scheme used in this chapter does not include the spectral influence of the surrounding zones (driver, breeder and reflector) upon the fuel depletion in the driver or breeder zone. This effect is included in the coupled calculations in chapter 4 and is found to give lower values for the conversion ratio. This only underlines this chapter's main observation that breeding can only be achieved when reprocessing the uranium content from all pebbles extracted from the system.

CORE design and fuel management studies are performed in this chapter to investigate whether a thorium breeder PBR is feasible and under which conditions. A method was developed to calculate the equilibrium core configuration of a thorium PBR, consisting of a driver and a breeder zone. Using this core depletion code, the breeding capability of a thorium PBR could be investigated as a function of the core geometry, operating conditions or fuel management scheme. Preferably, net-breeding can be achieved within a practical operating regime, in terms of power (> 25 MW$_{th}$), total pebble residence times and safety, by limiting the average power density in the driver zone to 3.2 MW/cm^3, the same as for the HTR-PM, and limiting the core radius to a maximum of 250 cm. For larger cores, it is unlikely that the decay heat removal will be sufficient.

From the neutronic studies of the fuel design in the previous chapter, it was concluded that the conversion of thorium can be maximized for fuel pebbles with a 30 g heavy metal loading, using the standard fuel kernel radius of 0.025 cm, irradiated at low specific power. An overview of the pebble data used in the previous, current and following chapters is given in tables 2.1 and 2.2. To raise the k_∞ of these pebbles above unity without fuel reprocessing, the addition of moderator pebbles is required. As a starting point for the core design studies in this chapter, it was therefore recommended to insert fresh pebbles with 30 g thorium into one or multiple breeder zones, without moderator pebbles, with the irradiated pebbles being recycled into one or multiple driver zones with moderator pebbles.

The calculational method to acquire the equilibrium core configuration will be discussed in section 3.1. The feasibility studies of achieving a breeder reactor are performed in section 3.2 for different fuel recycling strategies. From the feasibility studies, the core geometry, fuel management scheme and operating conditions necessary for a thorium breeder PBR can be determined. Conclusions are drawn in section 3.3.

3.1. EQUILIBRIUM CORE CALCULATION

BURNUP calculations inside a PBR are not trivial because of the movement of the fuel, the double-heterogeneous structure of the fuel, and the relatively long neutron migration length, typically of the order of several pebble diameters. Several codes used for the analysis of fuel depletion can be found in the literature. The distinctions between the codes mainly concern three points. First, some methods simultaneously solve the neutron diffusion equation and nuclide balance equations, whereas other methods interpolate cross sections from pre-generated burnup dependent cross section libraries. The second distinctive feature is the capability to model more complex fuel management schemes. Some codes can only model once-trough-then-out-cycles (OTTO), whereas others can also model multipass schemes. The third distinction between codes is whether they converge on the equilibrium core composition directly or calculate the transition from some initial core composition to a final, possibly equilibrium, core composition over time.

The VSOP (Very Superior Old Programs code) was developed in Germany during the High-Temperature Reactor Program [1]. The first edition of the VSOP code was published in 1980 and it was upgraded in 1994, 1997, 1999, 2005, 2009 and most recently 2011. Application of the code implies processing of cross sections, the setup of the reactor and fuel elements, neutron spectrum evaluation, neutron diffusion calculation, fuel burnup and movement, reactor control and thermal hydraulics. The VSOP code can calculate the core depletion from the initial core toward the equilibrium core and is probably the most

widely used code for pebble bed fuel cycle analysis. Other codes worth mentioning are NRG's PANTHERMIX code [2] and the method developed by Grimod [3, 4] in APPOLLO2.

In contrast to VSOP, the BATAN-MPASS code, developed by Liem [5], directly solves the core equilibrium condition for both multi-pass refueling schemes as well as the OTTO scheme. BATAN-MPASS uses a double iterative method to obtain the equilibrium condition of a critical pebble bed core. The inner iterative procedure determines an equilibrium core composition and an outer iterative procedure follows to achieve a critical state of the reactor by varying the pebble flow velocity, the fresh fuel enrichment, or the moderation ratio.

Terry [6] developed a deterministic method explicitly accounting for the flow of pebbles through the core and coupling this to the neutronics. This method can be used for both once-through cycles and multi-pass schemes. The work of Terry followed a systematic semianalytical approach and is the basis of the core depletion scheme in the PEBBED code [6]. The method obtains the asymptotic fuel loading pattern directly, without calculation of intermediate states. The core depletion scheme has been extended by Gougar [7, 8] to also account for more complex fuel management schemes, and it now allows for different pebble flow speeds and pebble types to be used in each channel.

The method used by Boer [9] and Boer et al. [10], similar to Terry et al. [6], tries to find the asymptotic nuclide distribution directly, without calculating any intermediate distribution. Instead of the analytical approach by Terry et al., a numerical iterative calculation scheme similar to that of Fratoni and Greenspan [11, 12] is followed using existing codes. SCALE5 is used for the cross-section preparation and depletion calculations. At the core level, the neutron diffusion equation is solved by the DALTON code [13]. The approach of the depletion method in this chapter is similar to the method developed by Boer et al.

3.1.1. CALCULATION SCHEME

The core depletion code scheme uses several modules from the SCALE6 code package [14] for cross-section preparation and depletion calculations. For computational efficiency, the ENDF-V5 44 group thermal reactor library is used for the core depletion calculations in this thesis. An average core temperature of 1100 K is assumed for the calculations and this temperature has been used throughout the cross section generation procedure for all calculations in this chapter. For neutron diffusion calculations at the core level, the DALTON code, which was developed in-house, is used.

To solve for the fuel depletion inside the pebble bed core, an iterative solution process is followed. A schematic overview of the core depletion code is given in figure 3.1. First a 2D(R,Z)-diffusion calculation is performed by DALTON using cross sections of a fresh fuel pebble with higher U-233 content and a high moderator-to-fuel ratio to mimic the driver zone and a low U-233 content for the breeder zone. These cross sections are generated using the CSAS sequence from SCALE6. DALTON determines the k_{eff} and eigenfunction of the system. The flux is then obtained by scaling this eigenfunction to the power production in the core, and used as an initial flux guess for the first depletion loop of the iterative solving process.

For the depletion calculation, the breed and driver channels are divided into several axial burnup zones, which consist of multiple radial grid cells and one or more of the axial grid cells used in the diffusion calculation. The thermal fluxes used in the ORIGEN de-

pletion calculation are obtained by volume averaging the thermal group flux (< 0.625 eV) obtained by DALTON over the volume of the burnup zone and by multiplying with the flux disadvantage factor of the fuel zone in the thermal energy range.

First, cross sections and neutron spectrum are generated using CSAS/XSDRN for the fresh thorium pebble, and an ORIGEN working library is created using COUPLE. The double-heterogeneous nature of the fuel has been accounted for by a Dancoff factor in the CSAS input file. The Dancoff factor is calculated according to the equations of Bende et al. [15]. The method of obtaining the fuel kernel cross sections, while including the spectral influence of the surrounding pebbles, is treated in detail in section 3.1.2. The change in the nuclide composition of the thorium pebble is then calculated by ORIGEN using the volume-averaged thermal flux of the first axial breeder zone during an irradiation of $\tau_{res,breed}\frac{dh}{H}$, where dh is the height of a single burnup zone, H is the height of the core, and $\tau_{res,breed}$ is the residence time of a fuel pebble in the breeder channel during one passage.

After the depletion step, new fuel kernel cross sections and spectrum are determined and the next depletion step is calculated by ORIGEN. This process is repeated until the pebble is at the bottom of the core. There it is recycled into the breeder channel until the final breed channel passage has finished. Three reprocessing or recycling schemes can then be applied to the discharged breeder pebbles. These three schemes will be discussed in section 3.1.4.

Inside the driver channel a similar process is followed as for the breed channel depletion calculation, except that the cross sections are now generated for a mixture of fuel and moderator pebbles or a mix of fuel pebbles with a lower metal loading. The presence of moderator pebbles is accounted for by the shell expansion method [15].

Besides the microscopic zone-weighted pebble cross sections generated for the depletion calculation, macroscopic homogenized cell-weighted cross sections are also calculated. The macroscopic cell-weighted pebble cross sections for all passages, at the top and the bottom of the axial burnup zone, are mixed by ICE with equal weights to obtain the average pebble material in a certain zone. At different heights, 1D XSDRN calculations are performed over radial slabs to collapse the cross sections from 44 to 5 groups with a proper weighting of the core neutron spectrum. The homogenized and collapsed pebble cross sections are then used to generate a 2D cross section mapping, and a 2D(R,Z)-diffusion calculation is performed with DALTON. The depletion loop described above is repeated using the updated flux profile from DALTON until convergence of the flux, k_{eff} and U-233 concentrations is reached and the core equilibrium configuration is determined. Then, the relevant output is stored, such as k_{eff}, burnup, flux profile and nuclide concentrations per zone and passage. The discharge burnup of the pebble is determined by summing over the burnups obtained during all the ORIGEN calculations. A schematic overview of the core depletion code is given in figure 3.1.

3.1.2. Cross sections and spectrum

The neutron migration length inside a PBR is much greater than the size of a single pebble. The neutron spectrum inside a pebble is therefore mainly determined by the average nuclide composition of the surrounding pebbles [16]. These spectral influences should be included in the fuel depletion calculation to obtain accurate results.

A schematic overview of the creation of the ORIGEN working library in the core deple-
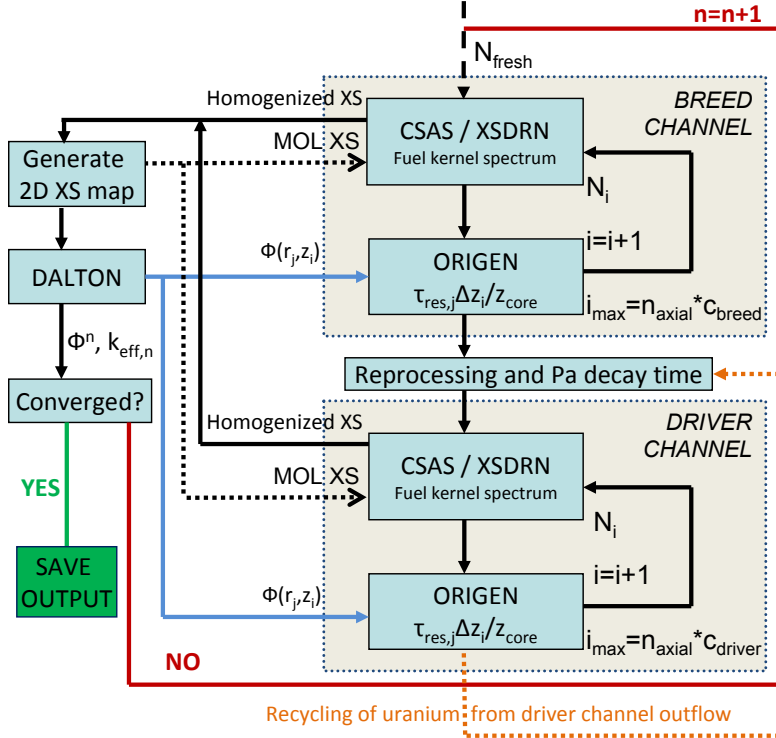
Figure 3.1: Overview of the iterative equilibrium core calculation scheme, containing cross section generation by CSAS/XSDRN and depletion by ORIGEN using fluxes from DALTON. Fluxes, k_{eff} and nuclide concentrations are updated repeatedly until convergence is reached.

tion scheme is shown in figure 3.2. As a first step, a CSAS calculation is performed at the level of a single fuel kernel. The fuel kernel is surrounded by a mixture of the TRISO coatings and the graphite matrix, with dimensions equivalent to a single fuel kernel, and this is again surrounded by a mixture of the pebble shell and the helium coolant. During the CSAS calculation, microscopic zone-weighted cross sections are generated for the fuel kernel and macroscopic zone-weighted cross sections for the two outer material regions. In a consecutive XSDRN calculation, an inner-zone weighting is performed to produce zone-weighted homogenized cross sections for a mixture of the fuel kernel, coating layers, and the graphite matrix.

During the first core iteration of the core depletion scheme, the microscopic fuel kernel cross sections obtained in this first step are used by COUPLE to create the ORIGEN working library, used for the depletion calculation in a specific zone. After the first core iteration, a second calculation step is performed by XSDRN. A 1D transport calculation is performed for a pebble with a fuel kernel in the center. The pebble is surrounded by the average pebble material in the burnup zone. The radius of this outer average pebble material layer is chosen to be large (200 cm) compared with the radius of a single pebble. To save computation time, the average pebble material cross sections are obtained from the
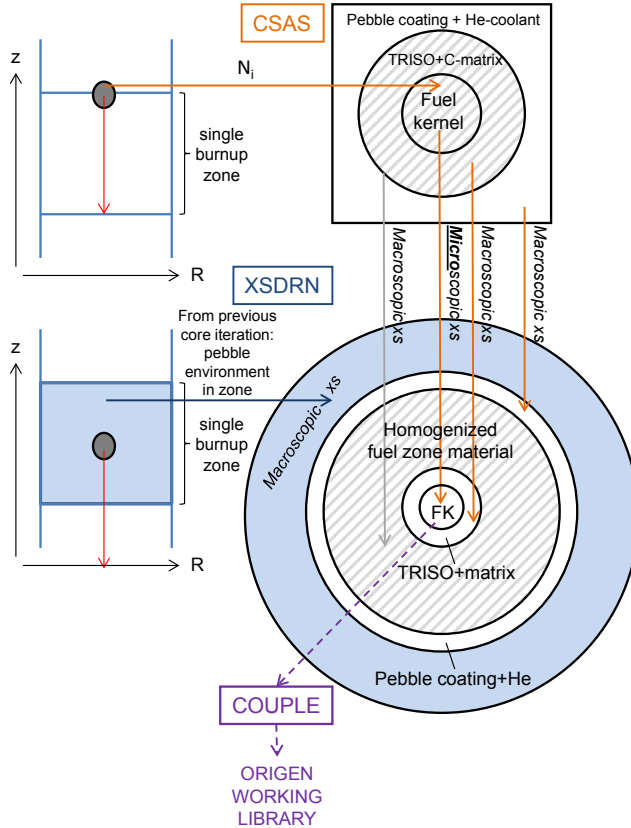
Figure 3.2: Schematic view of cross-section generation method (the diagrams are not to scale)

previous core iteration.

The average pebble material cross sections are referred to as MOL XS in figure 3.1. The cross sections for the center pebble were obtained by the CSAS and XSDRN calculations in the first step of the cross-section generation scheme. The microscopic zone-weighted cross sections obtained for the central fuel kernel are then used by COUPLE to generate the ORIGEN working library. This way, the neutron spectrum used during the depletion calculation includes the influence of the surrounding pebbles within the burnup zone.

3.1.3. Core geometry

The geometry used for the reflector and other regions outside the active core is roughly based on the geometry of the HTR-PM [17] and is shown in figure 3.3.

In the axial direction, the core is surrounded by several reflector layers, helium plena, or the top cavity and at the boundaries by the reactor carbon brick. To improve the convergence and accuracy of the neutron diffusion calculation, the use of neutronically thin media is avoided in the actual calculations. This is done by homogenizing helium regions with adjacent graphite regions. So, the helium of the core top cavity was homog-
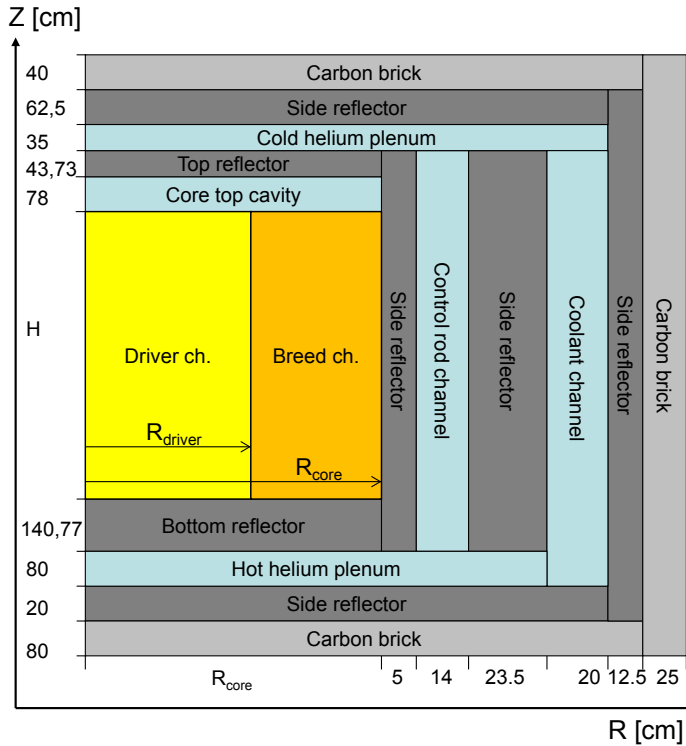
Figure 3.3: Schematic view of the thorium PBR geometry used for the neutronics calculations, consisting of a cylindrical core with driver and breeder zone, surrounded by different graphite, helium or carbon brick layers. Dimensions are based on numbers given by Zheng and Shi [18]. (not to scale)

enized with the top reflector, the hot helium plenum with the lower side reflector and the cold helium plenum with the upper side reflector. For pure graphite reflector material an atomic density of $8.8245 \cdot 10^{-2} \frac{atoms}{barn \cdot cm}$ (1.76 g/cm^3) is used, and for the carbon brick, $7.7716 \cdot 10^{-2} \frac{atoms}{barn \cdot cm}$ (1.55 g/cm^3) is used. During the diffusion calculations a 10 cm grid size is used within the core region in the radial direction and 50 cm in axial direction. For the surrounding reflector regions 9 additional cells are used in radial direction and 15 cells in axial direction.

In the radial direction, the core is surrounded by the side reflector and carbon brick. Inside the side reflector there is one region with openings for 8 control rods of 13 cm diameter and 22 absorber balls and one region with openings for 30 coolant channels of 18 cm diameter. The control rod and coolant channel regions have been modelled by mixing the helium openings with the surrounding graphite.

3.1.4. THREE REPROCESSING SCHEMES
For the core depletion scheme, three different fuel recycling strategies are applied, to check when breeding (CR>1) can be achieved using a minimum core power of 25 MW$_{th}$. The first scheme uses a decay time of 180 days, in order to allow for most of the Pa-233 to decay into

U-233, before fuel pebbles are recycled from the breed into the driver channel. In the second method, the fuel extracted from the breed channel is reprocessed, to make driver fuel pebbles with a higher U-233 weight fraction. In the third method, also the fuel extracted from the driver channel is reprocessed. For these three models, the aim is to maximize the equilibrium k_{eff} and check whether breeding[1] can be achieved, meaning k_{eff} is larger than unity. Ideally, breeding would be achieved without the expensive reprocessing of fuel pebbles, but this is also the most challenging option from a neutronic perspective. A graphical interpretation of the three reprocessing schemes is shown in figure 3.4.
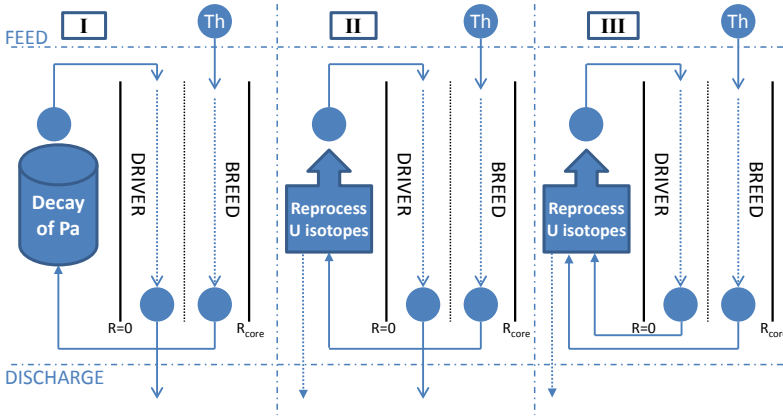
Figure 3.4: Overview of the three fuel recycling schemes

Scheme I: Without reprocessing

Thorium pebbles are inserted into the breed channel and recycled one or multiple times. After that the pebbles are stored, during a user specified decay time, to let most of the Pa-233 ($t_{1/2}$ = 26.967 d) decay into U-233. Then the pebbles are inserted into the driver channel for one or multiple passages, after which they are discarded. Assuming all breeder pebbles are eventually recycled into the driver channel, the residence time of a single passage of the pebble in the driver zone is given by

$$\tau_{res,driver} = \tau_{res,breed} \frac{c_{breed} V_{driver}}{c_{driver}(1 + f_{driver}) V_{breed}}, \tag{3.1}$$

where $\tau_{res,breed}$ is the single passage breeder pebble residence time, c_{breed} is the number of breed channel passages and c_{driver} the number of driver channel passages of the pebble, f_{driver} the dummy to fuel pebble fraction in the driver zone and V_{breed} and V_{driver} are the volumes of the breed and driver zone.

For a given V_{breed}, $\tau_{res,breed}$, c_{breed}, reactor power P, heavy metal loading per pebble m_{hm} (in grams), pebble radius r_{peb} and pebble packing fraction η, the average discharge burnup is given by

---

[1]The formal definition of breeding is a higher fissile atom production rate than consumption rate. For the third recycling scheme, where the fissile content of all the extracted pebbles is reprocessed, a k_{eff} above unity implies breeding. For the first two schemes, "self-sufficiency", i.e. only requiring Th-232 insertion for continuous operation, is a more correct phrasing if one would strictly adhere to the formal definition of breeding.

$$BU_{dis} = \frac{4P\pi r_{peb}^3 c_{breed}}{3 * 10^{-6} m_{hm} V_{breed} \eta} \tau_{res,breed} \ [MWd/t_{hm}].$$ (3.2)

This analytical expression can also be used to check the burnup values calculated by the core depletion code scheme.

SCHEME II: REPROCESSING FROM THE BREED CHANNEL

Thorium pebbles are inserted into the breed channel and recycled one or multiple times. After a user-specified decay time, the uranium isotopes in the pebbles are reprocessed into fresh fuel pebbles with a higher, user-specified, U-233 weight fraction and a lower heavy metal loading to improve the moderation in the driver zone. Then, the pebbles are inserted into the driver channel for one or multiple passages, after which they are discarded.

For a given U-233 weight fraction of the reprocessed fuel pebbles flowing into the driver channel, the residence time in the driver channel is given by

$$\tau_{res,driver} = \frac{c_{breed} V_{driver} m_{driver}^{hm} \epsilon_{driver}^{23,in}}{c_{driver} V_{breed} m_{breed}^{hm} \epsilon_{breed}^{23,out}} \tau_{res,breed},$$ (3.3)

where m_{driver}^{hm} is the heavy metal loading of the driver fuel pebbles and m_{breed}^{hm} the metal loading of the thorium breeder pebbles. The U-233 weight fraction of the fuel flowing out of the breeder zone is given by $\epsilon_{breed}^{23,out}$, and the user-specified U-233 weight fraction flowing into the driver channel is denoted by $\epsilon_{driver}^{23,in}$.

The weight fraction of any other uranium isotope after the reprocessing, $\epsilon_{driver}^{j,in}$, is calculated from

$$\epsilon_{driver}^{j,in} = \epsilon_{breed}^{j,out} \frac{\epsilon_{driver}^{23,in}}{\epsilon_{breed}^{23,out}},$$ (3.4)

where $\epsilon_{breed}^{j,out}$ is the weight fraction of uranium isotope j at the outlet of the breed channel.

SCHEME III: REPROCESSING FROM BREED AND DRIVER CHANNEL

In the previous recycling scheme, the uranium content left in the pebbles flowing out of the driver channel was discharged after their final passage. This time, all these uranium isotopes are also recycled into the fresh driver channel pebbles. Before reprocessing pebbles, a user-specified decay time is taken for conversion of Pa-233 into U-233.

For a given U-233 weight fraction of the reprocessed fuel pebbles flowing into the driver channel, the residence time in the driver channel is given by

$$\tau_{res,driver} = \frac{c_{breed} V_{driver} m_{driver}^{hm} (\epsilon_{driver}^{23,in} - \epsilon_{driver}^{23,out})}{c_{driver} V_{breed} m_{breed}^{hm} \epsilon_{breed}^{23,out}} \tau_{res,breed},$$ (3.5)

where $\epsilon_{driver}^{23,out}$ is the U-233 weight fraction of the fuel pebbles flowing out of the driver channel. Compared with recycling scheme II, which only reprocesses uranium from the breeder pebbles, the recycling of the fuel from the driver channel allows for a shorter driver

channel residence time, which in turn, leads to a higher U-233 concentration in the out-flow from the channel, and this leads to an extra shortening of the driver channel residence time, and so on. For this reason, the recycling of driver channel fuel might have quite a significant impact on the residence time and the k_{eff} of the equilibrium core.

The weight fraction of any other uranium isotope, $\epsilon_{driver}^{j,in}$, after the reprocessing is calculated by

$$\epsilon_{driver}^{j,in} = \epsilon_{driver}^{j,out} + \epsilon_{breed}^{j,out} \frac{\epsilon_{driver}^{23,in} - \epsilon_{driver}^{23,out}}{\epsilon_{breed}^{23,out}}, \tag{3.6}$$

where $\epsilon_{breed}^{j,out}$ is the weight fraction of uranium isotope j of the pebbles flowing out of the breeder channel.

3.2. Feasibility Studies

THE three recycling strategies discussed in the previous section are used to determine whether the design of a breeder is feasible for the different fuel reprocessing schemes and, if breeding is possible, under what operating conditions this is so.

The code developed offers the opportunity to vary many variables, such as residence times, moderator-to-fuel ratio, the number of pebble recyclings in breeder and driver channels, reactor power, core geometrical parameters, and even fuel geometrical and composition parameters. Because of the large number of variables involved, complete optimization is rather cumbersome, especially considering that a few days are required for each equilibrium core calculation. Therefore, the parameter studies presented in this section mainly focus on the variables that were found to have a significant influence on the breeding capability of the reactor, such as the radius of the driver and the breed channels and the reactor power.

3.2.1. Recycling strategy I

The ideal situation would be to achieve a critical core configuration without the expensive reprocessing of fuel pebbles. Only thorium pebbles would have to be added during reactor operation. Several parametric studies were performed to determine whether it is possible to design such a core.

Testcase

Section 3.1.2 explained how the influence of the surrounding pebbles upon the neutron spectrum is included in the ORIGEN calculation. However, the spectrum shifts due to the reflector surrounding the breed channel and the undermoderated breed channel surrounding the driver channel are not included in the ORIGEN calculation. For this reason, the power values obtained by the ORIGEN calculations may deviate somewhat from those of the DALTON calculation.

To quantify these effects and to check the accuracy of the code, the equilibrium core configuration was calculated when a pebble makes two passages through both the breeder and driver channel. Other parameters were R_{driver}=140 cm, R_{breed}=250 cm, H=1100 cm, P=250 MW$_{th}$, and f_{driver}=3. The residence time is chosen by equation 3.2 to give an analytical burnup of 100 GWd/t$_{hm}$. For this core, k_{eff} was found to be 0.8857.

The average discharge burnup of a pebble can be determined by summing over all burnup zones the product of the specific power and the pebble residence time in each zone. This way, the DALTON output gives a burnup of 99999 MWd/t$_{hm}$, as expected from the analytical burnup calculation. However, a summation over the burnup values obtained during all ORIGEN depletion steps yields a discharge burnup of 104028 MWd/t$_{hm}$. The thermal flux from DALTON (E < 0.625 eV) is used by ORIGEN to perform the depletion calculation in a certain burnup zone. The resonance flux (0.625 eV < E < 1 MeV), and consequently the specific power, is slightly too high for the breed channel in the ORIGEN calculation, as the influence of the reflectors is neglected. In the driver channel, this is the other way around. The influence of the undermoderated surrounding breeder channel is neglected, resulting in a lower resonance flux and specific power in the ORIGEN calculation. The difference between including the moderator density effect of the surrounding regions or not leads to a 4% larger pebble discharge burnup, which is acceptable for the purposes pursued in this chapter.

The number of axial burnup zones required to obtain accurate results was also investigated. Reducing the number of axial burnup zones from 22 to 11 had little influence on the results. Differences of 0.006% in k_{eff} and of 0.04% in discharge burnup were found. The relative change in the breed channel discharge U-233 concentration was slightly larger, but still marginal (0.28% higher using 22 zones). Since the use of 11 axial burnup zones nearly halves the calculation time compared with 22 zones and the induced error is reasonably small, this is the default choice for further calculations in this thesis.

PARAMETRIC STUDIES

To achieve the highest possible k_{eff} of the core design, different driver or breed channel radii, reactor powers and pebble residence times have been studied. Other parameters were chosen to be H_{core} = 1100 cm, f_{driver} = 3, c_{driver} = 2 and c_{breed} = 2.

For a 250 cm outer core radius, the radius of the central driver channel was varied from 80 to 200 cm, in steps of 20 cm, and the thickness of the breed channel was varied accordingly. The k_{eff}, the weight fraction of U-233 in the pebbles after the final passage through the breed channel and 180-day decay time, and the burnups accumulated by the pebbles at discharge from the breeder and the driver zone are shown in table 3.1.

Table 3.1: k_{eff}, U-233 weight fraction of discharged breeder pebbles, and breed and driver channel discharge burnup [GWd/t_{hm}] as a function of driver zone radius [cm] for a 250 cm core radius.

R_{driver} [cm]	k_{eff}	$\epsilon_{breed}^{23,out}$ [w%]	BU_{breed}^{dis} [GWd/t]	BU_{total}^{dis} [GWd/t]
80	0.8658	2.4888	96.1	103.5
100	0.8739	2.4775	91.7	103.7
120	0.8808	2.4620	86.3	103.6
140	0.8856	2.4459	80.8	104.2
160	0.8873	2.4252	74.2	104.5
180	0.8850	2.3983	66.5	104.9

A driver channel radius of about 160 cm leads to the highest k_{eff} of 0.8873 for the 250 cm core, but it is much smaller than unity. The total burnups are somewhat larger than the theoretical burnup of 100 GWd/t$_{hm}$ due to spectral influence of the reflectors.

This deviation from the theoretical burnup increases somewhat for larger driver zone radii, as the average location of the breeder pebble lies closer to the reflector and the reflector spectrum effect, as discussed in section 3.2.1, becomes more prominent.

A second relevant parameter is the residence time of the pebbles in the core. Using the 140/250 cm core configuration, the residence times were varied to yield discharge burnups of approximately 20, 40, 60, 80, 100, 120, 140 and 160 GWd/t$_{hm}$. Results in table 3.2 show that the highest burnup value leads to the highest k_{eff}. However, compared to 100 GWd/t$_{hm}$, the increase is quite marginal.

Table 3.2: k_{eff} and U-233 weight fraction of discharged breeder pebbles as a function of pebble discharge burnup [GWd/t_{hm}] or breeder pebble residence time [d] for a 140/250 cm core.

BU_{total}^{dis} [GWd/t]	$\tau_{res,breed}^{total}$ [d]	k_{eff}	$\epsilon_{breed}^{23,out}$ [w%]
20.5	1919	0.7238	1.7136
41.1	3838	0.8146	2.0960
62.0	5757	0.8538	2.2844
83.0	7676	0.8742	2.3877
104.2	9595	0.8856	2.4459
125.4	11514	0.8917	2.4779
146.5	13433	0.8953	2.4908
167.8	15352	0.8967	2.4907

Another relevant parameter for the breeding capability and equilibrium k_{eff} is the thermal power of the reactor. The k_{eff} was calculated for the 140/250 cm core configuration as a function of core power. The product of power and residence time was kept constant to ensure similar discharge burnups. Results are shown in table 3.3. The use of a lower power clearly leads to a significant increase in k_{eff}. Lowering the power results in lower Pa-233 and fission product concentrations, which reduces parasitic neutron capture. This leads to a higher equilibrium k_{eff} and more efficient conversion of thorium to U-233, at a price of extremely long, and therefore unrealistic, pebble residence times.

Table 3.3: k_{eff} and breed and driver channel discharge burnups [GWd/t_{hm}] for different reactor powers [MW_{th}] and breeder pebble residence times [d]

P [MW_{th}]	$\tau_{res,breed}^{total}$ [d]	k_{eff}	BU_{breed}^{dis} [GWd/t]	BU_{total}^{dis} [GWd/t]
25	95953	0.9045	80.9	104.0
100	23988	0.8961	80.8	104.0
250	9595	0.8856	80.8	104.2
500	4798	0.8741	80.5	104.2

Doubling the core radius to 500 cm might help raise k_{eff} above unity, as such an increase of the core radius will dwarf neutron leakage from the core. For a 500 cm core radius, a driver channel radius around 240 cm was found to yield the highest k_{eff}. Combined with a very low power of 25 MW$_{th}$ and average discharge burnup of 100 GWd/t$_{hm}$, an equilibrium k_{eff} of 0.9359 was obtained. Even for these exceptional reactor core designs, k_{eff} remains much smaller than unity. By optimizing c_{breed}, c_{driver}, and f_{driver}, a marginal

increase in k_{eff} may still be achieved, but not nearly enough to reach criticality. There-fore, reprocessing will be required to design a critical breeder reactor.

3.2.2. Recycling strategy II

The value of k_{eff} might be raised significantly by processing the uranium content of the breeder pebbles into newly made driver pebbles with a larger U-233 weight fraction. The uranium content of the driver fuel pebbles extracted from the system, after their final pas-sage through the core, is still treated as waste in this recycling scheme. Whether a critical core configuration can be achieved is investigated here.

Several parameter studies were performed for a 250 cm core. The core radius, driver channel radius, breeder pebble residence time, and reactor power were found to have a significant influence on the equilibrium k_{eff}, and these parameters will be discussed in more detail. If chosen within a feasible range, the U-233 weight fraction of the driver fuel ($\approx$7-10%), the number of breed ($\approx$2) and driver channel passages ($\approx$5-10) had only a small influence upon the equilibrium k_{eff}. For purposes beyond the scope of this chapter, such as flattening of the axial power profile, a further investigation of these variables might be desirable.

Driver channel radius

The driver channel radius was varied between 70 and 130 cm for a core with a radius of 250 cm. The total breeder pebble residence time was 5000 days, so a single breed channel passage takes 2500 days. Other core parameters were H_{core} = 1100 cm, m_{hm}^{driver} = 7.5 g, c_{driver} = 5, c_{breed} = 2, P_{core} = 250 MW$_{th}$ and $\epsilon_{driver}^{23,in}$ = 10 w%. Results for the different driver channel radii are shown in table 3.4.

Table 3.4: Driver pebble residence time [d], core equilibrium k_{eff}, and discharge burnup of breeder and driver pebbles [GWd/t_{hm}] as a function of R_{driver} [cm] for a 250 cm core

R_{driver} [cm]	$\tau_{res,driver}^{total}$ [d]	k_{eff}	BU_{breed}^{dis} [GWd/t]	BU_{driver}^{dis} [GWd/t]
70	535	0.9280	24.8	72.9
80	733	0.9492	23.2	87.9
90	967	0.9607	22.4	101.5
100	1242	0.9654	22.0	113.7
110	1584	0.9642	21.2	125.0
120	1973	0.9608	21.3	136.1
130	2429	0.9557	21.7	147.3

The radius of the driver channel has a significant influence on the k_{eff} of the equi-librium core. The highest k_{eff} is found for a driver channel radius of 100 cm. The res-idence time of the driver channel pebbles increases as the radius of the driver channel increases, as more pebbles have to be fueled into the driver channel from a smaller num-ber of breeder pebbles. Also, the driver pebble discharge burnup increases with increasing driver channel radius because of the increase in residence time.

The discharge burnup of the breeder pebbles initially decreases with increasing driver channel radius, but from 110 cm on it starts to increase again. This is caused by the combi-nation of two opposing effects. First, the fraction of the core power produced in the breed

channel decreases as the driver channel radius increases. This effect is most prominent for small driver channel radii. Second, the volume of the breed channel decreases more and more rapidly as the driver channel radius increases. The breed channel burnup is inversely proportional to the breed channel volume. This effect is most prominent for large driver channel radii, explaining the increase in the discharge burnup of the breeder pebbles.

BREEDER PEBBLE RESIDENCE TIME

The influence of the breeder pebble residence time on k_{eff} was also tested for the 250 cm core with a 90 cm driver channel radius. The results, as shown in table 3.5, indicate that quite long residence times are required to obtain a reasonably high k_{eff}.

Table 3.5: k_{eff} as a function of total breeder pebble residence time for a 90/250 cm core configuration

$\tau_{res,breed}^{total}[d]$	k_{eff}
1000	0.9073
2000	0.9303
3000	0.9451
5000	0.9607
7000	0.9671
10000	0.9693

OPTIMIZED 250 CM CORE

Combining the parameter choices leading to a high k_{eff}, a more or less optimal core configuration is found. Although this does not lead to one unique and truly optimal solution, it can be expected that the result is close to this optimum. During the calculation the following parameters are used: P_{core} = 25 MW$_{th}$, R_{driver} = 100 cm, R_{breed} = 250 cm, H_{core} = 1100 cm, m_{hm}^{driver} = 7.5 g, c_{driver} = 5, c_{breed} = 2, $\epsilon_{driver}^{23,in}$ = 7 w% and $\tau_{res,breed}^{total}$ = 50000 d. This residence time and power are completely unrealistic and not economical in practice, but is shows what equilibrium k_{eff} would be theoretically achievable with a 250 cm core with reprocessing of uranium from the breed channel. For this choice of parameters, a k_{eff} of 0.9881 was found, which is still smaller than unity.

VARYING CORE RADIUS

Increasing the radius of the core can improve the neutron economy and the achievable equilibrium k_{eff} significantly. For this purpose, the equilibrium k_{eff} was calculated for core radii ranging from 150 to 550 cm and a 100 cm driver channel radius. Whether the highest k_{eff} can actually still be achieved with a driver channel radius of 100 cm is investigated for a 500 cm core radius in section 3.2.2.

For this analysis, the power is kept constant and the breeder pebble residence time is varied proportionally to the core volume increase. This leads to a very good match between the radial power profiles for the different core radii, especially in the driver channel, as shown in figure 3.5. This approach is the most desirable one to model the reduced neutron leakage effect as the core radius increases. Alternatively, one could also increase the core power proportionally to the core volume increase, which makes sense from an economic perspective. However, it leads to a very high power density in the driver channel, which is undesirable from a safety perspective.

Figure 3.5 clearly shows the radial power profiles overlap in the driver channel. In the breed channel, there is an increase in power near the radial reflector. This effect is strongest for the smallest core radius. It can also be seen that the power production (per radial unit length) close to the reflector becomes smaller as the core size increases and, as a consequence, neutron leakage is also reduced. This can also be seen from the k_{eff} values, which strongly increase for a core size increase from 150 to 250 cm, whereas the breeding performance only improves modestly for a further increase of the core radius towards 350, 450 or 550 cm.

3
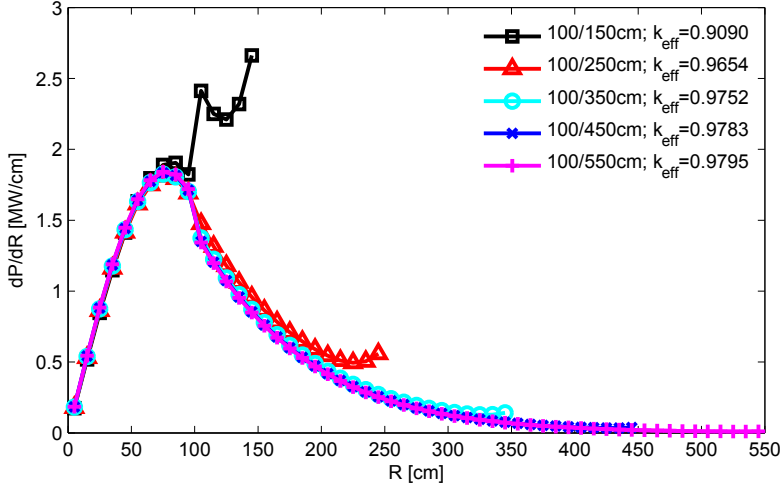
Figure 3.5: Power produced per radial length unit for different core radii, while varying $\tau_{res,breed}$ proportional to R^2_{core}; $P_{core} = 250\ [MW_{th}]$)

CORE RADIUS OF 500 CM

Now, the optimal ratio between driver and breeder zone radius is investigated for a core with a 500 cm radius. As demonstrated in figure 3.5, it is best to increase $\tau^{total}_{res,breed}$ to 20000 d, proportionally to the volume increase of the core. The core power is kept at 250 MW$_{th}$. Other parameters are H_{core} = 1100 cm, m^{driver}_{hm} = 7.5 g, c_{driver} = 5, c_{breed} = 2, $\epsilon^{23,in}_{driver}$ = 10 w%.

Using 50 radial grid cells the driver channel radius was varied from 80 to 120 cm, in steps of 10 cm. The results of these calculations are shown in table 3.6. The optimal driver channel radius is found to be around 110 cm, and only a very small shift occurs compared with the 250 cm core radius. In contrast to recycling scheme I, where no reprocessing is performed, the use of a larger core radius does not lead to a significant change in the optimal driver channel radius.

An attempt was made to find an equilibrium k_{eff} larger than unity for the 500 cm core radius. For this reason, a low power of 100 MW$_{th}$ and a very long total breeder pebble residence time of 50000 days was used. Although not very realistic in practice, this calculation provides some sort of upper boundary on the k_{eff} achievable if all the U-isotopes flowing

Table 3.6: Total driver pebble residence time $[d]$, core equilibrium k_{eff}, and discharge burnup of breeder and driver pebbles $[GWd/t_{hm}]$ as a function of driver zone radius using 50 radial core grid cells, $R_{breed} = 500$ $[cm]$

R_{driver} [cm]	$\tau_{res,driver}^{total}$ [d]	k_{eff}	BU_{breed}^{dis} [GWd/t]	BU_{driver}^{dis} [GWd/t]
80	701	0.9609	21.5	82.6
90	908	0.9740	20.3	95.5
100	1162	0.9790	18.4	106.8
110	1444	0.9803	17.3	116.9
120	1763	0.9786	16.4	126.2

out of the breeder channel are reprocessed. A driver channel radius of 100 cm was used and other parameters were H_{core} = 1100 cm, m_{hm}^{driver} = 7.5 g, c_{driver} = 5, c_{breed} = 2, $\epsilon_{driver}^{23,in}$ = 10 w%.

For this core, k_{eff} = 0.9876 was found, which is actually even smaller than the value of 0.9881 for the 250 cm core. This means that the gain by using a larger core radius is smaller than the additional neutron losses due to the increased power density in the driver channel, as a consequence of the power change from 25 to 100 MW$_{th}$. A higher power density leads to more parasitic neutron capture due to increased Pa-233 and fission product concentrations. A critical core could not be achieved for this favourable, but quite impractical, choice of parameters. The design of a breeder core under practical operating conditions will certainly require the reprocessing of uranium isotopes from the driver channel as well.

3.2.3. RECYCLING STRATEGY III

The third recycling strategy reprocesses the uranium isotopes from both the breeder and driver pebbles extracted from the system into fresh driver fuel pebbles. Compared with recycling strategy II, a significant reduction of the driver pebble residence time and increase of equilibrium k_{eff} are anticipated because of the addition of the extracted driver fuel in the recycling. It is hoped that this will allow the design of a critical equilibrium core with a more practical core power and pebble residence time.

CORE AND DRIVER CHANNEL RADII

The equilibrium k_{eff} was calculated for core radii of 150, 250, 350 and 450 cm and driver channel radii of 70, 80, 90 and 100 cm, while using a core power of 250 MW$_{th}$. The breeder pebble residence time was 5000 days for the 250 cm core, and varied proportionally to the core volume change for the other core radii. The large value of 5000 days was chosen for a proper comparison with the results obtained with recycling scheme II in table 3.4, where only uranium from the breeder pebbles is reprocessed. Other relevant parameters were H_{core} = 1100 cm, m_{hm}^{driver} = 7.5 g, c_{driver} = 5, c_{breed} = 2, and $\epsilon_{driver}^{23,in}$ = 10 w%. Compared with the results in table 3.4, the total driver pebble residence times were indeed reduced significantly because of the reprocessing of the driver pebbles. Reductions from 535 to 3.6 days (70/250 cm), 733 to 124 days (80/250 cm), 967 to 465 days (90/250 cm) and 1242 to 818 days (100/250 cm) were found, respectively. Especially for the smaller driver channel radii, the reduction in residence time is spectacular, but also unrealistic from a practical perspective.

The k_{eff} values calculated for the different core and driver channel radii are shown in table 3.7, from which it can be seen that it is physically possible to design a critical, and thus net-breeder, 250 MW$_{th}$ thorium PBR if the uranium from both the driver and breeder pebbles extracted from the system is reprocessed into the fresh fuel pebbles. Clearly, a larger core radius helps to increase k_{eff}, especially for smaller cores. Fewer neutrons are lost by leakage, so more are available to breed U-233. For larger cores, the gain in k_{eff} becomes smaller for a further increase in core radius and also the breeder pebble residence time becomes very long, as it was chosen proportional to the core volume change. For a small driver channel radius, the total residence time of the driver pebbles becomes smaller than 100 days, which is not very useful in practice.

Table 3.7: k_{eff} for different core and driver channel radii [cm]

| R_{core} [cm] | 150 | 250 | 350 | 450 |
R_{driver} [cm]				
70	0.9715^a	0.9977^a	1.0020^a	1.0044^a
80	0.9631	1.0203	1.0314^a	1.0348^a
90	0.9495	1.0160	1.0289	1.0324
100	0.9315	1.0091	1.0235	1.0259

a) $\tau_{res,driver}^{total} < 100$ days

The optimal driver channel radius for the 250 cm and larger cores lies around 80 cm, whereas in table 3.4 it was around 100 cm for the 250 cm core, where only the uranium content from the breeder pebbles was reprocessed (recycling scheme II).

The 250 cm core with a driver channel radius of 90 cm has also been studied with a shorter and more practical breeder pebble residence time of 500 days. In that case, $k_{eff} = 1.0259$ was found with a driver pebble residence time of 148 days, compared with 1.0160 and 465 days for the 5000-day breeder pebble residence time. For recycling scheme III, which reprocesses driver and breeder pebbles extracted from the system, it is possible to design a net-breeder thorium pebble bed reactor within a practical operating regime, in terms of power and residence times.

3.3. CONCLUSIONS

A calculation scheme was developed to assess the influence of the core geometry, operational parameters, and fuel management strategy on the breeding capability of a thorium PBR. Three variations of the calculation scheme were applied to model different reprocessing strategies. Feasibility studies, using these three reprocessing strategies, showed that the uranium content from both driver and breeder channel has to be reprocessed to achieve breeding (recycling scheme III). If done so, it seems possible to achieve breeding inside a thorium PBR for practical operating conditions.

The next chapter will investigate whether breeding can also be achieved in a practical operating regime when the spectral influence of the surrounding zones (driver, breeder and reflector) is included in the fuel depletion calculations, as well as a realistic steady-state temperature profile of the core. Furthermore, the passive safety features of potential breeder core designs will be evaluated.

3

REFERENCES

[1] H. J. Rütten, K. A. Haas, and C. Pohl, *Computer Code System V.S.O.P. (99/11): Update 2011 of V.S.O.P(99)-Version 2009 CODE MANUAL*, Forschungszentrum Jülich (2012).

[2] J. Oppe, J. B. M. D. Haas, and J. C. Kuijper, *PANTHERMIX (PANTHER-THERMIX) User Manual*, ECN Petten (1998).

[3] M. Grimod, R. Sanchez, and F. Damian, *Neutronic modeling for pebble bed reactors*, in *Proceedings of the M&C 2009 conference* (Saragota Springs, New York, 2009).

[4] M. Grimod, *Neutronic Modeling of Pebble Bed Reactors in APOLLO2*, Ph.D. thesis, L'universite Paris-Sud 11 (2010).

[5] H. P. Liem, *BATAN-MPASS: A general fuel management code for pebble-bed high temperature reactors*, Annals of Nuclear Energy **21**, 281–290 (1994).

[6] W. K. Terry, H. D. Gougar, and A. M. Ougouag, *Direct deterministic method for neutronics analysis and computation of asymptotic burnup distribution in a recirculating pebble-bed reactor*, Annals of Nuclear Energy **29**, 1345–1364 (2002).

[7] H. D. Gougar, *Advanced Core Design and Fuel Management for Pebble-Bed Reactors*, Ph.D. thesis, The Pennsylvania State University (2004).

[8] H. D. Gougar, A. M. Ougouag, W. K. Terry, and K. N. Ivanov, *Automated design and optimization of pebble-bed reactor cores*, Nuclear Science and Engineering **165**, 245–269 (2010).

[9] B. Boer, *Optimized Core Design and Fuel Management of a Pebble-Bed Type Nuclear Reactor*, Ph.D. thesis, Delft University of Technology (2008).

[10] B. Boer, J. L. Kloosterman, D. Lathouwers, and T. H. J. J. van der Hagen, *In-core fuel management optimization of pebble-bed reactors*, Annals of Nuclear Energy **36**, 1049–1058 (2009).

[11] M. Fratoni and E. Greenspan, *Determination of the equilibrium composition of cores with continuous fuel feed and removal using MOCUP*, in *Joint international topical meeting on Mathematics & Computation and Supercomputing in Nuclear Applications* (Montery, California, 2007).

[12] M. Fratoni and E. Greenspan, *Equilibrium core composition search methodologies for pebble bed reactors*, Nuclear Science and Engineering **166**, 1–16 (2010).

[13] B. Boer, D. Lathouwers, J. L. Kloosterman, T. H. J. J. van der Hagen, and G. Strydom, *Validation of the DALTON-THERMIX code system with transient analyses of the HTR-10 and application to the PBMR*, Nuclear Technology **170**, 306–321 (2010).

[14] Radiation Safety Information Computational Center, Oak Ridge National Laboratory, *"SCALE: A Modular Code System for Performing Standardized Computer Analyses for Licensing Evaluations"*, Vols. I-III, Version 6, CCC-750; ORNL/TM-2005/39 (2009).

[15] E. E. Bende, A. H. Hogenbirk, J. L. Kloosterman, and H. van Dam, *Analytical calculation of the average Dancoff factor for a fuel kernel in a pebble bed high-temperature reactor,* Nuclear Science and Engineering **133**, 147–162 (1999).

[16] L. Massimo, *Physics of high-temperature reactors* (Pergamom Press, 1976).

[17] Z. Zhang, Z. Wu, D. Wang, Y. Xu, Y. Sun, F. Li, and Y. Dong, *Current status and technical description of Chinese 2 x 250 MW$_{th}$ HTR-PM demonstration plant,* Nuclear Engineering and Design **239**, 1212–1219 (2009).

[18] Y. Zheng and L. Shi, *Characteristics of the 250MW Pebble-Bed Modular High Temperature Gas-Cooled Reactor in Depressurized Loss of Coolant Accidents,* in *High Temperature Reactor Conference 2008* (Washington, DC USA, 2008) HTR2008-58299.

3

4

COUPLED DESIGN STUDIES OF A PASSIVELY SAFE THORIUM BREEDER PBR

This chapter investigates whether it is possible to combine passive safety and breeding, within a practical operating regime, inside a thorium Pebble Bed Reactor. Therefore, the influence of several fuel design, core design and operational parameters upon the conversion ratio and passive safety is evaluated. Depressurized Loss of Forced Cooling (DLOFC) transients, with and without scram, are evaluated with a coupled DALTON/THERMIX code scheme.

High conversion ratios (CR > 0.96) and passive safety can be combined in a thorium PBR within a practical operating regime, in terms of thermal power, residence times and pebble handling speed. With an increased U-233 content of the fresh driver pebbles (18 w%), breeding (CR=1.0135) can already be achieved for a 220 cm core and 80 cm driver zone radius. While the decay heat removal is sufficient in this design, the temperature feedback of the undermoderated driver pebbles is too weak to compensate the reactivity insertion due to the xenon decay during a DLOFC without scram.

With a lower U-233 content per driver pebble (10 w%), breeding (CR=1.0036) and passive safety can be combined for a 300 cm core and 100 cm driver zone radius, but this requires a doubling of the pebble handling speed and a high fuel pebble reprocessing rate. The maximum fuel temperature during a DLOFC without scram was simulated to be 1481 °C for this design, still quite a bit below the TRISO failure temperature of 1600 °C. The maximum reactivity insertion due to water ingress is also limited (+1497 pcm).

T HE aim of this chapter is to investigate if both passive safety and breeding can be achieved, within a practical operating regime, within a thorium Pebble Bed Reactor. Neutronic studies of the fuel design and the equilibrium core design were performed for the previous chapters 2 and 3. The results indicated that reprocessing will be required to achieve breeding in a thorium PBR. So, an underlying assumption in the following chapters is that the U-233 content in the discharged pebbles can be reprocessed at a sufficient rate. Not so long ago, this reprocessing assumption might have been rather unrealistic due to the difficulties with mechanical separation methods for coated particle fuels [1], but Fütterer et al. [2] recently made very promising progress in fragmenting coated particle fuels. Using high voltage discharges inside a water vessel, the contents of the fuel kernels can be separated with little energy consumption.

In this chapter, an important addition is made to the original calculation scheme from chapter 3 by including the spectral influence of surrounding zones (driver, breeder and reflector) into the fuel depletion calculations. This was found to have a significant impact on the conversion ratio. With this improved calculation scheme, it will be investigated for which fuel, core and operational parameters breeding might be achieved within a safe and practical operating regime. This practical operating regime is characterized by a thermal power of 100 MW or higher for economical reasons, 1000 days total residence time of the breeder pebbles to limit the length of the running-in phase and a fuel pebble handling time longer than 14.5 s, like in the High Temperature Reactor-Pebble-bed Module (HTR-PM), to prevent engineering issues with the fuel handling system.

One of the key safety aspects of a thorium breeder core design is the reactor behavior during a Depressurized Loss of Forced Cooling (DLOFC) transient. Due to the depressurization, conduction and radiation become the main heat transfer mechanisms for decay heat removal, while the contribution from (natural) convection is almost negligible. Due to the very limited heat transfer from the fuel to the surroundings the fuel will initially heat up significantly until the decay power equals the amount of heat transferred to the Reactor Heat Removal System (RHRS), located on the outer side of an airgap surrounding the reactor pressure vessel [3]. The maximum fuel temperature should remain below 1600 °C to ensure all the radioactive fission products are retained within the fuel's tristructural-isotropic (TRISO) coating layers [4].

Both the DLOFC with scram, which is solely a heat transfer problem, and without scram, involving fully coupled neutronics and thermal hydraulics, will be investigated. For the different breeder designs, it has to be demonstrated if the maximum fuel temperature can remain below the TRISO limit temperature of 1600 °C purely by passive means or not. So, also in the worst case scenario where control rods will not drop automatically for whatever reason. During the transient, an initial build-up of the concentration of Xe-135, a strong neutron absorber, is followed by a strong decrease, leading to a significant reactivity insertion into the core. Thus, besides the decay heat removal capacity, also the core's response to recriticality due to the reduced xenon concentration must ensure fuel temperatures below 1600 °C.

In thorium PBRs, an additional reactivity insertion may originate from the decay of Pa-233 into U-233. However, this only becomes a significant effect in the very long run, as the half-life of Pa-233 is nearly 27 days, as compared to 9.14 hours for Xe-135. So, this effect has not been considered in the transients in the present chapter.

To perform the analysis of the transient behaviour of the thorium PBR, a coupled code scheme involving the SCALE6 code package [5] for cross section generation, the DALTON neutron diffusion solver [6] and the THERMIX thermal hydraulics code [7] for pebble bed reactors, is used. The updated conversion ratio calculation scheme of the thorium PBR core configurations is discussed in section 4.1. The coupled code scheme and the modelling approach for the transients will be introduced in section 4.2. The conversion ratio is investigated for different core, fuel and operational parameters in section 4.3, as well as the response of the relevant core designs to the DLOFC transients with and without scram. Based on these results, possible design choices for a passively safe and/or breeder thorium PBR within a practical operating regime are discussed in section 4.4, also with regard to the maximum possible reactivity increase due to water ingress.

4.1. UPDATED EQUILIBRIUM CORE CALCULATION SCHEME

I$_N$ chapter 3, the neutronic design of a thorium breeder PBR was investigated for a cylindrical core consisting of an outer breeder zone and a central driver zone. Figure 3.3 gives a schematic view of the reactor geometry used for the neutronic studies. Pebbles with 30 g thorium (in the form of ThO$_2$) are inserted in the breeder zone, while driver pebbles with 10 w% (or more) U-233 and a much lower heavy metal loading, for improved moderation, are inserted into the driver zone. Besides the U-233, the driver pebble fuel kernels mainly consist of thorium with traces of the other uranium isotopes, according to their ratios in the combined outflow of the driver and breeder zone. An overview of other pebble parameters used throughout the previous and the current studies was given in tables 2.1 and 2.2.

The equilibrium core calculation scheme uses the CSAS and XSDRN modules from the SCALE6 code package for neutron cross section generation, COUPLE and ORIGEN (also SCALE6) for fuel depletion, and the DALTON code to perform 2D(R,Z) neutron diffusion calculations of the core. During the first iteration, an initial flux guess is used for the depletion calculations of the breeder and driver pebbles while they move downwards, in 11 steps of one meter, in the core. First, cross sections are generated for a fresh fuel pebble at the top position (11 m), followed by a depletion calculation using the time period taken by the pebble to descend one meter to obtain nuclide concentrations for the fuel at a height of 10 m. This is repeated until the pebble reaches the bottom of the core. After this, a pebble is either re-inserted into the core or extracted for reprocessing. The flux used in the depletion calculation is volume-averaged in the radial direction for the breeder and driver zone, obtaining a single radial nuclide concentration for the breeder and the driver zone at each pebble passage and height. The use of multiple radial depletion zones for driver and breeder, would have added many different refueling possibilities to a core design problem already involving many variables in the present conceptual design stage. Furthermore, the use of a single radial depletion zone for driver and breeder only has a limited impact upon the conversion ratio and leads to conservative results in terms of maximum power density and fuel pebble handling speed. This is demonstrated in section 4.4.5 by also analysing the three most promising core designs of this chapter with an extended model with eight radial depletion zones.

Using the updated set of nuclide concentrations and cross sections obtained for the driver and breeder zone over the height of the core, the flux profile can be updated by

DALTON. This sequence of fuel depletion calculations, for the different pebble passes and heights in the two channels, and a core calculation is repeated until convergence of the flux and k_{eff} is achieved. An outer-iterative loop adjusts the residence time of the driver pebbles to obtain a critical core configuration, while the breeder pebble residence time remains fixed. A detailed description of the equilibrium core calculation scheme is given in chapter 3.

One important modification was made to the original equilibrium core calculation scheme in chapter 3 with respect to the neutron spectrum used in the fuel depletion calculation. The influence of the surrounding zones (driver, breeder and reflector) upon the fuel depletion in the driver or breeder zone is now also taken into account by using the spectra calculated during the previous core iteration by 1D radial slab calculations for the different core heights. As there is no direct way to include these spectra in SCALE6.0, they are introduced into COUPLE and ORIGEN by overwriting the MT=1099 card, which contains the neutron spectrum of the nuclides included in the AMPX-library. Figure 4.1 gives a schematic view of the updated cross section and depletion spectrum generation scheme.
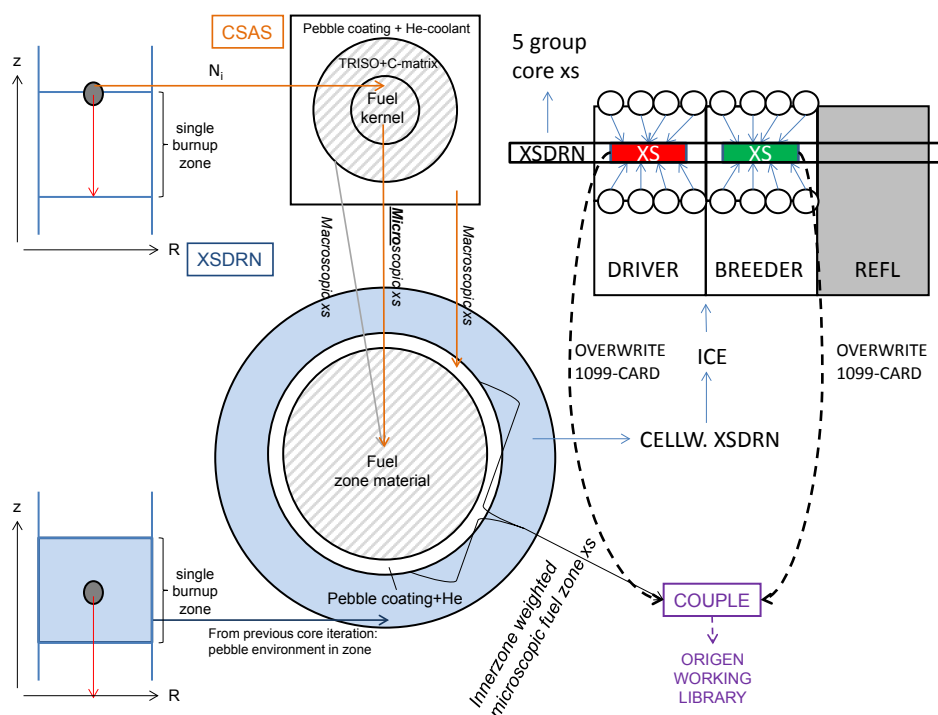
Figure 4.1: Schematic view of the updated cross section generation method (the diagrams are not to scale)

Including the spectral influence of the surrounding zones (driver, breeder or reflector) has a significant negative impact on the conversion ratio (12% for one specific case). Especially in the breeder zone, the conversion rate of thorium into U-233 was exaggerated due to the combination of the thermal flux normalization convention used by ORIGEN and the spectrum mismatch between the whole core DALTON-calculation and the fuel depletion

spectra.

Another relevant modification to the scheme was made with respect to the fuel recycling scheme. The strict coupling between the fuel discharge rate from the core and the driver pebble residence time, as in recycling scheme III of chapter 3, is abandoned. Instead, the driver pebble residence time is adjusted (for a given breeder pebble residence time) until a critical core is found. A major advantage of this approach is that a physically realizable state of the reactor is always achieved. In this case, the aim is not to achieve k_{eff} larger than unity, but to find a negative mass balance for U-233 (and Pa-233), so that more U-233 (including Pa-233) is discharged from the system than inserted. A schematic comparison between recycling scheme III and the new mass balance approach, denoted as scheme IV, is made in figure 4.2.
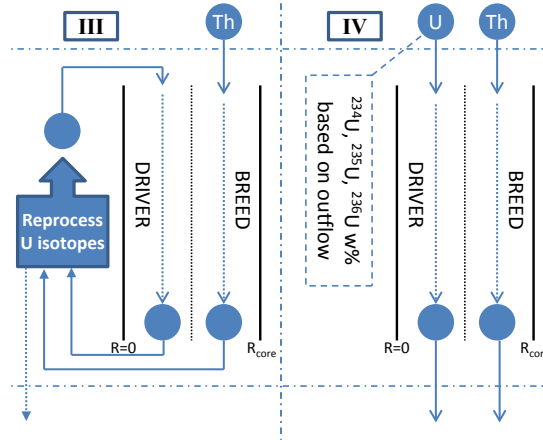
Figure 4.2: Comparison between recycling scheme III from chapter 3 and the new mass balance approach (scheme IV) used in this chapter. Both schemes assume reprocessing of the uranium contents from the extracted driver and breeder pebbles after their final passage. The breeding capability is determined from the mass balance of a critical core in scheme IV, instead of evaluating k_{eff} for a zero net mass balance of U-233 (and Pa-233) in scheme III.

After the calculation scheme converges and a critical core configuration is achieved, the code calculates the U-233 mass balance of the system, being the feed rate of U-233 ($\dot{m}_{U3,in}$) minus the extraction rate of U-233 ($\dot{m}_{U3,out}$) and Pa-233 ($\dot{m}_{Pa3,out}$). Core configurations with a negative overall mass balance of U-233 plus Pa-233 are considered being a breeder reactor, assuming the uranium contents of the driver and breeder pebbles extracted from the core are fully reprocessed. The composition of the driver fuel, or more specifically the ratio between the concentrations of the other uranium isotopes and U-233, is determined by their ratio in the combined outflow of the driver and the breeder zone.

The conversion ratio (CR) is defined by Duderstadt and Hamilton [8] as the average rate of fissile atom production divided by the average rate of fissile atom consumption. For the results presented in this chapter, a more practical approximate definition is used for the conversion ratio, since the absorption rate in the fissile atoms is not tracked separately in the code scheme.

$$CR \approx 1 + \frac{\dot{m}_{U3,out} + \dot{m}_{Pa3,out} - \dot{m}_{U3,in}}{\dot{m}_{U,fission}}. \tag{4.1}$$

The absorption-to-fission ratio for thermal neutrons in U-233 is approximately 1.0876 [9]. So, dividing by the fission rate instead of the fissile consumption rate leads to a slight over-prediction of conversion ratios above unity and a slight underprediction of conversion ratios below unity, while the definition is exact for a conversion ratio of 1. The main interest from a core design perspective is to know whether the CR is above unity or not. In the latter case, a value close to unity would be desirable.

4.2. Coupled DALTON/THERMIX code scheme

A code scheme coupling neutronics and thermal hydraulics was used for the analysis of the DLOFC transients in this chapter. The SCALE6 code package is used for the generation of the neutron cross sections libraries, the in-house developed diffusion solver DALTON to describe the core neutronics, and the THERMIX code is used for the thermal hydraulics calculation. A similar geometrical model as used by Zheng et al. [3] and Zheng and Shi [10] for the HTR-PM was used to model the thermal hydraulics of the thorium breeder Pebble Bed Reactor within THERMIX.

4.2.1. Temperature dependent cross section library
The nuclide concentrations used in the determination of the temperature dependent cross section library are obtained using the previously described equilibrium core calculation scheme. A steady-state THERMIX run is included in each core iteration, so the influence of the temperature feedback upon the fuel depletion is properly included in the nuclide concentrations, though this hardly affects the breeding potential of the thorium PBR.

The first step to perform coupled neutronics and thermal hydraulics calculations is the generation of a cross section library for the pebble bed reactor depending on fuel, moderator and reflector temperatures. Cross sections in these libraries are condensed to five energy groups using 1D XSDRN calculations over representative radial slabs of the core at eleven different core heights. These radial slabs consist of a driver zone, breeder zone and the various side reflector and surrounding regions depicted in figure 3.3. A buckling correction is applied to approximate axial leakage. Cross sections for the top and bottom reflectors are condensed using an axial XSDRN calculation. This process is performed in a similar way as in the equilibrium core calculation scheme, described in chapter 3. In total 25 cross section libraries are generated for 5 different fuel and 5 different moderator+reflector temperatures, and merged into a single library. The temperatures used are 300 K, 700 K, 1100 K, 1500 K and 1900 K.

Using the ICE module of SCALE6, cross sections are mixed using interpolation on the basis of the actual fuel and moderator temperature (so using 4 interpolation coefficients) or the reflector temperature for each core region included in the neutron diffusion calculation. If a value above 1900 K occurs, the cross section at the limit temperature of 1900 K is used. Note that this value is above the TRISO safety limit temperature of 1600 °C.

When the steady-state temperature distribution of the core, $T(r, z)$, is known, uniform reactivity coefficients of the core can be calculated based on these temperature dependent

libraries according to

$$\alpha_{uniform} = \frac{\rho(T(r,z) + \Delta T) - \rho(T(r,z))}{\Delta T}. \tag{4.2}$$

In the results section, the uniform reactivity coefficients are evaluated for a temperature increase, ΔT, of 500 °C.

During the generation of the cross section library, the microscopic xenon cross sections are also generated for the different positions in the core, which can be used to include the xenon effect into the cross sections during a transient, as explained in appendix A.

4.2.2. STEADY-STATE COUPLED CALCULATION

The following approach is used to acquire the steady-state temperature distribution of a pebble bed reactor. An initial guess is used for the temperature (for instance a uniform 1100 K) and a cross section set for this temperature is used by the neutron diffusion solver DALTON, which calculates k_{eff}, the flux and power density distribution over the core. The power density is handed over to THERMIX, which calculates the updated steady-state temperature profile, and from this a new cross section library is interpolated from the temperature dependent library. This process can be repeated until convergence is reached.

However, there is one complicating factor in the case of the two-zone thorium breeder PBR: Only the coolant flowing through the driver zone heats up significantly, but the largest fraction of the coolant flows through the breeder zone. So, the coolant flows extracted from the driver zone and the breeder zone have to be separated in the design. The hot helium flowing out of the driver zone is led to the steam generator (or turbine), while the slightly heated helium from the breeder zone is mixed with the cold helium (250 °C) to preheat it before entering the core. A schematic view of the helium coolant flow scheme inside the thorium breeder PBR is shown in figure 4.3. Note that in reality, as well as in the THERMIX model, there is just one helium flow from top to bottom through the whole core (so breeder and driver zone combined). For this reason, on average, a fraction of the flow is forced to move from the driver zone into the breeder zone due to the expansion of the hotter helium in the driver zone. Similar to the work of Zheng et al. [3], the THERMIX model also includes bypass flows through the control rod channels, which account for roughly 1% of the total mass flow, and a leakage flow of 4% to 5% to simulate the flow through the gaps between the graphite components. These bypass flows are not shown in figure 4.3.

Such a complex scheme, i.e. the mixing of the preheated helium of the breeder zone outlet with the cold helium of 250 °C is not easy to model directly in the THERMIX code. Therefore, the inlet temperature of the THERMIX calculation, $T_{in,core}$, is adjusted. It is also difficult to model two outlet regions in THERMIX, so one for the driver and one for the breeder zone, because this is only possible if the user prescribes the mass flows at both the outflow regions, but in reality these are unknown a-priori. So, the helium flows exiting the driver and breeder zones only remain separated up to a final single outflow zone where they are mixed. The advantage of this approach is that the helium mass flow is distributed over the driver zone and breeder zone in a natural way, since only the total core helium outflow is prescribed by the user. The mass flow and temperature of the breeder and driver zone outflow are read from the THERMIX output by choosing the appropriate cells, just before the streams are mixed in the final outflow zone.

4
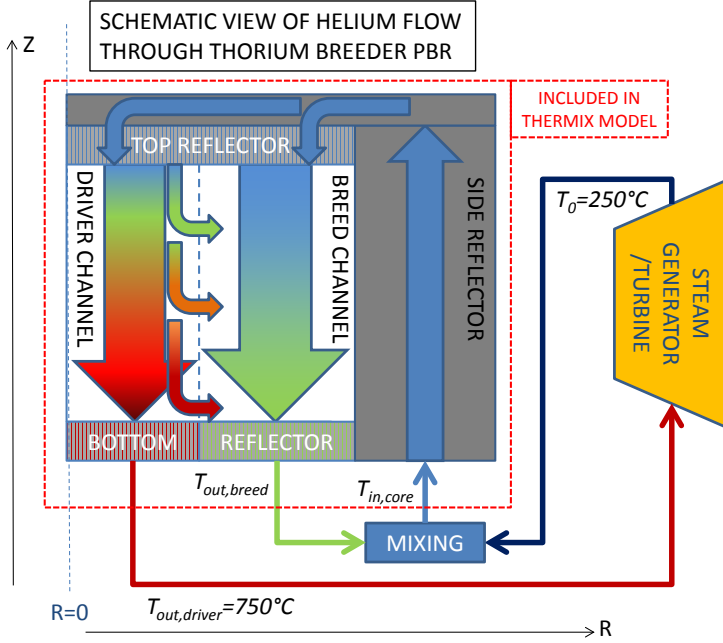
Figure 4.3: Schematic view of the helium coolant flow scheme in the Thorium Breeder PBR

With the outer system temperature, T_0, fixed at 250 °C, as with the regular HTR-PM, and the mass flows over the driver zone, $\dot{m}_{driver}$, and the breeder zone, $\dot{m}_{breed}$, obtained from the THERMIX output, the new inlet temperature $T_{in,core}$ follows from a simple balance

$$T_{in,core} = \frac{\dot{m}_{driver}T_0 + \dot{m}_{breed}T_{out,breed}}{\dot{m}_{total}}. \tag{4.3}$$

The total mass flow entering the core, $\dot{m}_{total}$, is the sum of $\dot{m}_{breed}$ and $\dot{m}_{driver}$. To ensure the (driver zone) outlet temperature remains at 750 °C, the total mass flow of the coolant is increased (or decreased) iteratively in the numerical scheme.

A higher mass flow rate requires an increase of the pumping power which decreases the efficiency of the reactor. According to chapter 3 from Melese and Katz [11], the pumping power increases linearly with the mass flow rate for a fixed pressure drop, e.g. if the mass flow rate increases proportionally to the pebble bed volume with increasing core diameter. But Melese and Katz [11] also show that the pressure drop depends quadratically on the ratio between the mass flow rate and the flow surface area. So, any increase of the mass flow rate above proportional to the flow surface area increase, increases the required pumping power with the third power of the mass flow rate. An increase of the system pressure can help to reduce the required pumping power, as it varies inversely quadratically with the system pressure [11]. However, the pumping power decrease comes at the price of an increase in construction costs of the reactor.

In the iterative steady-state scheme, the core inlet temperature of THERMIX and the mass flow are adjusted in an iterative inner loop until convergence of the core inlet and outlet temperature is reached. The cross section and power profile are updated until convergence of k_{eff} and the power profile in an outer iterative loop.

The method described above has also been implemented into the equilibrium core calculation scheme. However, in that case only a single volume-averaged temperature (and concentration) is used in the radial direction for the driver zone and a single volume-averaged temperature for the breeder zone. During the interpolation from the temperature dependent libraries, which will also be used during the coupled transient calculations, different temperatures are used for each radial grid zone. For the initial core configuration, this leads to a slight deviation from the original k_{eff} of $1(\pm0.0002)$ obtained with the core depletion scheme. To ensure the system is really in a steady-state at the start of the time-dependent calculation, a small correction is applied twice (to eliminate second order effects) to the fission cross section, $\Sigma_f = \Sigma_f/k_{eff}$, to force k_{eff} to be 1.

4

4.2.3. TRANSIENTS

The DLOFC transients modelled in this chapter assume that the reactor depressurizes instantaneously from 70 bar to 1 bar between 0 and 0.1 s, which is a conservative estimate for the heat transfer [10]. Due to the depressurization, conduction and radiation are the dominant mechanisms to transfer the decay heat from the fuel to the reactor pressure vessel and the water cooling panel, while heat transfer due to natural convection is almost negligible. Due to the very small heat transfer from the fuel to the surroundings, the fuel will initially heat up until the decay power becomes smaller than the heat transfer to the Reactor Heat Removal System (RHRS), which consists of a water cooling panel kept at a constant temperature of 70 °C. The maximum fuel temperature should remain below 1600 °C to ensure all the radioactive fission products remain contained within the fuel's TRISO coating layers.

DLOFC WITH SCRAM

In a DLOFC with scram, it is assumed that the fission power is reduced instantaneously due to the scram, so all the heat produced in the core originates from the decay heat. The decay heat profile of U-235, according to the 23 exponents of the ANS decay heat standard from 1993 [12], is used throughout the transients in the present chapter, as U-233 is not included in the ANS decay heat standard. Better decay heat data for U-233 would be desirable to improve the modelling of transients in U-233 fueled reactors.

Alternatively, the evolution of the decay heat fraction over time can roughly be described by the Way-Wigner equation [13], which is the standard method in older versions of the THERMIX code [7]. The Way-Wigner equation describes the decay heat fraction as a function of time by

$$\eta = 0.0622(t^{-0.2} - (t_0 + t)^{-0.2}), \tag{4.4}$$

where t is time elapsed after the start of the transient in seconds and t_0 is the time the fuel has been irradiated at nominal power in seconds. The Way-Wigner approximation somewhat underpredicts the decay heat fraction during the initial stage of the transient,

but gives a very similar decay heat fraction later on in the transient. Assuming the pebbles were irradiated for 365 days at the nominal operating power, the decay heat curves of the ANS-1993 standard and the Way-Wigner approximation are both plotted in figure 4.4 ranging from 1 s to 100 h.
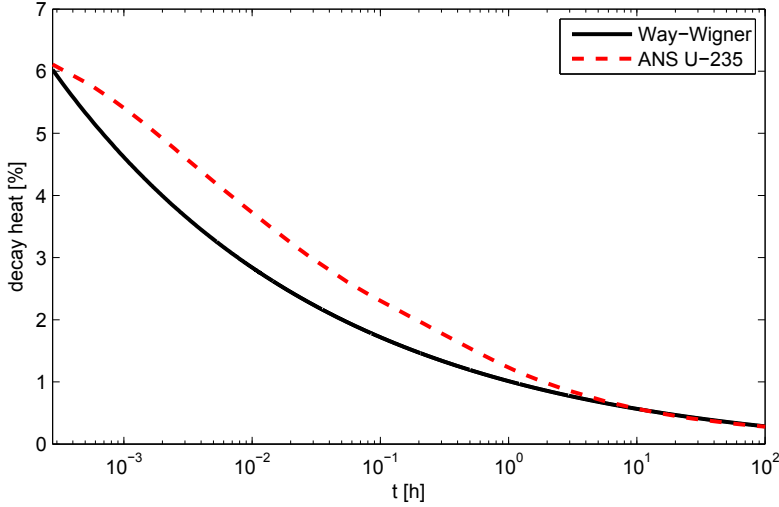
Figure 4.4: Decay heat as a function of time using the Way-Wigner approximation [13] of equation 4.4 [t_0=365 days] and using the ANS decay heat standard for U-235 [12].

DLOFC without scram

Without scram, the power in the reactor will slowly decrease due to the negative temperature feedback as the fuel temperature increases after the DLOFC. During this period, the heat generated in the fuel is the sum of the actual fission power and the decay heat generated in the fuel. In the calculation scheme, the actual heat generated in the fuel is approximated by adding up the actual fission power $P_{fission}$, calculated by DALTON, and the decay heat fraction at time t after the start of the transient times the difference between the nominal operating power P_0 and the actual fission power $P_{fission}$,

$$P_{total}(t) = P_{fission}(t) + \eta(t)\left(P_0 - P_{fission}(t)\right). \qquad (4.5)$$

For a correct understanding of this definition, one should be aware that the steady-state fission power calculated by DALTON contains contributions from both the prompt fission power and a delayed heat release, which one refers to as the decay heat after the start of the transient.

Using the decay heat fraction starting from $t = 0$ for all the decay heat generated may lead to some inaccuracy during the initial minutes of the transient, but the effect is negligible for the peak fuel temperatures, which occur after many hours in the transient. It does not matter that much anymore for the decay heat fraction $\eta(t)$ whether t is 10 hours or 10 hours and a few minutes.

During the first period of the transient, the calculation is run in a fully coupled mode, so THERMIX frequently exchanges the updated fuel temperatures with SCALE and DALTON to update cross sections and the power profile. At the moment the ratio of the fission power over the decay heat power becomes smaller than 0.1 the calculation switches over to a loosely coupled mode and the time step size is increased. A threshold of 0.1 ensures no computational time is wasted, because the contribution of fission to the core temperature increase becomes marginal (≈ 0.1 °C) after reaching the threshold. In the loosely coupled mode THERMIX is run solely using the decay heat power obtained by the ANS-1993 Standard, DALTON is now run in static mode to calculate k_{eff}.

The xenon concentration, i.e. Xe-135, will initially increase during the transient to give a negative reactivity contribution and later on decrease and give a positive reactivity contribution. The method to include the xenon effect into the calculation scheme is explained in appendix A. At a certain moment, the decrease of the xenon concentration results in re-criticality of the core. In the loosely coupled mode, the time step size is reduced as k_{eff} approaches unity. The calculation switches to dynamic (so fully coupled) mode again when k_{eff} becomes unity, and the fission power restarts at a value of 100 W. 100 W is still a very small fraction of the total heat production, but also ensures no computation time is wasted for very small fission powers. DALTON and THERMIX exchange power and temperature profile every 20 s, this is increased up to 80 s if the change in fission power becomes very small during a time step. A schematic view of the time-dependent DALTON/THERMIX coupling scheme is shown in figure 4.5.
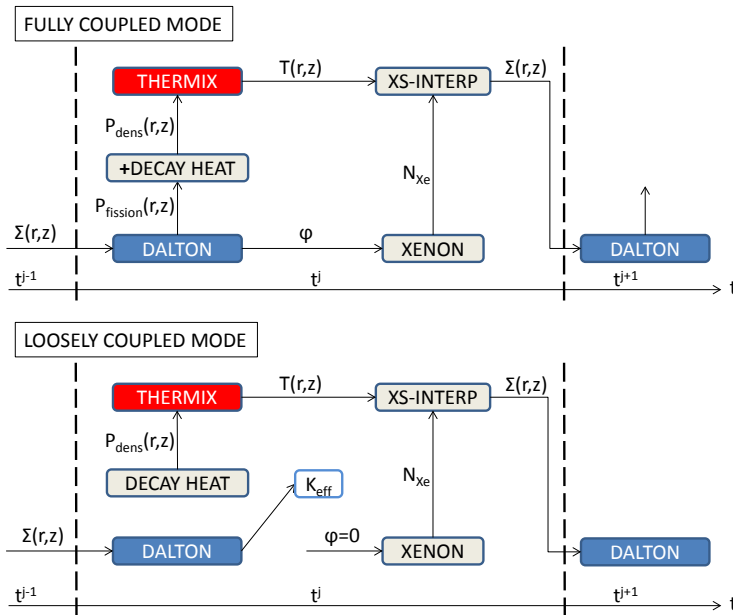

Figure 4.5: Schematic view of the coupled DALTON/THERMIX code scheme during fully coupled and loosely coupled run

4.3. Core parameter studies

MANY parameters that influence the conversion ratio of a thorium PBR might be varied in the core design. The main parameters are the heavy metal loading of the driver and the breeder pebbles, the U-233 weight fraction of the driver fuel, the radius of the core and the driver zone, the residence time of the breeder pebbles, reactor power and the number of passes a pebble makes through the driver and the breeder zone.

In view of the calculation time of a single equilibrium core simulation, it is certainly not possible to study all possible parameter combinations. The number of options can be narrowed down significantly by taking into account practical constraints and by excluding parameter choices with a certain negative impact on safety, such as a very high reactor power. Furthermore, the results obtained in chapter 3 did not include the spectral influence of the surrounding zones (driver, breeder, reflector), but many of the trends observed still provide a useful starting point in order to achieve a core configuration with a high conversion ratio. Finally, design variations are mostly investigated for one parameter at a time to limit the number of core calculations.

4.3.1. U-233 weight fraction of driver fuel

Ideally, the combination of the U-233 weight fraction of the driver fuel and the heavy metal loading per driver pebble are chosen around the optimal moderator-to-fuel ratio of the core, so ensuring the highest fission over absorption ratio in the driver zone. A U-233 weight fraction of 12% is used for the driver fuel as a starting point for this section. A lower weight fraction would result in difficulties reaching criticality with a small driver zone radius. A small driver zone ensures a high fraction of neutrons leak into the breeder zone which enhances conversion. A higher U-233 weight fraction of the driver fuel, with the same metal loading, may be desirable to reduce the pebble handling speed for the core and/or allow for a smaller driver zone radius, which could improve the conversion ratio. This option will be investigated later on. On the downside, a higher U-233 weight fraction may present problems in terms of passive safety, as reactivity coefficients become less negative and the reactivity increase due to water ingress becomes stronger as the core becomes undermoderated.

4.3.2. Heavy metal loading

The breeder pebbles are filled with 30 g thorium, a conservative estimate of the maximum possible loading from a fuel fabrication perspective [14]. Each breeder pebble makes two passes through the core in the calculations in the present chapter. Adding more passes does not significantly improve the conversion ratio, but might put a very high demand on the fuel handling system.

For the driver pebbles, a 3 g HM loading is used in the following sections. This is bit above the optimal moderator-to-fuel ratio, as shown in figure 2.1, if a U-233 weight fraction of 12% is used, but low enough to ensure that water ingress cannot lead to a large reactivity insertion (see section 4.4.3). The reactivity coefficients are also more negative for lower driver pebble heavy metal loadings [15], which improves the safety of the core during a DLOFC without scram.

4.3.3. Reactor power

A minimum constraint of 100 MW is used for the thermal power of the reactor. Lower values are undesirable from an economical perspective and it will also take a very long time to achieve the equilibrium core configuration as the irradiation of the breeder pebbles becomes very slow. A maximum of 250 MW is used for the thermal power, similar to the HTR-PM. As the core radius of a high-conversion thorium PBR is generally much larger than for the HTR-PM, decay heat removal is probably insufficient for a higher power, so fuel temperatures are likely to exceed 1600 °C in that case.

The influence of the reactor power on the conversion ratio, calculated by equation 4.1, was determined for a typical thorium PBR of 300 cm radius with a 100 cm driver zone radius. A breeder pebble residence time of 2000 days was used, which is rather high from a practical perspective, but it ensures sufficient irradiation of the breeder pebbles. Shorter and more practical residence times of the breeder pebbles will also be investigated later on.

Table 4.1: Overview of conversion ratio, fuel management and safety parameters for different reactor powers ($\tau_{res,tot}^{breed}$ = 2000 [d], $\epsilon_{driver}^{U-233,in}$ = 12 [w%], R_{core} = 300 [cm], R_{driver} = 100 [cm], 15 driver pebble passes and 2 breeder pebble passes)

Case	I	II	III	IV
Thermal power [MW]	100	150	200	250
Conversion ratio	0.9913	0.9915	0.9914	0.9932
$\tau_{res,tot}^{driver}$ [d]	323	229	183	157
$P_{density}^{max}$ [MW/m^3]	6.2	8.6	10.6	12.4
Pebble handling time [s]	8.5	6.3	5.1	4.5
Reprocessing rate [p/day]	1322	1560	1766	1935
Max. burnup [MWd/t_{hm}]	52966	54020	55223	57025
$T_{scram}^{max,DLOFC}$ [°C]	1240	1448	1623	1789
$\alpha_{uniform}^{+500K}$ [pcm/K]	-3.52	-3.38	-3.28	-3.14

The results in table 4.1 indicate that the conversion ratio does not vary a lot with reactor power. For 100 MW$_{th}$, 150 MW$_{th}$ and 200 MW$_{th}$ the CR is almost equal, and close to 1. It increases a bit at a power of 250 MW$_{th}$ because a larger fraction of the power is produced in the breeder zone and this enhances conversion more than the decrease caused by additional neutron capture due to the higher Pa-233 concentrations. This also indicates that the optimal breeder pebble residence time for this configuration would even be larger than 2000 days. A breeder pebble residence time of 5000 days (P=100 MW$_{th}$) would increase the conversion ratio up to 1.0011, but this is impractical considering the typical lifetime of a reactor.

As could be expected, the driver pebble recycling speed and pebble reprocessing rate also increase with increasing reactor power. The maximum fuel temperatures during a DLOFC with scram, shown in table 4.1, indicate that decay heat removal is a problem for reactor powers of 200 MW$_{th}$ and larger, since fuel temperatures exceed the TRISO limit temperature of 1600 °C. From a decay heat removal perspective, it would be wise to limit the core power to 150 MW$_{th}$ for a core configuration with a 300 cm core radius.

The maximum fuel temperature during a DLOFC with and without scram is shown in figure 4.6 for reactor powers of 100 MW$_{th}$ and 150 MW$_{th}$. For the transients with scram,

the maximum fuel temperature increases rapidly during the initial stage of the transient and reaches its maximum after 47 h (100 MW$_{th}$) or 48 h (150 MW$_{th}$). It slowly decreases afterwards as the decay heat production becomes smaller.
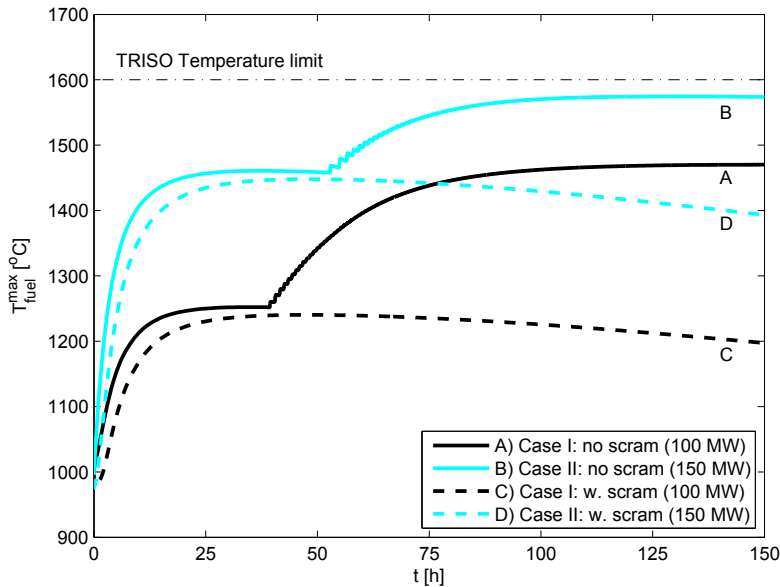
4

Figure 4.6: Maximum fuel temperature over time during a DLOFC with and without scram for reactor powers of 100 MW$_{th}$ and 150 MW$_{th}$ in a 300 cm core with a 100 cm driver zone radius

For the transients without scram, the interruption of the coolant flow and depressurization of the core, heat up (the largest part of) the core and the core becomes subcritical leading to a slow decrease of the fission power. The power production in the core is mainly due to decay heat after a few minutes, which leads to a further increase of the maximum fuel temperature in the core. The additional fission power during the first minutes causes a slightly stronger temperature increase during the initial stage of the transient without scram.

After 39 h (100 MW$_{th}$) or 53 h (150 MW$_{th}$) recriticality occurs as the positive reactivity effect of the reduced Xe-135 concentrations becomes equal to the negative reactivity effect of the temperature feedback. After the recriticality, the fission power and temperature increase rapidly, making the core subcritical till the core cools down again or a sufficient amount of xenon has decayed again to induce another fission power increase.

The maximum fuel temperatures, 1470 °C (100 MW$_{th}$) and 1575 °C (150 MW$_{th}$), during the transient without scram are significantly higher than for the case with scram. This is generally not the case for modular pebble bed reactors fueled with U-235/U-238, since these reactors have stronger temperature reactivity coefficients than a thorium fueled pebble bed reactor.

The difference in maximum fuel temperature due to a power increase from 100 MW$_{th}$ to 150 MW$_{th}$ is a lot smaller in the transient without scram, as it has reduced from 228 °C

(curve D vs C in Fig 4.6) to 105 °C (curve B vs A). This is because the decay heat production scales linearly with the nominal power of the reactor. The maximum temperature after the recriticality is also determined by the prompt fission power, which depends on the combination of the temperature feedback and the xenon reactivity effect. The temperature feedback is slightly weaker for the 150 MW$_{th}$ case (table 4.1), while the xenon reactivity contribution only increases slightly, i.e. +2494 pcm (100 MW$_{th}$) and +2594 pcm (150 MW$_{th}$) after all Xe-135 in the steady-state core decays.
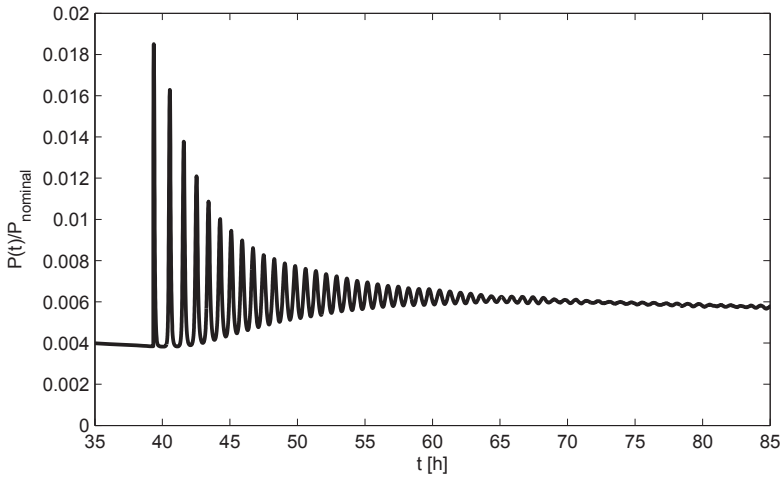

Figure 4.7: Ratio between actual power (fission plus decay heat) over nominal power during the coupled transient for the 100 MW$_{th}$ core configuration.

The total power production after the recriticality is shown as a fraction of the nominal power for the 100 MW$_{th}$ design in figure 4.7. The oscillations in fission power after the recriticality can persist for quite a long time due to the relatively slow thermal response inside a pebble bed reactor [16]. The phenomenon behind the power oscillations in figure 4.7 is certainly physical, but numerical difficulties in the current code scheme also cause the power oscillations to persist for quite a long time. The numerical difficulties can be seen as the oscillations do not fully damp out later in the transient, e.g. after 65 hours in figure 4.7. It has been tested that these oscillations damp out quicker if smaller time steps are used, but this comes at a price of extremely long computation times for the full transient. So, this is unfeasible for the calculation of a significant number of transients. It is important to realize that these oscillations do not affect the trend of the maximum fuel temperature for the different designs as the temperature is physically bounded by the decay of xenon and the reactivity coefficients.

4.3.4. CORE RADIUS
A larger core radius leads to a reduction of neutron leakage and is expected to increase the conversion ratio. Table 4.2 shows the conversion ratio increases significantly if the core radius is increased from 200 cm to 250 cm, while further extension of the core radius only leads to a marginal increase. So, core radii larger than 300 cm are not very interesting.

Table 4.2: Overview of conversion ratio, fuel management and safety parameters for different core radii ($P = 100\ [MW_{th}]$, $\tau_{res,tot}^{breed} = 2000\ [d]$, $\epsilon_{driver}^{U-233,in} = 12\ [w\%]$, $R_{driver} = 100\ [cm]$, 15 driver pebble passes and 2 breeder pebble passes)

Case	I	II	III	IV
Core radius [cm]	200	250	300	350
Conversion ratio	0.9597	0.9870	0.9913	0.9921
$\tau_{res,tot}^{driver}$ [d]	427	356	323	306
$P_{density}^{max}$ [MW/m^3]	4.9	5.6	6.2	6.5
Pebble handling time [s]	12.2	9.8	8.5	7.7
Reprocessing rate [p/day]	716	1012	1322	1658
Max. burnup [MWd/t_{hm}]	62459	56060	52996	51412
$T_{scram}^{max,DLOFC}$ [°C]	1161	1211	1240	1259
$\alpha_{uniform}^{+500K}$ [pcm/K]	-3.41	-3.52	-3.52	-3.51

The residence time of the driver pebbles decreases for larger core radii, and consequently lower burnups are attained in the driver pebbles. The reduced residence times are somewhat surprising, but can be understood from the fact that a single concentration is used (radially) for driver and breeder zone. For larger breeder zones, the average flux and U-233 concentration in the breeder zone becomes lower and hence also the power production. So, a larger fraction of the power is produced in the driver zone and a larger fuel insertion rate is required in the calculations. This is a limitation of the current model, though it can be argued that this also occurs in reality with a larger number of breeder pebble recyclings and random re-insertion. It would be interesting to investigate the conversion ratio using more detailed radial fuel depletion models.

The maximum fuel temperature during a DLOFC with scram increases as the core radius increases, as shown in figure 4.8. As discussed above, the maximum power density increases for larger core radii and also the thermal resistance for decay heat removal has increased due to the larger breeder zone radius, explaining the rise of the maximum fuel temperature. Later on in the transient, the fuel temperature also decreases slower for the larger core size. For the DLOFC without scram, the maximum fuel temperature is quite a bit lower (1404 °C vs 1470 °C) if the core radius is reduced to 200 cm. This ensures a reasonable margin remains with the TRISO limit temperature of 1600 °C, also in view of modelling uncertainties and assumptions used, but it comes at the price of a significantly lower conversion ratio.

4.3.5. Driver zone radius

Besides the core radius, which should be sufficiently large to reduce neutron leakage, the driver zone radius has a large influence upon the conversion ratio, as shown in table 4.3. Enlarging the driver zone radius from 100 cm to 110 cm (P=100 MW$_{th}$) leads to a significant reduction of the conversion ratio, from 0.9913 to 0.9616, while a reduction of the driver zone radius to 90 cm leads to an increase of the conversion ratio to 1.0328, at the price of a very high pebble handling speed requirement. This is around five times faster than the average fuel handling speed of the HTR-PM, where a single pebble is handled each 14.52 s (see section 4.3.6). This may provide a big engineering challenge. The re-
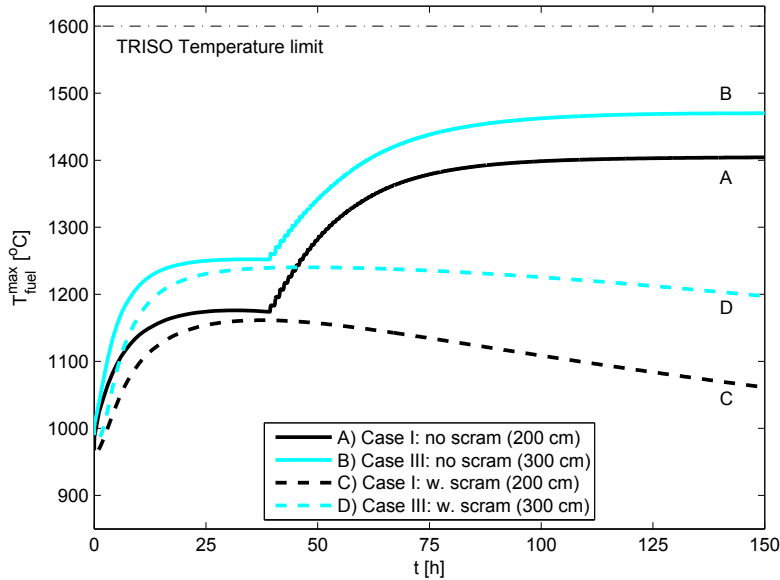
Figure 4.8: Maximum fuel temperature over time during a DLOFC with and without scram for core radii of 200 cm and 300 cm with a 100 cm driver zone radius and a 100 MW$_{th}$ nominal power

processing rate also increases significantly for a smaller driver zone radius, which is also marked by the low burnup (16.8 GWd/t$_{hm}$) attained in the driver pebbles.

Another important issue of a smaller driver zone radius is that the temperature feed-back becomes weaker, as the driver zone becomes more undermoderated due to the higher average U-233 weight fraction caused by the increased pebble handling speed. An under-moderated state of the driver zone also makes the core more vulnerable to water ingress.

Figure 4.9 shows the maximum fuel temperature during a DLOFC with and without scram for the different driver zone radii considered. The differences for the transient with scram are quite small, with the highest maximum fuel temperature occurring for the small-est driver zone. For the transient without scram, the maximum fuel temperature becomes significantly higher with a smaller driver zone due to the weaker temperature feedback and higher power density, which also results in higher steady-state Xe-135 concentrations.

The maximum fuel temperature still remains below 1600 °C for all three driver zone radii, but the 90 cm driver zone comes very close to this limit, also keeping in mind the modelling assumptions made, which will be addressed in section 4.5. Another issue, the high pebble handling speed with a 90 cm driver zone, may be resolved by using less driver pebble passes and by using a higher U-233 weight fraction in the driver pebbles. Less driver pebble passes leads to a higher axial power peaking, while a higher U-233 content per driver pebble might reduce the temperature feedback further and cause difficulties in case of water ingress. From this perspective, safety and breeding act in opposite directions. So, it remains to be seen whether a compromise involving breeding and passive safety within practical constraints is possible.

Table 4.3: Overview of conversion ratio, fuel management and safety parameters for different driver zone radii ($P = 100$ [MW_{th}], $\tau_{res}^{breed} = 2000$ [d], $\epsilon_{driver}^{U-233,in} = 12$ [$w\%$], $R_{core} = 300$ [cm], 15 driver pebble passes and 2 breeder pebble passes)

Case	I	II	III
Driver zone radius [cm]	90	100	110
Conversion ratio	1.0328	0.9913	0.9616
$\tau_{res,tot}^{driver}$ [d]	84	323	581
$P_{density}^{max}$ [MW/m^3]	7.1	6.2	5.6
Pebble handling time [s]	3.0	8.5	11.9
Reprocessing rate [p/day]	2561	1322	1114
Max. burnup [MWd/t_{hm}]	16800	52996	79381
$T_{scram}^{max,DLOFC}$ [$°C$]	1257	1240	1237
$\alpha_{uniform}^{+500K}$ [pcm/K]	-3.22	-3.52	-3.82

4.3.6. Number of driver pebble passes

The handling time per pebble was quite short in most of the results till now. From a practical perspective, it would be desirable to avoid pebble handling speeds (significantly) above those in the HTR-PM. A single 250 MW_{th} HTR-PM core contains 420000 pebbles with a 7 g HM loading and the average burnup of discharged pebbles is 90 GWd/t_{hm} [3]. This means the average pebble resides for 1058 days in the core. So, the HTR-PM discards 397 depleted fuel pebbles each day. Since each pebble makes 15 passes through the core the fuel handling system has to be capable of handling a pebble each 14.52 s on average. All of the configurations presented so far require a faster pebble handling speed than the HTR-PM. The pebble flow rate can be reduced by lowering the number of recyclings of the driver pebbles. The impact of using 6 or 10, instead of 15, driver pebble passes upon the conversion ratio and decay heat removal is shown in table 4.4.

Table 4.4: Overview of conversion ratio, fuel management and safety parameters for different number of driver pebble passages ($P = 100$ [MW_{th}], $\tau_{res}^{breed} = 2000$ [d], $\epsilon_{driver}^{U-233,in} = 12$ [$w\%$], $R_{core} = 300$ [cm], $R_{driver} = 100$ [cm], 2 breeder pebble passes)

Case	I	II	III
Driver pebble passes	6	10	15
Conversion ratio	0.9908	0.9912	0.9913
$\tau_{res,tot}^{driver}$ [d]	317	321	323
$P_{density}^{max}$ [MW/m^3]	6.9	6.4	6.2
Pebble handling time [s]	17.2	11.8	8.5
Reprocessing rate [p/day]	1334	1326	1322
Max. burnup [MWd/t_{hm}]	51961	52677	52966
$T_{scram}^{max,DLOFC}$ [$°C$]	1285	1256	1240
$\alpha_{uniform}^{+500K}$ [pcm/K]	-3.53	-3.53	-3.52

The use of a lower number of driver pebble passes hardly influences the conversion ratio and the handling time per pebble is significantly slower. With 6 passes, it is slower than the requirement of the HTR-PM's fuel handling system. A lower number of passes reduces the flattening of the power profile and makes decay heat removal a bit worse (+45 °C for 6
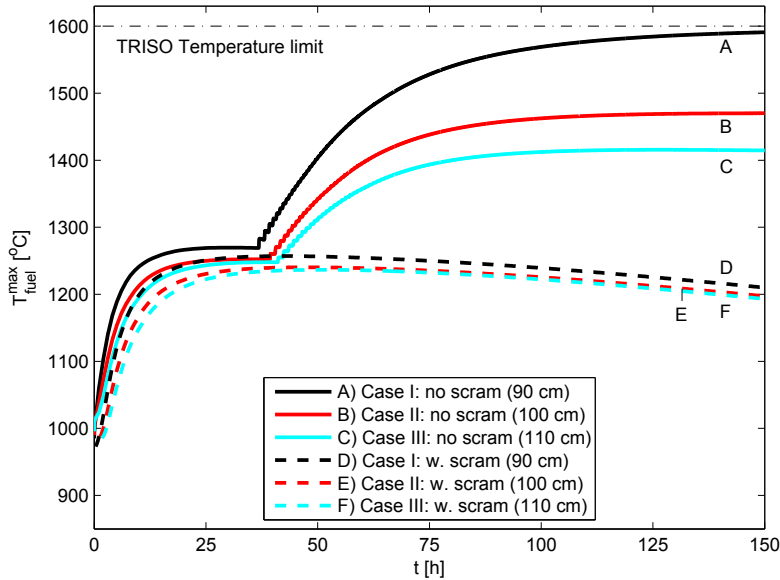
Figure 4.9: Maximum fuel temperature over time during a DLOFC with and without scram for driver zone radii of 90, 100 and 110 cm and a core radius of 300 cm

passes), while the reactivity coefficients are hardly influenced.

The impact of using 6 instead of 15 driver pebble passes upon the DLOFC temperatures with and without scram is shown in figure 4.10. Without scram, the maximum fuel temperature increase is only 15 °C. So, the pebble handling speed can be reduced safely to meet the specifications of the fuel handling system of the HTR-PM design, with a 100 cm driver zone radius. However, a smaller driver zone radius (90 cm) is required to increase the conversion ratio above unity. In that case, a sufficient reduction of the pebble handling speed may only be achieved by an increase of the U-233 content in the driver pebbles, but this weakens the temperature feedback.

4.3.7. BREEDER PEBBLE RESIDENCE TIME
A breeder pebble residence time shorter than 2000 days leads to a slight decrease of the conversion ratio for a 300/100 cm core configuration operating at 100 MW$_{th}$ power, as shown in table 4.5.

The handling speed of the driver pebbles and the maximum power density increases due to the lower fissile content and power production in the breeder zone. This also results in slightly higher maximum fuel temperatures during a DLOFC with scram.

The difference in maximum temperature is of similar magnitude for a DLOFC without scram, as shown in figure 4.11. So, both from the perspectives of the conversion ratio, safety, the reprocessing rate and the fuel handling system, a longer breeder pebble residence time of 2000 days would be desirable. Nonetheless, a breeder pebble residence time of 1000 or 1500 days is more feasible from a practical perspective as it also reduces
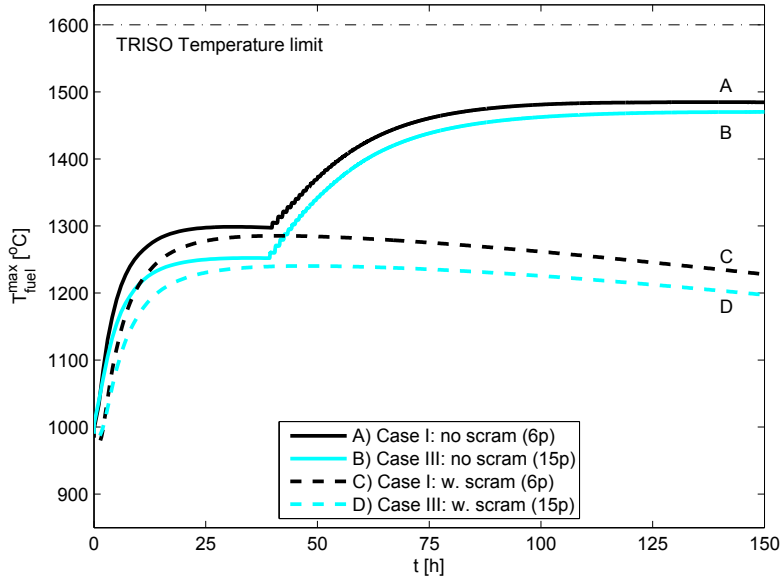
Figure 4.10: Maximum fuel temperature over time during a DLOFC with and without scram for 6 and 15 driver pebble passes for a core with a 100 cm driver zone and a 300 cm core radius
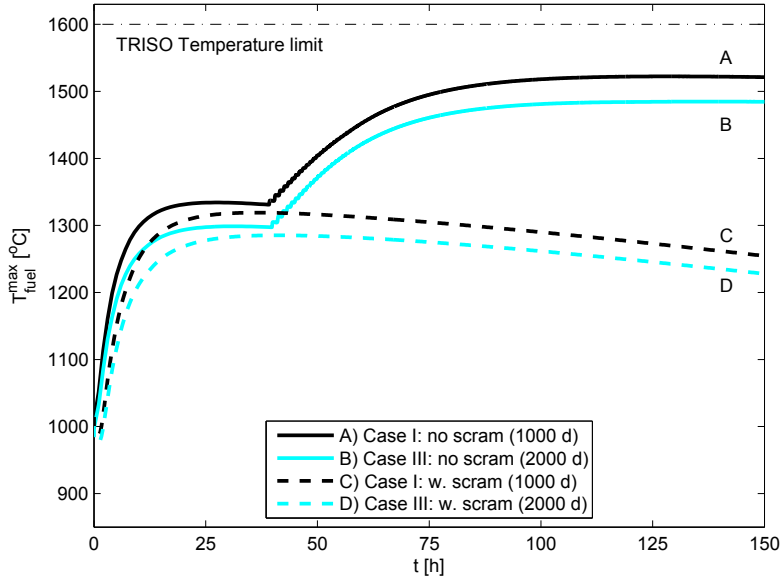

Figure 4.11: Maximum fuel temperature over time during a DLOFC with and without scram for a 1000 and 2000 days breeder pebble residence time for a core with a 100 cm driver zone and a 300 cm core radius

Table 4.5: Overview of conversion ratio, fuel management and safety parameters for different breeder pebble residence times, ($P = 100$ [MW_{th}], $\epsilon_{driver}^{U-233,in} = 12$ [$w\%$], $R_{core} = 300$ [cm], $R_{driver} = 100$ [cm], 6 driver pebble passes and 2 breeder pebble passes)

Case	I	II	III
$\tau_{res,tot}^{breed}$ [d]	1000	1500	2000
Conversion ratio	0.9850	0.9893	0.9913
$\tau_{res,tot}^{driver}$ [d]	279	300	317
$P_{density}^{max}$ [MW/m^3]	7.5	7.2	6.9
Pebble handling time [s]	12.4	15.1	17.2
Reprocessing rate [p/day]	2159	1615	1334
Max. burnup [MWd/t_{hm}]	47904	50364	51961
$T_{scram}^{max,DLOFC}$ [°C]	1319	1303	1285
$\alpha_{uniform}^{+500K}$ [pcm/K]	-3.49	-3.51	-3.53

the length of the running-in phase of the reactor, especially in relation to the lifetime of a typical reactor.

4.4. DESIGN CHOICES

The previous section has given an overview of the impact of several core design and fuel management parameters upon the conversion ratio, passive safety and the requirement of the fuel handling system. Based on these results, different core designs with either improved conversion ratio (>1) or improved passive safety within practical constraints are investigated, as well as the potential to combine both of these goals.

4.4.1. IMPROVING THE CONVERSION RATIO

The results in table 4.3 give a clear indication that a significant increase of the conversion ratio can be achieved by reducing the driver zone radius to 90 cm. On the downside, the driver pebble residence time becomes very short, so the fuel handling system would need to handle one pebble every 3 seconds, as compared to the 14.52 s of the HTR-PM. Though it may be possible to construct a fuel handling system capable of such short handling times (3 s), e.g. by using multiple outlets, a reduction of the pebble handling speed is preferable from an engineering perspective. The pebble handling speed can be reduced by limiting the number of driver pebble passages to six and by increasing the U-233 weight fraction of the driver pebbles. These options are investigated in table 4.6.

Case II shows that an increase of the U-233 content of the driver pebbles and a reduction of the number of driver pebble passes to six, lead to a slight reduction of the conversion ratio (CR=1.0072) as compared to case I, which was already presented in table 4.3. The handling time per pebble has significantly increased and is feasible from an engineering perspective, i.e. the handling speed is slower than for the HTR-PM. The reprocessing rate is also significantly reduced by the higher U-233 content of the driver pebbles, which is also marked by the higher burnup attained in the driver pebbles. Although the power density increases a bit, the maximum fuel temperature during a DLOFC with scram is still far below 1600 °C. A bigger concern is caused by the weaker temperature feedback, which could cause fuel element temperatures to exceed 1600 °C during a DLOFC without scram.

Table 4.6: Overview of conversion ratio, fuel management and safety parameters for different core configurations with a smaller driver zone radius and higher U-233 weight fraction of the driver fuel ($R_{core} = 300$ [cm], 2 breeder pebble passes)

Case	I	II	III	IV
$R_{driver}[cm]$	90	90	90	80
$\epsilon_{driver}^{U-233,in}[w\%]$	12	15	15	18
Driver pebble passes	15	6	6	6
$\tau_{res,tot}^{breed}[d]$	2000	2000	1500	1500
$P[MW_{th}]$	100	100	120	120
Conversion ratio	1.0328	1.0072	1.0044	1.0268
$\tau_{res,tot}^{driver}$ [d]	84	315	250	161
$P_{density}^{max}$ [MW/m^3]	7.1	8.0	9.8	10.6
Pebble handling time [s]	3.0	19.6	15.3	13.3
Reprocessing rate [p/day]	2561	1242	1621	1776
Max. burnup [MWd/t_{hm}]	16800	63397	61104	49593
$T_{scram}^{max,DLOFC}$ [°C]	1257	1310	1428	1423
$\alpha_{uniform}^{+500K}$ [pcm/K]	-3.22	-2.89	-2.80	-2.05

Case III adds to this an increase of the core power to 120 MW$_{th}$ in conjunction with a reduction of the breeder pebble residence time to 1500 days, for economical and practical considerations. These changes only have a limited effect on the conversion ratio, which is still above unity, and lead to a slightly higher power density and maximum fuel element temperature during a DLOFC with scram, but still 172 °C below the failure temperature of the TRISO particles. But some margin should also remain in consideration of modelling uncertainties and assumptions in the relatively coarse models used for the parametric studies in this chapter. Improved decay heat models, i.e. containing specific data for U-233 and including the influence of pebble movement upon the power history of the pebbles, and more radially detailed fuel depletion models may cause an increase of maximum fuel temperatures, but they could also decrease.

Case IV considers a further increase of the U-233 content of the driver pebbles to 18 w%, in combination with a further reduction of the driver pebble radius to 80 cm. This increases the conversion ratio to 1.0268, while the handling time per pebble is still acceptable, as well as the maximum fuel element temperature (1423 °C) during a DLOFC with scram. The main problem of this design, is the significant reduction of the temperature feedback, which means overheating is likely to become a problem in case of a (long-term) failure to scram the reactor. Though such an event is extremely unlikely, it is a requirement to call a reactor passively safe.

Since the conversion ratio of the last design (CR=1.0268) is a bit above unity, there is some margin to reduce the core radius, and thus reduce costs, and the breeder pebble residence time. Some options are shown in table 4.7.

Table 4.7 shows that a reduction of the core radius to 250 cm (CR=1.0224, case I) and 220 cm (CR=1.0119, case II) can be performed while maintaining breeding. For a 200 cm radius, the conversion ratio (=0.9982) drops below unity due to the increased neutron leakage. For a 220 cm core radius, a reduction of the breeder pebble residence time to 1000 days leads to a small increase of the conversion ratio to 1.0135 (case III). This is different

Table 4.7: Overview of conversion ratio, fuel management and safety parameters for different core configurations with an 80 cm driver zone radius, an 18 w% U-233 weight fraction of the driver fuel and 6 driver and 2 breeder pebble passes

Case	I	II	III	IV
$R_{core}[cm]$	250	220	220	220
$\tau_{res,tot}^{breed}[d]$	1500	1500	1000	1500
$P[MW_{th}]$	120	120	120	150
Conversion ratio	1.0224	1.0119	1.0135	1.0091
$\tau_{res,tot}^{driver}$ [d]	185	203	171	177
$P_{density}^{max}$ [MW/m^3]	9.9	9.2	10.1	10.7
Pebble handling time [s]	16.4	18.9	15.0	17.0
Reprocessing rate [p/day]	1343	1110	1482	1195
Max. burnup [MWd/t_{hm}]	54325	57626	51197	60623
$T_{scram}^{max,DLOFC}$ [°C]	1389	1358	1400	1474
$\alpha_{uniform}^{+500K}$ [pcm/K]	-2.11	-2.12	-2.05	-2.07

4

from the trend observed in table 4.5 for a 300 cm core, due to the higher average U-233 and Pa-233 concentrations in the smaller breeder zone of the 220 cm core.

Based on the third design of table 4.7, alternative core design options with a central breeder zone surrounded by a driver zone were also investigated. Unfortunately, the increase of neutron leakage severely reduces the conversion ratio (between 0.59 and 0.66) of such designs. These studies have been included in appendix B.

Case IV of table 4.7 shows the reactor power can be increased to 150 MW$_{th}$, as compared to case II, without compromising breeding (CR=1.0091). Furthermore, the maximum fuel temperature during a DLOFC with scram still remains quite a bit below 1600 °C. The handling time per pebble is also acceptable.

Figure 4.12 shows the maximum fuel temperature for case I and III of table 4.6 and case III of table 4.7 after a DLOFC with and without scram. As discussed, the DLOFC with scram does not pose a problem for any of these designs. Without scram, the maximum fuel temperature remains below the TRISO limit temperature only for the design with 12 w% driver pebbles, but only by less than 10 °C. In view of the modelling assumptions, this does not offer real certainty that fuel temperatures will indeed remain below 1600 °C in reality. On the other hand, slightly exceeding 1600 °C does not necessarily lead to a (significant) release of radioactive fission products from the fuel kernels, especially for relatively low burnups [4]. For the other two designs, the temperature feedback is not strong enough to compensate the reactivity increase due to the xenon decay without exceeding the TRISO temperature limit. So, active reactivity control measures are required during a DLOFC event.

So, in view of the conversion ratio, reactor size, demand on the fuel pebble handling system and practical value of the breeder pebble residence time, the last two designs of table 4.7 are promising thorium breeder PBR design options. A major drawback is that safety cannot be achieved by fully passive means, because of the relatively small temperature feedback. Another potential risk is that water ingress causes a large reactivity insertion due to the undermoderated state of the driver zone. So, choosing one of these breeder configurations for future design studies, places a very high demand on the reactivity control
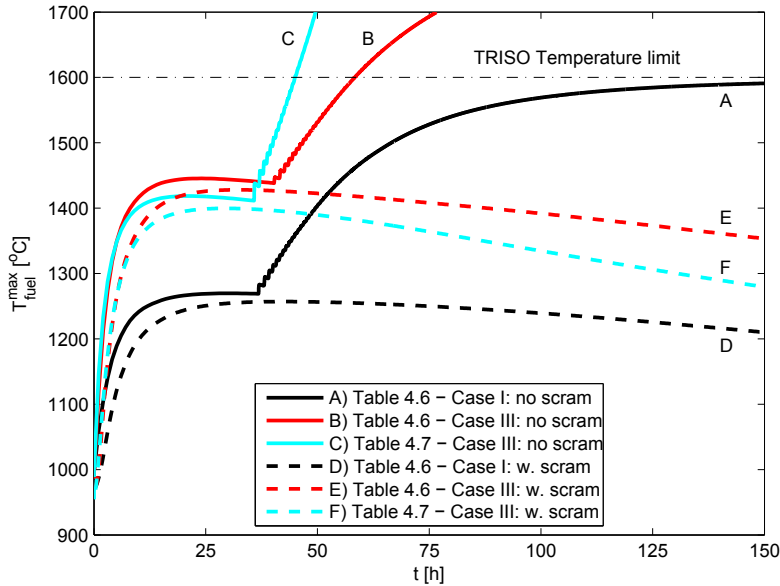
Figure 4.12: Maximum fuel temperature over time during a DLOFC with and without scram for cases I and III of table 4.6 and case III of table 4.7

system, in terms of reliability and control rod worth.

4.4.2. Improving passive safety

The main problem in terms of passive safety of a thorium breeder PBR is the weak reactivity feedback. The reactivity feedback becomes stronger for a lower U-233 weight fraction in the driver fuel. This section investigates the use of a 10 w% U-233 fraction per driver pebble. The disadvantage is that the fuel pebble handling speed increases significantly. So, the driver zone radius cannot be too small ($\geq$ 100 cm), which may limit the breeding potential of such designs. On the other hand, as shown by cases I and II of table 4.6, a lower U-233 weight fraction can also have a positive effect on the conversion ratio.

Four different core designs are considered in table 4.8. Case I and II have a driver zone radius of 100 cm and a core radius of 300 cm. These configurations are breeders (CR > 1) and have relatively strong reactivity coefficients (-3.67 pcm/K). The uniform, fuel and moderator temperature reactivity coefficient of case II is analysed in more detail in appendix C. The number of driver pebble passes is reduced from 6 to 4 in case II. This helps to reduce the fuel pebble handling speed and only has limited influence on the maximum fuel temperature during a DLOFC with scram (+12 °C). These values for the maximum fuel temperatures are still far below the maximum TRISO failure temperature of 1600 °C. The fuel pebble handling speed for case II is still more than twice as fast as in the regular HTR-PM design, but this engineering challenge seems inevitable for a breeder design with a sufficiently strong reactivity coefficient. An economical challenge might be posed by the enormous increase of the required reprocessing rate, which has more than tripled per unit

Table 4.8: Overview of conversion ratio, fuel management and safety parameters for different core configurations with P=100 MW$_{th}$, τ_{res}^{breed} = 1000 [d], 10 w% U-233 in the 3 g HM driver pebbles, a 100 cm driver zone radius, 6 driver and 2 breeder pebble passes)

Case	I	II	III	IV
R_{core} [cm]	300	300	300	250
R_{driver} [cm]	100	100	110	110
Driver passes	6	4	6	5
Conversion ratio	1.0037	1.0036	0.9708	0.9660
$\tau_{res,tot}^{driver}$ [d]	81.8	80.4	293.6	306.2
$P_{density}^{max}$ [MW/m^3]	6.7	6.9	6.5	6.3
Pebble handling time [s]	5.2	7.0	11.5	15.5
Reprocessing rate [p/day]	3770	3810	2220	1676
Max. burnup [MWd/t_{hm}]	14017	13778	41763	42698
$T_{scram}^{max,DLOFC}$ [°C]	1268	1280	1288	1280
$\alpha_{uniform}^{+500K}$ [pcm/K]	-3.67	-3.67	-3.93	-3.90

of energy produced as compared to case III of table 4.7.

Case III has a 300 cm core radius and a 110 cm driver zone radius. The increased size of the driver zone leads to a reduction of the conversion ratio to 0.9708, but does contribute to a slightly stronger reactivity coefficient (-3.93 pcm/K). Case IV is still a high-conversion reactor (CR=0.9660) with a relatively strong reactivity coefficient and a fuel pebble handling speed similar to the HTR-PM.

The maximum fuel temperature during a DLOFC with and without scram is shown in figure 4.13 for case II and case IV of table 4.8. With scram, the maximum fuel temperature is the same for these designs, but the smaller core cools down more rapidly later on in the transient. During a DLOFC with scram, the smaller core also profits from its smaller core radius and the stronger reactivity feedback. In both cases, the maximum fuel temperature, i.e. 1481 °C and 1430 °C respectively, remains quite a bit below the TRISO failure temperature.

One final remark should be made about the reactivity effect of the decaying Pa-233, which has been neglected in the transient calculations in this chapter. For case II of table 4.8, a complete decay of all Pa-233 into U-233, would result in a reactivity addition of 466 pcm. In reality, around 15% of the Pa-233 has decayed after 150 hours, so an additional reactivity effect of +69 pcm may be anticipated from linear interpolation. A complete decay of Xe-135 results in a reactivity effect of +2531 pcm. So, for this case, neglecting the Pa-233 effect does not have a large impact upon the results of the transient.

4.4.3. Water ingress

Besides the response to a DLOFC with and without scram, the maximum possible reactivity insertion due to water ingress is an important safety aspect. In a worst case scenario, such an ingress of water vapour would occur in combination with a DLOFC without scram. Ideally, for complete passive safety, the temperature feedback can overcome both the reactivity insertion due to water ingress and xenon decay. But this is a very strict demand, since water ingress and xenon decay occur at completely different time-scales. The water ingress is an almost instantaneous effect, while decay of xenon causes a reactivity increase
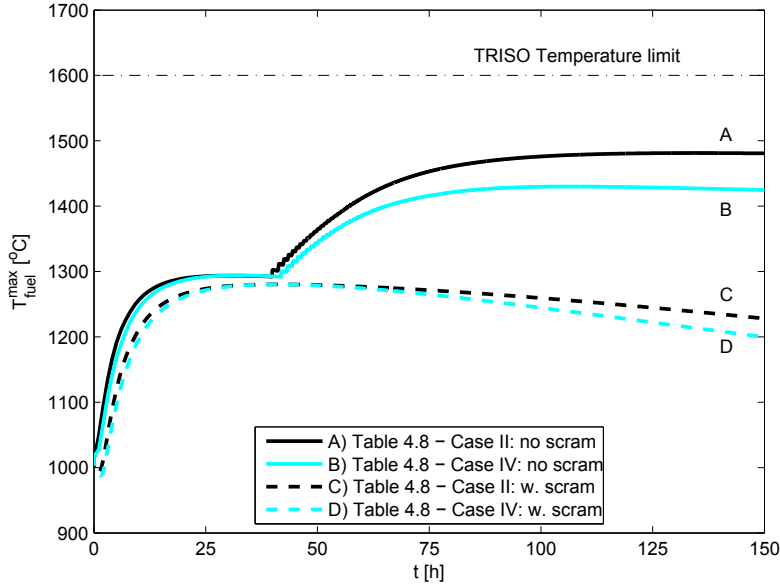
Figure 4.13: Maximum fuel temperature over time during a DLOFC with and without scram for cases II and IV of table 4.8

after many hours.

To minimize the risks caused by water ingress, the temperature feedback has to be quite strong or the reactivity insertion due to water ingress has to be very small (or negative), which requires the driver zone to be around an optimal to overmoderated state. However, the temperature feedback of the HTR-PM design is not sufficient to compensate for a worst-case water ingress, as can be observed in the work by Zheng et al. [17]. In the HTR-PM, the maximum reactivity increase due to water ingress is around 4.3%. According to Zheng et al. [17], the fuel temperature feedback coefficient of $-4.36 \cdot 10^{-5} \Delta k / k / °C$ can compensate around 3% of this 4.3% by a temperature increase without exceeding the TRISO coating's temperature limit of 1600 °C. The remaining reactivity increase (1.3%) due to water ingress would have to be compensated by the reflector rods.

Figure 4.14 shows the reactivity insertion due to an ingress of water vapour for three promising thorium PBR configurations. The water density is specified in kg/m^3 of the total core volume, so the helium volume plus the pebble volume. In the calculations, water is added into the helium region surrounding the pebbles in the cross section generation by CSAS, while the other nuclide concentrations remain the same as they have been determined by the equilibrium core calculation scheme. Two-dimensional cross section sets are created for the k_{eff}-calculation by DALTON for different water densities. This way, the maximum reactivity increase could be determined for the three designs.

The maximum reactivity insertion is +6147 pcm for the first configuration, with an 80 cm driver zone radius and 18 w% U-233 per fresh driver fuel pebble (table 4.7 - case III). The high average U-233 weight fraction of the driver pebbles makes the driver zone
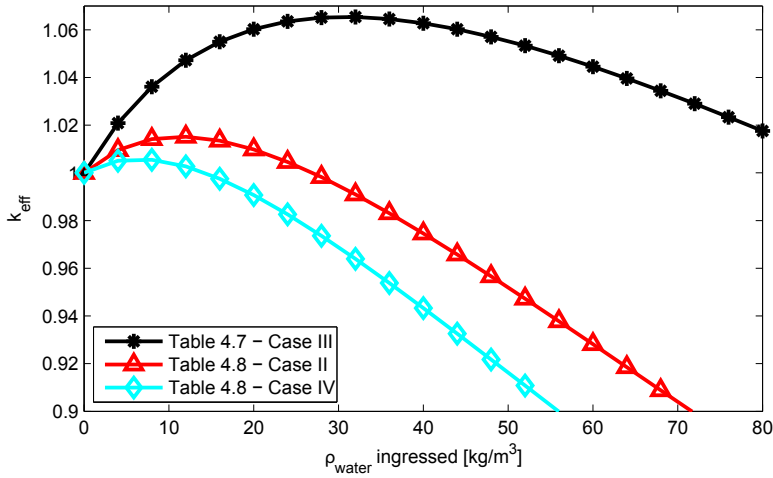
Figure 4.14: k_{eff} as a function of water ingressed [kg/m^3 of the total core volume] for three promising core designs

strongly undermoderated, so a large reactivity insertion occurs if water vapour enters the primary loop. A reactivity increase of 6147 pcm cannot be compensated by the temperature feedback and thus puts a large demand on the required reactivity worth of the reactivity control system, i.e. the control rods and absorber balls. Furthermore, this system is also not passively safe in case of a water ingress, as was also the case during a DLOFC without scram (see figure 4.12). Nonetheless, the design might still be interesting in view of the relatively small core radius for which breeding can be achieved within practical constraints, i.e. fuel pebble handling speed and breeder pebble residence time.

For the second configuration (table 4.8 - case II), which combines breeding and a maximum fuel temperature below 1600 °C during a DLOFC without scram, the maximum reactivity increase due to water ingress is limited to 1497 pcm. Compared to the first case, the average U-233 weight fraction is much lower in the driver zone with 10 w% U-233 in the fresh driver pebbles, and the core is only slightly undermoderated. Contrary to the first case and the HTR-PM, a reactivity insertion of 1497 pcm can be compensated by the temperature feedback only without exceeding the failure temperature of the TRISO particles. Such a design represents a good compromise between breeding and (passive) safety, but it does require an increase of the pebble handling rate of the fuel handling system, as compared to the HTR-PM. It also requires a significant increase of the reprocessing rate, compared to the other options, which may present an economic challenge.

For the third configuration (table 4.8 - case IV) with 10 w% U-233 per driver pebble, the use of a larger driver zone (110 cm) leads to a longer driver pebble residence time and thus a lower average U-233 weight fraction in the driver zone, as compared to the second case. Therefore, the maximum reactivity insertion due to water ingress is reduced to +544 pcm. This reactor can be considered the best choice among the cores considered in terms of passive safety while still providing a high-conversion reactor (CR=0.9660) within practical constraints, such as the pebble handling speed.

4.4.4. ENGINEERING ISSUES

Figure 4.15 gives a more detailed look into the spatial temperature distribution and its influence on the mass flow for case II of table 4.8. This case is taken out as a reference, but the analysis and issues that will be addressed in the following occur in a similar way, perhaps to a somewhat weaker or stronger extent, in the other configurations.
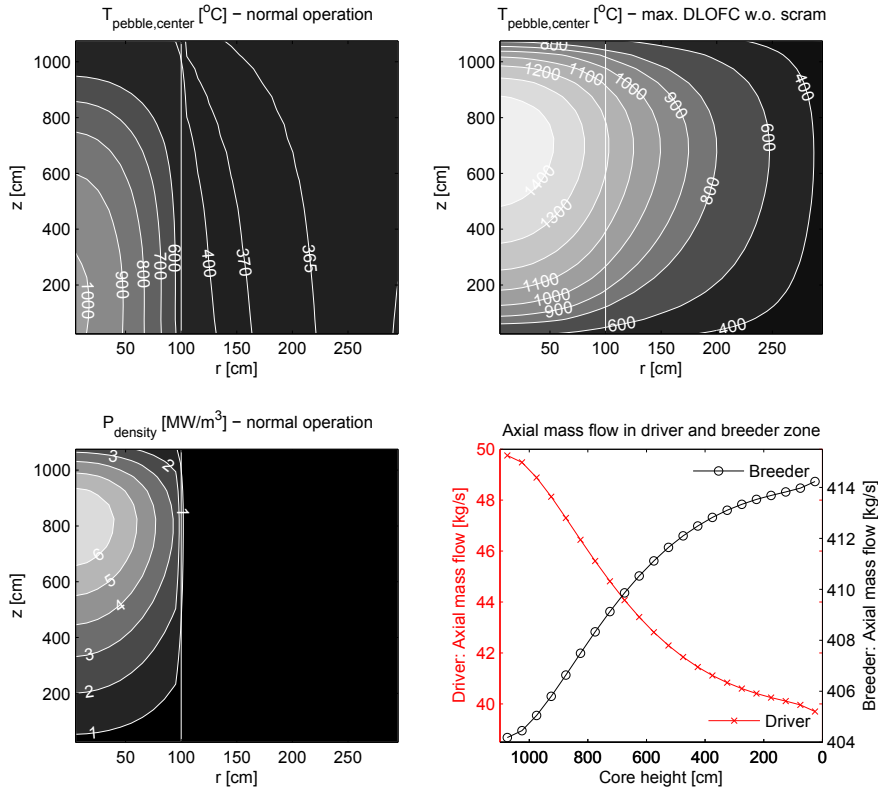

Figure 4.15: Additional results for the second design of table 4.8: Central fuel pebble temperature during normal operation (*top left*) and at maximum temperature during DLOFC without scram (*top right*). The *lower left* plot shows the steady-state power density and the *lower right* graph shows the cumulative axial mass helium flow rates through the driver zone (R < 100 cm) and through the breeder zone (R > 100 cm) as a function of core height.

During normal operation, the highest temperatures occur in the central region near the bottom of the core, as cold helium enters the core at the top and hot helium leaves at the bottom. The coolant hardly heats up in the breeder zone, where the power density is low, and significantly in the driver zone, where most of the power is produced. This clearly shows the need to separate the driver zone hot helium outflow from the relatively cold helium flowing out of the breeder zone. Figure 4.15 also shows that, as expected, the maximum fuel temperature during a DLOFC without scram occurs close to the position where the maximum power density occurs during normal operation. The power density drops rapidly near and inside the breeder channel, which probably makes the reactivity

worth of control rods in the side reflector insufficient. The reactivity control system for the two-zone passively safe thorium breeder PBR is investigated in chapter 5.

The total helium mass flow rate (480.2 kg/s, including a total bypass flow rate of 26.3 kg/s through the side reflector) is also very high for a 100 MW_{th} core, as compared to 96 kg/s in the 250 MW_{th} HTR-PM. This is because only a small fraction of the helium coolant flows through the driver zone, which only constitutes 11.11% of the total core volume. Especially for cores with a large breeder zone, a large mass flow rate is required to ensure the (average) driver zone outlet temperature is 750 °C. This may significantly reduce the efficiency of the reactor due to the large pumping power requirement.

Furthermore, as discussed in section 4.2.2, the helium expands much more in the hot driver zone than in the breeder zone, so there is a net deflection of the mass flow from the central driver zone into the breeder zone. This is clearly shown in the lower right graph of figure 4.15, which shows the evolution of the axial mass flow through the driver zone and the breeder zone as a function of core height (1100 cm is the top of the core). The axial mass flow rate of the helium through the driver zone drops with 20% due to this effect. So, besides a factor 9 increase in the mass flow rate due to the large volume of the breeder zone, an additional 25% increase of the mass flow rate is required for sufficient cooling of the driver zone. On top of this, the average inlet temperature of the helium in the core has increased to 364.5 °C, due to the mixing with the pre-heated helium exiting the breeder zone. This requires a higher helium mass flow rate to limit the outlet temperature of the driver zone to 750 °C.

One possible solution for these issues, i.e. the large helium mass flow rate and the probably insufficient worth of the control rods, could be provided by using a graphite layer to separate the driver from the breeder zone. This way, the pebble flow speed and helium mass flow rate in the driver and breeder zones can be selected separately, also in practice. This graphite layer could also be used to accommodate control rods and absorber balls. Disadvantages are that this graphite layer may have to be relatively thick to ensure the structural integrity of the core. The influence of such a layer upon the conversion ratio, i.e. increased moderation of neutrons travelling from the driver into the breeder zone and the different geometrical distribution of the core, should also be investigated.

An interesting alternative approach might be the use of a radially cooled pebble bed [18–20]. First of all, the helium coolant will flow through both the driver and breeder zones, so a lower helium mass flow is required. The pressure drop is much lower, further decreasing power losses to the coolant pump. A radially cooled reactor design requires the use of a central reflector, which is a very suitable location to position control rods close to the driver zone, ensuring sufficient reactivity worth. On the other hand, it is the question whether a radially cooled design can also perform similar in terms of breeding.

For a further improvement of the decay heat removal, allowing for higher operating powers, the use of a liquid salt coolant might also be considered. The use of a liquid salt coolant has previously been investigated for a regular uranium fueled Pebble Bed Reactor [21] and liquid salts are also used in the design of the Pebble Bed-Advanced High Temperature Reactor [22]. Another interesting advantage is that the system can operate at ambient pressure.

A further relevant engineering question is how much time it will take to achieve the equilibrium core and what start-up strategy should be followed during the running-in

phase.

4.4.5. Multiple radial burnup zones

The results presented in this chapter should be interpreted with the limitations and as-sumptions of the present code scheme in mind. Especially, the use of a single radial bur-nup zone for driver and breeder, and subsequent use of uniform pebble flow speeds in driver and breeder zone, may influence the conversion ratio obtained by the depletion cal-culations. Extensive studies with more radially detailed models would be desirable for fu-ture validation and optimization, but these were considered beyond the scope of this the-sis. Using multiple radial depletion zones and a radial velocity profile, adds many degrees of freedom to the core design, because of the large variety in pebble recycling options. One could always recirculate pebbles within the same radial burnup zone or they can be randomly reinserted. Pebble recirculation can also be done in many structured ways, e.g. making a first pass through the inner zone and moving outward in the next pass, without violating pebble flow conservation constraints. This fuel management scheme can be op-timized with regard to safety, i.e. reduce the maximum power density, conversion ratio or fuel pebble handling speed, by increasing the driver pebble residence time. The concep-tual core designs presented in the present chapter are a good starting point for such more detailed future studies. However, this is only the case if the use of additional radial zones has a limited influence upon the conversion ratio. For this reason, some additional calcu-lations were performed to investigate the effect of adding more radial depletion zones.

Two additional simulations were performed for the passively safe breeder configura-tion (case II of table 4.8) using 8 radial burnup zones (3 driver zones with a 40 cm, 30 cm and 30 cm thickness respectively and 5 breeder zones, all with a thickness of 40 cm) within an extended version of the equilibrium core calculation model. In the first additional sim-ulation, the discharged pebbles are reinserted within the same radial zone, while in the second simulation this was done randomly for both driver and breeder zone. The random reinsertion was simulated by equalizing the mass and concentrations of all nuclides ac-cording to their average mass fractions in the pebbles flowing out of the different radial burnup zones. The weight fraction of isotope x, $\epsilon_{x,insert}^{pass+1}$, in the randomly reinserted peb-bles, was calculated according to

$$\epsilon_{x,insert}^{pass+1} = \frac{\sum_{j=1}^{zones} \epsilon_{x,out}^{j,pass} \dot{m}_j}{\sum_{j=1}^{zones} \dot{m}_j}, \tag{4.6}$$

where the index j sums over the number of radial zones of the driver zone or the breeder zone, and $\dot{m}_j$ is the mass flow rate of heavy metal through radial burnup zone j.

A constant driver and breeder pebble residence time was assumed over the whole driver or breeder zone, in consistence with the results previously shown in this chapter. Secondly, a velocity profile with faster speeds in the inner part of driver and breeder zone is expected to weaken the effect of using multiple radial zones, as pebbles reside shorter in the high flux regions leading to a more even distribution of fuel depletion in the driver zone and thorium conversion in the breeder zone. The results are shown in table 4.9.

Clearly, the simulation with recirculation of pebbles in the same zone, shows the most

Table 4.9: Comparison of conversion ratio, driver pebble residence time and maximum power density for the original scheme with two radial burnup zones and the updated scheme using 8 radial zones with pebbles reinserted in the same zone and with random reinsertion.

	2 zones	8 z. same	8 z. random
Conversion ratio	1.0036	1.0040	1.0024
$\tau_{res,tot}^{driver}$ [d]	80.4	138.9	112.7
$P_{density}^{max}$ [MW/m^3]	6.9	5.3	5.7

extreme effect of adding multiple zones. The U-233 concentration builds up more rapidly in the most inner breeder burnup zone of the multi-zone model. As a consequence, the k_{eff} would increase with the original 80.4 days residence time, requiring an increase of the driver pebble residence time to obtain a critical core configuration. This effect is somewhat weaker with random pebble reinsertion, explaining the more limited increase in driver pebble residence time. However, the change of the conversion ratio is somewhat larger (and negative) for the case of random re-insertion, but the impact is still very limited. If pebbles would make many (random) pebble passages, results should become very close to the original model with one radial burnup zone for driver and breeder zone.

The most important observation is that the conversion ratio changes only very little after adjusting the driver pebble residence time, while the fuel pebble handling speed and the maximum power density decrease with the multi-zone depletion model. For this specific case, the use of one radial burnup zone for driver and breeder has produced an accurate estimate of the conversion ratio, while the results are conservative in terms of safety, i.e. maximum power density, and practical constraints, i.e. fuel pebble handling speed.

Also for other configurations, it can be expected that using multiple radial burnup zones leads to an increase of U-233 concentrations in the inner part of the breeder zone with similar consequences as for the specific case demonstrated, being an increase of the breeder pebble residence time and a decrease of the maximum power density. However, the change of the conversion ratio is expected to be limited. In order to support this, two additional calculations (with random reinsertion) were performed for case III of table 4.7 and case IV of table 4.8. These designs have been presented as optimal in terms of either a high conversion ratio or passive safety within practical constraints. The results are shown in table 4.10.

Table 4.10: Comparison of conversion ratio, driver pebble residence time and maximum power density for the original scheme with two radial burnup zones and the updated scheme using 8 radial zones with random pebble reinsertion for three cases.

	CR	$\tau_{res,tot}^{driver}$ [d]	P_{dens}^{max} [MW/m^3]
Table 4.8 C. II (2 z)	1.0036	80.4	6.9
Table 4.8 C. II (8 z)	1.0024	112.7	5.7
Table 4.8 C. IV (2 z)	0.9660	306.2	6.3
Table 4.8 C. IV (8 z)	0.9670	332.3	5.5
Table 4.7 C. III (2 z)	1.0135	170.6	10.1
Table 4.7 C. III (8 z)	1.0027	207.4	8.5

For the first additional case considered, i.e. case IV of table 4.8, the effect of adding

more radial burnup zones is similar as for the first configuration. So, there is an increase of the driver pebble residence time and a decrease of the maximum power density, while the conversion ratio is hardly affected. For the second additional case, i.e. case III of table 4.7, the driver pebble residence time also increases and the power peak decreases. Although the conversion ratio drops by more than 1%, the reactor is still a breeder.

This analysis shows that the conversion ratios obtained with a single radial burnup zone for driver and breeder provide a reasonable estimate of the breeding potential of the different core configurations, while the results are conservative in terms of safety and fuel pebble handling speed.

4.5. CONCLUSIONS AND RECOMMENDATIONS

THE breeding potential and passive safety of a two-zone thorium Pebble Bed Reactor was investigated in this chapter. With reprocessing, it is possible to achieve breeding in a thorium Pebble Bed Reactor. Using an 18 w% U-233 content for the driver fuel, breeding can already be achieved for a 220 cm core radius within a practical operating regime, in terms of power ($\geq$ 100 MW$_{th}$), breeder pebble residence time ($\leq$ 1000 days) and fuel pebble handling time ($\geq$ 14.5 s per pebble). On the downside, such a design is not passively safe due to the strongly undermoderated state of the driver zone, which results in a weak temperature feedback and a possibly strong reactivity increase in case of water ingress.

An alternative design uses a lower U-233 content in the fresh driver pebbles (10 w%) and has a 250 cm core radius and a 110 cm driver zone. This configuration presents a passively safe thorium PBR and also operates within the same practical operating regime. The maximum fuel temperature reaches 1430 °C during a DLOFC without scram, which is sufficiently below the TRISO failure temperature. The core is also quite insensitive to a reactivity increase due to water ingress (+544 pcm). Disadvantage is that this design is not a breeder reactor, but it is still a high conversion reactor (CR=0.9660).

If the fuel pebble handling speed can be increased by a factor two, as compared to the regular HTR-PM, a compromise combining breeding (CR=1.0036) and passive safety ($T_{scram}^{max,DLOFC}$ = 1481 °C; $\Delta\rho_{water}^{max}$ = 1497 pcm) can be achieved for a 300 cm core and 100 cm driver zone radius. Obviously, this represents the most attractive option in terms of safety and sustainability.

REFERENCES

[1] M. Lung, *EUR 17771: A present review of the thorium nuclear fuel cycles (European Commission)*, Tech. Rep. ISSN 1018-5593 (1997).

[2] M. A. Fütterer, F. von der Weid, and P. Kilchmann, *A high voltage head-end process for waste minimization and reprocessing of coated particle fuel for high temperature reactors,* in *Proceedings of ICAPP'10* (San Diego, CA, USA, 2010).

[3] Y. Zheng, L. Shi, and Y. Dong, *Thermohydraulic transient studies of the Chinese 200MWe HTR-PM for loss of forced cooling accidents,* Annals of Nuclear Energy **36**, 742–751 (2009).

[4] W. Schenk, G. Pott, and H. Nabielek, *Fuel accident performance testing for small HTRs,* Journal of Nuclear Materials **171**, 19–30 (1990).

[5] Radiation Safety Information Computational Center, Oak Ridge National Laboratory, *"SCALE: A Modular Code System for Performing Standardized Computer Analyses for Licensing Evaluations", Vols. I-III, Version 6, CCC-750; ORNL/TM-2005/39* (2009).

[6] B. Boer, D. Lathouwers, J. L. Kloosterman, T. H. J. J. van der Hagen, and G. Strydom, *Validation of the DALTON-THERMIX code system with transient analyses of the HTR-10 and application to the PBMR,* Nuclear Technology **170**, 306–321 (2010).

[7] S. Struth, *Thermix-Direkt: Ein Rechenprogramm zur instationären zweidimensionalen Simulation thermohydraulischer Transienten* (FZ Jülich, Germany, 1995).

[8] J. J. Duderstadt and L. J. Hamilton, *Nuclear Reactor Analysis* (John Wiley and Sons Inc., 1976).

[9] International Atomic Energy Agency (IAEA), *Thorium fuel cycle - Potential benefits and challenges,* Tech. Rep. IAEA-TECDOC-1450 (Vienna, 2005).

[10] Y. Zheng and L. Shi, *Characteristics of the 250MW Pebble-Bed Modular High Temperature Gas-Cooled Reactor in Depressurized Loss of Coolant Accidents,* in *High Temperature Reactor Conference 2008* (Washington, DC USA, 2008) HTR2008-58299.

[11] G. Melese and R. Katz, *Thermal and Flow Design of Helium-Cooled Reactors* (American Nuclear Society, 1984).

[12] American Nuclear Society, *ANSI/ANS-5.1-1993: Decay Heat Power in Light Water Reactors,* (1993).

[13] K. Kugeler, E. Kugeler, N. Pöppe, Z. Alkan, and W. Grätz, *Nuclear Energy, Volume 3B of Landolt-Börnstein - Group VIII: Advanced Materials and Technologies Series* (Springer Berlin Heidelberg, 2005) p. 147.

[14] E. Teuchert, *Brennstoffzyklen des Kugelhaufen-Hochtemperaturreaktors in der Computersimulation* (Kernforschungsanlage Jülich GmbH., 1986).

[15] F. J. Wols, J. L. Kloosterman, D. Lathouwers, and T. H. J. J. van der Hagen, *Preliminary safety analysis of a thorium high-conversion pebble bed reactor,* in *PHYSOR-2014* (Kyoto, Japan, 2014).

[16] H. Van Dam, *Dynamics of passive reactor shutdown,* Progress in Nuclear Energy **30(3)**, 255–264 (1996).

[17] Y. Zheng, L. Shi, and W. Yan, *Water-ingress analysis for the 200MWe pebble-bed modular high temperature gas-cooled reactor,* Nuclear Engineering and Design **240**, 3095–3107 (2010).

[18] Y. Muto and Y. Kato, *A new pebble bed core concept with low pressure drop,* in *Transactions of the Global 2003 Conference* (New Orleans, LA, 2003) pp. 1202–1209.

4

[19] Y. Muto, Y. Kato, and R. Udagawa, *Improvement of fuel temperature characteristics in a pebble bed core with horizontal flow by means of fuel zoning,* in *Proceedings of ICAPP'05* (Seoul, Korea, 2005).

[20] B. Boer, D. Lathouwers, J. L. Kloosterman, T. H. J. J. van der Hagen, and H. van Dam, *Optimization of a radially cooled pebble bed reactor,* Nuclear Engineering and Design **240**, 2384–2391 (2010).

[21] S. J. De Zwaan, B. Boer, D. Lathouwers, and J. Kloosterman, *Static design of a liquid-salt-cooled pebble bed reactor (LSPBR),* Annals of Nuclear Energy **34**, 83–92 (2007).

[22] M. Fratoni and E. Greenspan, *Neutronic feasibility assessment of liquid salt-cooled pebble bed reactors,* Nuclear Science and Engineering **168**, 1–22 (2011).

4

5

NEUTRONIC DESIGN STUDIES OF THE REACTIVITY CONTROL SYSTEM

The neutronic design of the reactivity control system for the 100 MW$_{th}$ Passively Safe Thorium Breeder PBR design, introduced in chapter 4, is investigated in this chapter. The low fissile content of the breeder zone leads to low fluxes in the radial reflector region. Therefore, a significant decrease of the control rod worth is anticipated at this position.

The reactivity worth of control rods in the side reflector and at alternative in-core positions is calculated using different techniques, being 2D neutron diffusion, perturbation theory and more accurate 3D Monte Carlo models. The reactivity worth in the radial reflector is found far insufficient to achieve cold reactor shutdown, which requires a control rod worth of over 15000 pcm. Three dimensional heterogeneous KENO calculations show that placing 20 control rods just outside the driver zone, between 100 cm and 110 cm radius, does provide sufficient reactivity worth, also if one or two control rods would fail to insert.

As an additional emergency shutdown system, the insertion of a neutron absorber gas is investigated. Perturbation theory is found to give a good estimate of the reactivity effect for this type of problem, because a relatively small perturbation $\Delta\Sigma_a$ is now applied over the whole volume of the core. BF$_3$ is found to be the most suitable absorber gas candidate, among four gases investigated, due to its wide availability and the relatively low amount required to achieve a sufficient reactivity worth.

I N modular PBR designs, the radial reflector is the preferred option for the placement of control rods with metallic parts [1], because the control rods can move freely and the rods can be cooled sufficiently. Furthermore, the thermal neutron flux close to the reflector is quite high due to the thermalized neutrons reflected back into the core, which ensures a sufficient control rod worth can be achieved. Therefore, this approach is also taken in the HTR-PM [2], which also has a secondary shutdown system by dropping graphite balls containing neutron absorber material into holes inside the radial reflector.

However, the power production is very low close to the radial reflector for the 100 MW_{th} Passively Safe Thorium Breeder Pebble Bed Reactor (PBR), introduced in chapter 4. So, the effectiveness of control rods is expected to be very small. Therefore, the insertion of control rods into the active core region might be unavoidable for a sufficient reactivity worth.

This might be achieved by using guide channels in which the control rods can be inserted or extracted from the core, like in the German AVR [3]. Driving control rods directly into the pebble bed is less desirable to avoid pebble crushing, although this method was used effectively for reactor shutdown in the Thorium High Temperature Reactor (THTR-300) [4]. An alternative option would be a reactor design with control rods inside a central reflector. This could also offer the opportunity for radial cooling of the pebble bed [5, 6], which might increase the thermal and pumping efficiency of the design as all of the coolant would flow through both the hot driver and the cold breeder zone in the two-zone thorium breeder PBR.

First, it is investigated where control rods might be positioned in the design to obtain a sufficient reactivity worth. These studies are performed using different calculation techniques, being forward 2D(R,Z) diffusion calculations with the inhouse developed neutron diffusion solver DALTON [7], perturbation theory and 3D KENO [8] models. As control rods give a strong local perturbation, a 3D method like KENO is expected to yield the most accurate results. But the simplified 2D DALTON models can be used to provide an upper limit of the reactivity worth at a certain radial control rod position, because the self-shielding effect of the neutron absorber material is underestimated due to its homogeneous distribution.

Secondly, the insertion of an absorber gas is studied as an emergency shutdown system. The achievable reactivity worth as a function of the amount of absorber gas inserted is calculated for different gases, using 2D(R,Z) forward neutron diffusion calculations and perturbation theory. For this application, first order perturbation theory might still provide a good estimate of the reactivity worth as the perturbation introduced is rather homogeneous.

The reactivity worth required to achieve cold shutdown and the temperature constraints of the control rod positioning problem are treated in section 5.1. In section 5.2, the methodology for the control rod positioning calculations and the results are discussed, followed by the absorber gas studies for emergency shutdown and conclusions.

5.1. Requirements of the control system

S EVERAL effects should be taken into account in order to determine the required reactivity worth for the 100 MW_{th} Passively Safe Thorium Breeder PBR, introduced as Case II of table 4.8. Quite extensive descriptions of these effects are given for High Temperature

Reactors by Massimo [9] and Kugeler et al. [10]. In case of a cold shutdown, three important effects with a positive reactivity contribution occur: There is a positive feedback due to the temperature decrease of the core until the cold state of the reactor, decay of xenon-135 leads to reduced neutron absorption and, over time, most of the Pa-233 decays into fissile U-233.

To calculate the reactivity contribution of the temperature feedback, cross sections were generated using the equilibrium core composition, according to the method used to generate the temperature dependent cross section libraries in section 4.2, for both a uniform core temperature of 300 K and for the equilibrium core temperature distribution. Two core calculations are then performed by DALTON to obtain the reactivity effect of the core cooling down to 300 K. The Xe-135 effect is calculated in a similar way by generating cross sections for the equilibrium core temperature and composition, with and without Xe-135, followed by comparing the values of k_{eff} calculated by DALTON. Similarly, the Pa-233 concentration is set to zero and added to the U-233 concentration in all core regions to calculate the Pa-233 effect. The combined effect is calculated by combining these steps in the cross section generation. An overview of the reactivity effect of these three (and other) effects for the 100 MW_{th} thorium PBR is given in table 5.1.

Table 5.1: Reactivity requirement of the reactivity control system of the thorium PBR

Cold shutdown	8361 pcm
T=300 K	(4748 pcm)
Xe-135 decay	(2765 pcm)
Pa-233 effect	(466 pcm)
Water ingress	1497 pcm
Excess reactivity	1000 pcm
Under-criticality	500 pcm
Margin for control rod failure (12.5%)	1419 pcm
Uncertainty/computational inaccuracy (20%)	2555 pcm
Total worth requirement	15328 pcm

Clearly, the temperature reduction of the core leads to the largest reactivity increase, followed by the xenon decay. The contribution of Pa-233 decay is relatively small, but it cannot be neglected for long term cold shutdown, as its half life is 27 days. Note that the sum of the three separate reactivity effects (+7979 pcm) is slightly less than the combined reactivity effect of the three (+8361 pcm), which can be attributed to second order effects.

Furthermore, one should also take into account the maximum possible reactivity increase caused by the ingress of water. For the equilibrium core of the thorium PBR, this effect is quite small (+1497 pcm) because the driver fuel is very close to the optimal moderation ratio when 3 g HM per pebble is used, as shown in section 4.4.3. This effect would be more problematic for greater metal loadings per driver pebble [11].

In general, the possible excess reactivity of the core during normal operation should also be taken into account. This value is relatively small inside a PBR in equilibrium operation due to the continuous refueling, but it might be larger for the start-up core composition. For the breeding potential of the core, the overreactivity should also be kept as small as possible, e.g. below 1000 pcm, though this could cause some complications from an operational perspective if the reactor should be restarted again within several hours after

reactor shutdown, due to the increased Xe-135 concentration. A value of 500 pcm is also added to the excess reactivity to ensure the core is really subcritical [10].

There is also the possibility that one or two control rods fail to enter the core. For this reason a margin of 12.5% is added to the reactivity worth requirement, so that one out of eight control rods is allowed to fail, under the assumption of a symmetrical system like in the current analysis. Next to these physical effects, one should also take into account margins due to computational or data uncertainties. For both the reactivity requirement as well as the calculated control rod worth, an uncertainty in the order of 5 to 10% should be considered according to Massimo [9]. Though it can be argued that the uncertainty has decreased significantly with modern calculation techniques, a conservative estimate of 20% is added to the reactivity worth requirement to account for both uncertainties in the present study. So, a total reactivity worth of over 15000 pcm would be desirable for long-term cold shutdown of the thorium PBR.

5.1.1. TEMPERATURE CONSTRAINT

An important constraint on the positioning of control rods is their temperature during normal operation and transients. The power profile of the thorium PBR, as shown in the upper left graph of figure 5.1, clearly shows that the power production in the breeder zone is quite low. It seems likely that absorber material, like a control rod in a guide channel, should be brought into the active core region to ensure sufficient reactivity worth for reactor control and shutdown. Figure 5.1 also shows the temperature distribution in the active core region both during normal operation and during a DLOFC transient with and without scram, at the moment the maximum temperature occurs.

The maximum temperature allowed for the in-core control rods used in the THTR is 650 °C [10]. However, this design could rely on metallic rods in the relatively cold side reflector for reactivity control during normal operation. So, the material of these rods would not be ideal if control rods were to be inserted into the active core region during normal operation. A more suitable material was used for the control rods of the high temperature engineering testing reactor (HTTR) in Japan, which consist of Alloy 800H for the metallic parts, resulting in a maximum allowable temperature of 900 °C for repeated use after scrams [12]. These control rods are inserted in guide columns located between and around the fuel blocks. According to the HTTR's design guidelines, the control rod should be replaced if its temperature exceeds 900 °C, forming an important constraint for the positioning of metallic control rods.

During normal operation or a regular shutdown of the core, i.e. with active cooling, a maximum allowable temperature of 900 °C, does not pose a problem if the control rods would be positioned just outside the driver zone. It is a problem during a DLOFC, with temperatures up to 1000 °C (with scram) and 1200 °C (without scram) in this region. Materials with a better high temperature characteristic, for instance without metallic parts, would be advisable for these cases. Alternatively, the control rods could also be positioned more outward, but this reduces the reactivity worth. It is the question whether a sufficient reactivity worth for long-term cold shutdown can also be achieved on a more outward location. Even if so, additional control rods are required.
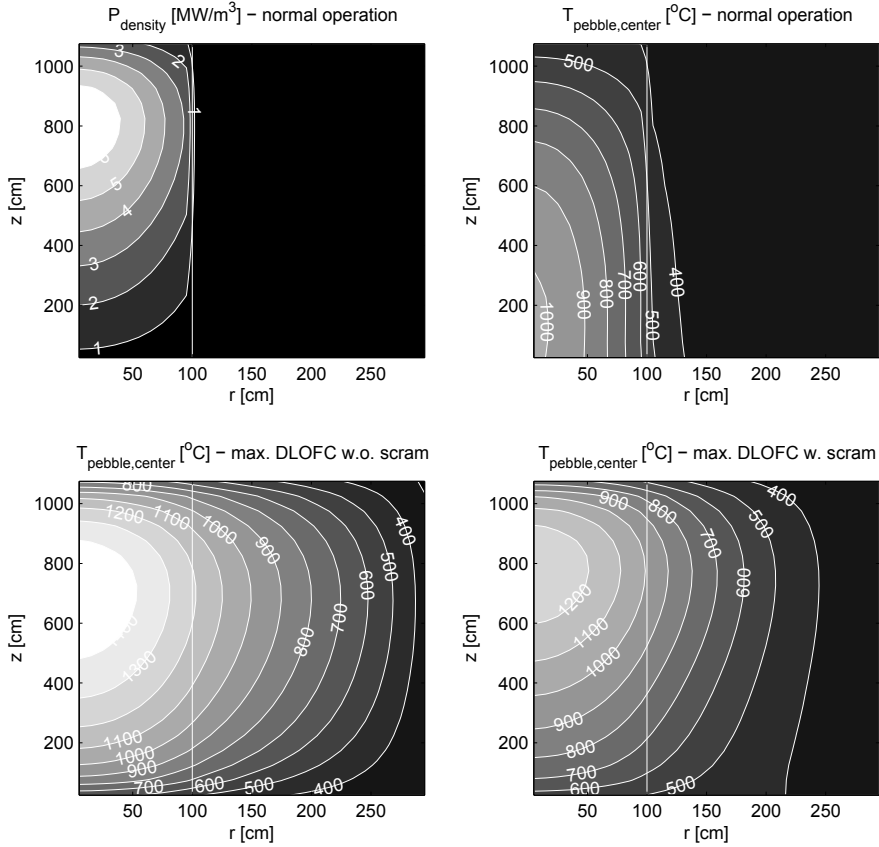
Figure 5.1: Power density (*upper left*) and fuel temperature profile at pebble center during normal operation (*upper right*) and fuel temperature profile during DLOFC without (*lower left*) and with scram (*lower right*) at the moment the maximum fuel temperature occurs.

5.2. CONTROL ROD POSITIONING STUDIES

T HIS section investigates at which control rod positions the required reactivity worth of over 15000 pcm can be achieved.

5.2.1. COMPUTATIONAL MODELS

A 2D(R,Z)-model is used to estimate the maximum achievable worth at a certain radial control rod position. In this model, the control rod material is homogenized within a radial ring over the full height of the active core (11 m). A 3D KENO model with discrete rods was also developed to obtain more accurate results. The models used are discussed in the following.

85

DALTON MODEL

Using DALTON, the reactivity effect can easily be calculated for a homogeneous 2D(R,Z)-model. Cross sections of B_4C absorber material, ρ=2.52 g/cm^3, are added in the affected regions of the original equilibrium core cross section set, obtained for the 100 MW$_{th}$ thorium breeder PBR in chapter 4.

Several modules from the SCALE6 code package [8] are used, in particular CSAS, XS-DRN and ICE, to generate cross sections for the absorber material. As a first step, cross sections are generated with CSAS using the 44-group ENDF/B-V library, included in SCALE6, for an infinite homogeneous medium of B_4C. A 1D radial XSDRN calculation is performed where a very small fraction (1E-20) of the 44-group B_4C cross section is added to the regular core cross sections at central height in the core. At the end of the XSDRN calculation, the 44-group B_4C cross sections are collapsed to 5 groups and, for the core zones under consideration, mixed with the original 5-group core cross sections, by the ICE module of SCALE6 within the forward calculation scheme. Finally, k_{eff} is calculated by DALTON. A significant radial grid refinement, with a factor 100, of the affected and neighbouring radial regions is applied in the DALTON diffusion calculations to model the addition of a strong neutron absorber more accurately.

PERTURBATION THEORY

First order perturbation theory has been implemented and applied with the 2D model. The sensitivity coefficients calculated by perturbation theory provide a first indication on control rod positions yielding a high reactivity worth. It is also interesting to see how useful first order perturbation theory is for an accurate prediction of the reactivity worth in this type of problem, though very accurate results cannot be expected for strong local perturbations. In the next section, first order perturbation theory is also applied for the addition of absorber gases into the core. This is a very homogeneous perturbation, so first order perturbation theory is expected to give accurate results.

The reactivity effect of adding some absorber material can be approximated by first order perturbation theory. Writing the neutron diffusion problem in operator notation:

$$\mathbf{L}\phi = \frac{\mathbf{F}}{k_{eff}}\phi, \tag{5.1}$$

a general expression for the reactivity change $\Delta\rho$ due to a perturbation $\Delta\mathbf{F}$ of the fission operator $\mathbf{F}$, and/or a perturbation $\Delta\mathbf{L}$ of the diffusion operator $\mathbf{L}$, which also includes scattering and absorption, is given corresponding to eq. 4.36a from Ott and Neuhold [13]:

$$\Delta\rho = \frac{\left\langle \phi^\dagger, \frac{\Delta\mathbf{F}}{k_{eff}} - \Delta\mathbf{L}\phi \right\rangle}{\langle \phi^\dagger, \mathbf{F}\phi \rangle}, \tag{5.2}$$

where $\phi^\dagger$ and ϕ are the unperturbed adjoint and forward neutron flux, and $\mathbf{F}$ and $\mathbf{L}$ are also the unperturbed operators. In order to write $\langle \phi^\dagger, \Delta\mathbf{L}\phi \rangle$, the contribution from the boundary term of the leakage term has been assumed to be negligible in accordance with appendix B.5 of Ott and Neuhold [13]. The inner product means integration over space and energy. For the current application, where neutron absorber material (B_4C) is added, the fission operator will remain the same. So the equation reduces to:

$$\Delta\rho = \frac{\langle\phi^\dagger, \Delta L\phi\rangle}{\langle\phi^\dagger, F\phi\rangle} = \frac{\langle\phi^\dagger, \nabla\cdot\Delta D\nabla\phi\rangle - \langle\phi^\dagger, \Delta\Sigma_a\phi\rangle}{\langle\phi^\dagger, F\phi\rangle}, \tag{5.3}$$

The contribution from the change of the diffusion operator will be neglected, as this term is rather small. The validity of this assumption will be demonstrated later on by performing the forward calculations with and without changing the diffusion coefficient. So the reactivity change due to the addition of a neutron absorber, $\Delta\Sigma_a$, is now approximated by:

$$\Delta\rho = -\frac{\langle\phi^\dagger, \Delta\Sigma_a\phi\rangle}{\langle\phi^\dagger, F\phi\rangle} \tag{5.4}$$

Using the output from the finite volume multi-group neutron diffusion code DALTON, the inner products can be calculated in the following way:

$$\Delta\rho = -\frac{\sum_i\sum_j\sum_k V_{i,j,k}\sum_g \phi^\dagger_{g,i,j,k}\Delta\Sigma^{i,j,k}_{a,g}\phi_{g,i,j,k}}{\sum_i\sum_j\sum_k V_{i,j,k}\sum_g \phi^\dagger_{g,i,j,k}\chi_{g,i,j,k}\sum_{g'}\nu\Sigma^{i,j,k}_{f,g'}\phi_{g',i,j,k}}, \tag{5.5}$$

where g refers to the neutron group number and i, j and k refer to the spatial indices and $V_{i,j,k}$ is the volume of a specific grid cell. Due to the angular symmetry in the homogeneous model, the summations only run over two spatial indices, i.e. corresponding to the r and z-direction, in this chapter. The same 5-group B_4C cross sections, as for the forward calculations, were used in combination with the forward and adjoint 5-group fluxes from DALTON.

KENO (HOMOGENEOUS AND HETEROGENEOUS)

A reference 2D KENO-model was also made using 44-group cross sections for the core materials and B_4C. KENO is a Monte Carlo solver included in SCALE6 [8]. This KENO model is used to verify the accuracy of the results from the DALTON calculation, since locally adding a strong neutron absorber could be less accurate for a diffusion solver. Secondly, a heterogeneous 3D KENO model has been developed to model the reactivity effect of discrete rods.

5.2.2. RESULTS AND DESIGN IMPLICATIONS

Results and the different control rod positioning options will be discussed in this section, while a more detailed comparison of the different computational models is given in section 5.2.3.

HOMOGENEOUS MODEL

Figure 5.2 shows k_{eff} as a function of the B_4C volume fraction at four radial positions for both DALTON, perturbation theory and the homogeneous KENO-model. The radial control rod positions considered range between 0 and 10 cm, 50 cm and 60 cm, or 100 cm and 110 cm radius, or the original control rod section in the radial reflector, as shown in figure 3.3. The B_4C absorber is added in volume fractions ranging from 10^{-6} to 1. As a first observation, the results from DALTON and KENO are generally in close agreement, while

perturbation theory is only accurate for small perturbations. This will be investigated more quantatively in section 5.2.3.
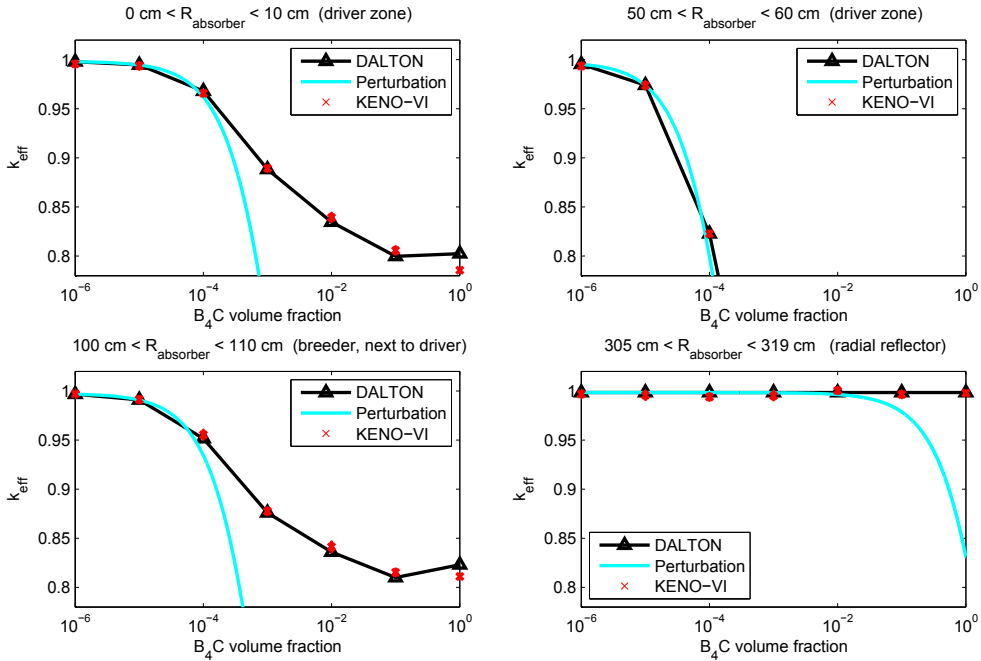

Figure 5.2: Comparison of achievable control rod worth (i.e. reduction of k_{eff}), due to homogenized modelling, for B_4C volume fractions between 10^{-6} and 1 in four radial regions, using (forward) DALTON, perturbation theory and KENO (Monte Carlo). The KENO results are shown within the 95% or 2σ confidence interval.

Placing control rods in the side reflector (305 cm < R < 319 cm) clearly gives an insufficient reactivity worth for reactor shutdown, even with homogeneous modelling of the control rods, which exaggerates the reactivity effect. Other positions are more suitable. In the center of the core, the highest flux (and adjoint) occurs making it the most effective position to add some absorber. However, the reactivity effect achieved in figure 5.2 is much larger between 50 cm and 60 cm radius, because a much larger volume fraction of the core is affected. Just outside the driver zone, the reactivity worth is probably also sufficient for reactor shutdown. This position might be more desirable from a design perspective in terms of control rod operating temperatures and irradiation damage. Furthermore, it might also be beneficial to have some physical separation between the driver and the breeder zone. This could offer the opportunity to separate the driver from the breeder pebbles and to have two separate helium flows through driver and breeder zone, allowing for a significant decrease of the required pumping power, as recommended in section 4.4.4.

HETEROGENEOUS KENO-MODEL

The heterogeneous KENO model was used to determine the reactivity worth of solid B_4C rods (4.95 cm radius) positioned just outside the driver zone at a radius of 105 cm. Figure 5.3 shows the multiplication factor as a function of the number of control rods for both the 2D homogeneous KENO model and the 3D heterogeneous KENO model. Clearly, the homogeneous model significantly overestimates the negative reactivity insertion by the absorber material, especially for a small number of control rods.
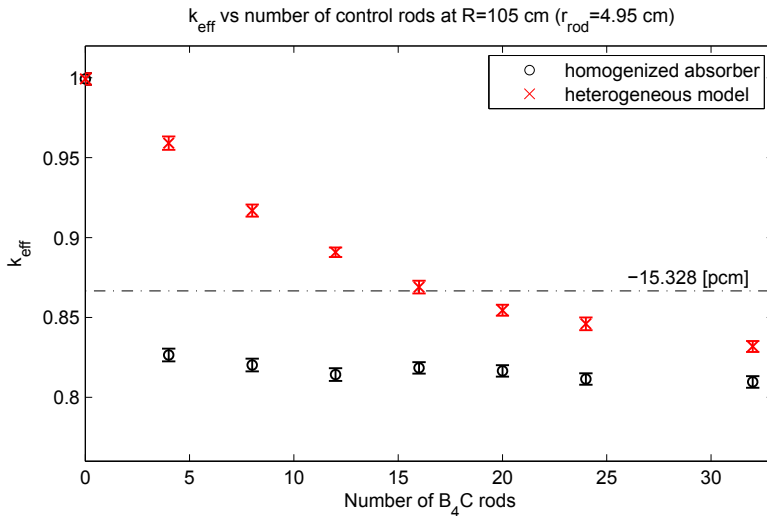

Figure 5.3: Comparison of achievable control rod worth (i.e. reduction of k_{eff}), for different number of control rods with a homogeneous and a heterogeneous KENO-model. Results are shown within the 95% or 2σ confidence interval.

The required reactivity worth of 15328 pcm can be achieved with the implementation of 20 control rods, insertable in guide tubes just around the driver zone. Such a control rod system might be operated in two groups of ten, for improved reliability in case of short term reactor shutdown requirements. By the chosen margins in table 5.1, these 20 rods should also provide sufficient reactivity worth in case one or two rods fail to enter the core.

The temperature constraint for repeated use of metallic control rods after scrams, i.e. 900 °C [12], will be violated during a DLOFC at the location just outside the driver zone (100 cm $< R <$ 110 cm). So, control rods, completely made out of ceramic materials, might be preferable from this temperature perspective, otherwise the control rods might have to be replaced after a DLOFC transient. Still, this is not a big concern, since a DLOFC is unlikely to take place.

A combined system of metallic control rods and graphite absorber balls can also be considered. The graphite absorber balls, containing B_4C, can be inserted in guide channels just outside the driver zone (100 cm $< R <$ 110 cm) to provide sufficient reactivity worth for long term cold shutdown of the core. The metallic control rods are positioned at a more outward position (i.e. $R > 120$ cm) for fine regulation of the reactivity and short term shutdown of the core, but these rods alone may not provide sufficient worth for cold

shutdown. In such a configuration, the control rod temperature also remains below 900 °C during a DLOFC with scram, allowing for repeated use of metallic control rods.

Alternative systems using absorber balls for reactivity control have already been considered more than fifty years ago [14]. In such a system, the balls would move in and out of the core by a regulable fluid flow. This would also resolve issues with the temperature constraint of metallic control rods, but may meet additional difficulties for accurate control of the reactivity.

5.2.3. COMPARISON OF COMPUTATIONAL MODELS

HOMOGENOUS MODELS

Results from forward DALTON calculations, perturbation theory and reference calculations by KENO-VI were compared in figure 5.2. The results obtained by DALTON and KENO are very similar. At a volume fraction of 1, k_{eff} slightly increases again in the DALTON calculation, which seems unphysical. Clearly, diffusion theory has some difficulty with modelling the strong neutron absorber region despite a 100 times grid refinement in the radial direction. Within the active core region, perturbation theory gives reasonable results up to a volume fraction of 10^{-4}, and after that the result starts to deviate as the linear dependence on the amount of absorber added is not valid anymore.

In table 5.2, a comparison is made between first order perturbation theory and the forward DALTON calculations. As mentioned in section 5.2.1, the change of the diffusion coefficient has not been included in the application of the perturbation theory in equation 5.5. To verify this simplification, the forward DALTON calculation has been performed both with changing the diffusion coefficient, due to the change of Σ_a, and by changing only Σ_a. The relative differences, due to the change of D, are also shown in table 5.2. Comparing the third with the fourth column, one can see that the influence of the diffusion coefficient is very small. For the purposes of this chapter it has been a valid assumption to neglect this term in the application of the perturbation theory.

For a volume fraction of 10^{-6}, perturbation theory compares quite well with the forward calculations, i.e. relative differences range from 0.2% to 3.0% depending on the radial position, but this rapidly increases from 1.7% to 17.0% for a volume fraction of 10^{-5} and from 16.7% up to 167% for a volume fraction of 10^{-4}. So, it has once more been demonstrated that first order perturbation theory can model small local perturbations and give an indication of effective control rod positions, but it is inappropriate for an accurate modelling of strong local perturbations. Therefore, it can be anticipated that perturbation theory leads to even worse results if a 3D model with discrete rods is used instead of the 2D homogenous model.

HETEROGENEOUS MODEL

As shown in figure 5.3, the homogeneous model significantly overestimates the negative reactivity insertion, especially in case of a small number of control rods. With a small number of rods, only a small part of the azimuthal domain is affected in the heterogeneous model, while the homogeneous model affects the whole azimuthal domain. If the number of control rods is increased, the control rods start to fill up the radial ring. So, a larger fraction of the azimuthal domain becomes affected in the heterogeneous model and results become more similar to the homogeneous model. Clearly, heterogeneous models

Table 5.2: Comparison of $\Delta\rho$, due to B_4C addition, according to perturbation theory, and forward calculations, with and without changing the diffusion cross section. The relative differences caused by ΔD are shown in parentheses.

0<R<10 cm	$\Delta\rho_{pert.th.}$ [pcm]	$\Delta\rho_{fwd}$ [pcm]	$\Delta\rho_{fwd}(\Delta D = 0)$ [pcm]
10^{-6}	-38.0	-37.9	-37.9 (0.003%)
10^{-5}	-379.7	-371.8	-371.9 (0.003%)
10^{-4}	-3797.1	-3136.4	-3137.4 (0.032%)
10^{-3}	-37971	-12405	-12534 (1.040%)
50<R<60 cm			
10^{-6}	-249.0	-248.5	-248.7 (0.052%)
10^{-5}	-2489.8	-2447.4	-2448.7 (0.053%)
10^{-4}	-24898	-21331	-21346 (0.070%)
10^{-3}	-248976	-94988	-95771 (0.761%)
100<R<110 cm			
10^{-6}	-67.7	-67.2	-67.5 (0.436%)
10^{-5}	-677.4	-648.7	-651.7 (0.450%)
10^{-4}	-6773.5	-4831.2	-4860.0 (0.596%)
10^{-3}	-67735	-13891	-14150 (1.865%)
305<R<319 cm			
10^{-6}	-0.0201	-0.0196	-0.0196 (0.102%)
10^{-5}	-0.2015	-0.1722	-0.1724 (0.110%)
10^{-4}	-2.015	-0.754	-0.757 (0.256%)
10^{-3}	-20.15	-1.19	-1.20 (1.093%)

are required for an accurate calculation of the control rod worth at a certain radial position, especially for a small number of control rods. Still, the homogeneous models are very useful to provide an upper limit of the maximum achievable control rod worth at a certain radial position.

The results discussed in section 5.2.2 were obtained by modelling solid pure B_4C control rods. For comparison, the reactivity worth of 20 rods (4.95 cm radius) containing only a 7 mm thick annular layer of absorber material has also been calculated. In reality, control rods are likely to be constructed in the latter way. A 7 mm B_4C layer was also used in the control rods of the AVR [3].

The use of 20 solid pure B_4C control rods leads to a k_{eff} of 0.8545 with a standard deviation of 0.0017, while the use of 20 rods with a thin layer of B_4C (7 mm, like in the AVR) yields a k_{eff} of 0.8603 with a standard deviation of 0.0015. For practical applications, the control rods effectively work as a black absorber and their modelling by a solid rod is justified for the purposes of the present study.

5.3. REACTOR SHUTDOWN BY ABSORBER GAS INSERTION

IN emergency situations, a neutron absorber gas might be inserted into the core to achieve reactor shutdown, i.e. in extreme cases where control rods and absorber balls fail to drop. It is an easy way to insert neutron absorber material into the most reactive parts of the core. This is of particular interest for the thorium breeder Pebble Bed Reactor, where the reactivity worth of neutron absorber material in the side reflectors is insufficient for

reactor shutdown.

On the downside, it may provide some issues in case of a depressurization incident of the core, because the absorber might leak out of the core along with the coolant and a strong absorber will be required for a sufficient reactivity worth at atmospheric pressure. Furthermore, it may be difficult to remove the absorber gas from the system again. For these reasons, the method is only practical as an additional shutdown system in emergency conditions [15].

In contrast to the control rod positioning problem, perturbation theory is expected to be a powerful method to estimate the reactivity worth due to an absorber gas addition, since it leads to a rather homogeneous perturbation.

5.3.1. Absorber Gases

Candidates for a reactor shutdown gas, studied in this section and described in literature, are the following:

- N_2 is not a very strong neutron absorber, but it is widely available and easy to handle. In sufficient quantity it can still yield a significant reactivity effect [9].

- Kr [9, 16]; It is quite rare in nature (1 ppm), but a slightly stronger absorber than N_2 [9]. Kr-82 (11.6% natural abundance) and Kr-83 (11.5%) are thermal neutron absorbers.

- BF_3; Boron trifluoride gas is mentioned in several patents about reactor control or shutdown mechanisms [15, 17–19]. In theory, it could achieve $\Delta\rho = -0.14$ in the THTR [9], but there is no mention of absorber gas shutdown systems in the actual THTR design [20]. Advantage of BF_3 is that boron is a strong neutron absorber, which can even be made five times more effective if it is enriched in B-10, and boron is also widely available. Disadvantage is that BF_3 is highly corrosive, so only feasible in emergency situations and less desirable for repeated use [15].

- He-3 [16, 18]. Helium-3 is a very strong neutron absorber gas, even better than B-10, though in present times it has also become very expensive. He-3 may also be difficult to separate from the regular helium coolant.

An alternative to BF_3, mentioned in two patents [16, 18], are boron hydrides, specifically B_2H_6. Since this is not expected to yield a fundamentally different effect upon the neutronics, this has not been considered in the remainder of this chapter. Another strong neutron absorber gas is Xe-135 [16], but the relatively short half-life (9.14 h) makes it rather impractical as the Xe-135 stock has to be refilled continuously. Therefore, this option is also not considered.

Figure 5.4 shows the neutron capture cross sections of the gas absorber isotopes considered in this section. The (n,γ)-cross sections for Kr-82 and Kr-83 were added according to their natural abundance. He-3 is the best thermal neutron absorber, but also the most rare and expensive. B-10 also has a large absorption cross section for thermal neutrons. Natural boron is quite widely available and consists for almost 20% of B-10. Nitrogen has the smallest neutron capture cross section, so large quantities will be required. On the other hand, nitrogen is cheap and easy to handle.
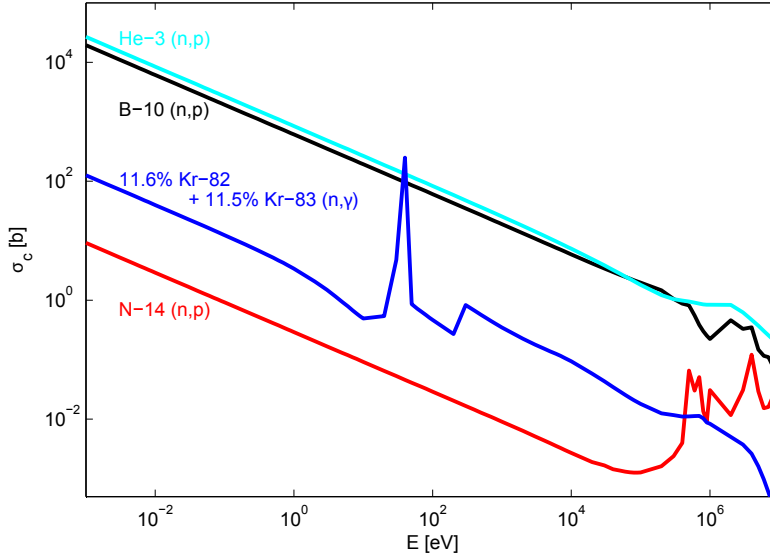
Figure 5.4: Microscopic capture cross sections of the most relevant neutron capture processes for N-14, Kr, B-10 and He-3 according to the ENDF-VII library included in the JANIS-database [21].

5.3.2. HOMOGENEOUS AND INHOMOGENEOUS MODEL

To model the reactivity effect, 44-group cross sections are generated for an infinite homogeneous medium using CSAS. They are added in a very small concentration (1E-20) to the regular core cross sections within 1D radial XSDRN calculations, at different core heights, to collapse to 5 energy groups with a representative energy spectrum at the different core locations. These cross sections are used in the perturbation theory implementation. The forward calculations use the ICE module to mix the original core cross sections and the microscopic absorber gas cross sections multiplied with the desired concentrations for the different core regions.

A homogeneous and an inhomogeneous model is used for the concentrations of the absorber gas. In the homogeneous case, the absorber gas is homogeneously (so same concentration everywhere) added into the active core region, and the change of k_{eff} is determined for the four absorber gases for different masses added in the active core region. Forward DALTON calculations and perturbation theory are used to obtain the results.

The inhomogeneous model is much closer to reality, where the absorber gas will be inserted at one or multiple positions in the core and mix with the helium in the primary loop. After some time, it can be assumed that the absorber gas has perfectly mixed with the helium. The helium density variation strongly depends on the temperature in the core and can be described by [22]:

$$\rho_{he} = 48.14 \frac{p}{T} \left[1 + 0.4446 \frac{p}{T^{1.2}} \right], \tag{5.6}$$

where p is the pressure in bars and T is the temperature in Kelvin and ρ_{he} the density in kg/m^3.

The temperature (and density) variation between the hot driver and the cold breeder zone is quite significant. Therefore, the concentration of the absorber gas also varies in the core. The inhomogeneous model accounts for this effect by varying the absorber gas concentration proportional with the helium density according to the steady-state temperature profile by THERMIX at a pressure of 70 bar. This assumption can be made in case of perfect mixing and if the amount of absorber added is relatively small compared to the amount of helium in the core. For large amounts of absorber, more advanced gas mixing models are advisable for an accurate description of the helium and absorber gas density in relation to pressure.

In reality, the temperature in the core changes significantly after the absorber gas is added and reactor shutdown is achieved. This also affects the distribution of the absorber gas in the core and the reactivity effect. If forced cooling is continued, the coolant temperature inside the core probably drops more significantly than in other parts of the primary loop, so a relative increase of the density and reactivity effect is expected. With a strong temperature increase in the core, as in case of a Pressurized Loss of Forced Cooling, the reactivity effect of the absorber gas might strongly reduce. But a detailed study of this effect is beyond the scope of the work in this chapter. Obviously, the reactivity effect is minimized during a Depressurized Loss of Forced Cooling, so other shutdown systems are always required.

5.3.3. Results

Results for both the homogeneous and inhomogeneous treatment are shown in table 5.3. The absorber gas masses shown in table 5.3 only account for the amount of absorber gas inserted into the active core region. So, the ratio between the helium mass inside the whole primary loop and the mass inside the active core region should be taken into account to determine the total mass of absorber gas required in the whole primary loop.

Comparison of calculation models

The results shown in table 5.3 demonstrate an almost linear dependence of $\Delta\rho$ on the amount of absorber gas added over a large range of concentrations, which justifies the application of perturbation theory. The reactivity worth is predicted somewhat worse by perturbation theory if the inhomogeneous density effect is taken into account. But in any case, it still gives a good estimate of the reactivity effect.

Forward DALTON calculations, with and without changing the diffusion operator, have been performed to estimate the effect of neglecting the change of the diffusion operator in equation 5.3. Neglecting the ΔD-term leads to overprediction of the reactivity worth by approximately 3.0% (not shown in table 5.3) for all concentrations of N_2 added. This is probably due to the influence of the non-zero scatter cross section of N_2 upon the diffusion coefficient. The effect is only 0.3% for Krypton, while it is just above 0.1% for BF_3 and He-3. For large absorber gas concentrations, the effect of neglecting the ΔD-term is very small compared to the total difference between the forward and perturbation theory results.

According to perturbation theory, the density variation of the helium causes the reactivity effect of the absorber gas to reduce by 24.4% since the absorber gas concentration is reduced strongest in the core parts with the highest power density. The reactivity change is similar for the forward calculations for small absorber gas insertions, but the reactivity

Table 5.3: Comparison of $\Delta\rho$, as a function of absorber gas mass added in the active core region, according to perturbation theory, and forward calculations using a homogeneous and inhomogeneous absorber gas distribution

	Inhomogeneous		Homogeneous	
	$\Delta\rho_{pert.th.}$	$\Delta\rho_{fwd}$	$\Delta\rho_{pert.th.}$	$\Delta\rho_{fwd}$
N$_2$	[pcm]	[pcm]	[pcm]	[pcm]
2.5 kg	-12.1	-11.6	-15.0	-14.4
25 kg	-120.8	-115.7	-150.4	-144.4
250 kg	-1208.3	-1148.1	-1503.9	-1441.8
500 kg	-2416.7	-2276.5	-3007.9	-2879.5
1000 kg	-4833.4	-4474.4	-6015.7	-5741.6
1500 kg	-7250.1	-6598.4	-9023.5	-8587.2
2000 kg	-9666.8	-8657.5	-12032	-11416
2500 kg	-12084	-10663	-15039	-14230
3000 kg	-14500	-12624	-18047	-17029
3500 kg	-16917	-14550	-21055	-19813
4000 kg	-19334	-16447	-24063	-22583
	$\Delta\rho_{pert.th.}$	$\Delta\rho_{fwd}$	$\Delta\rho_{pert.th.}$	$\Delta\rho_{fwd}$
He-3	[pcm]	[pcm]	[pcm]	[pcm]
0.2 g	-12.5	-12.4	-15.5	-15.2
2 g	-124.8	-124.7	-155.3	-155.1
20 g	-1248.1	-1235.5	-1553.1	-1548.9
40 g	-2496.2	-2449.3	-3106.3	-3093.8
80 g	-4992.5	-4810.7	-6212.6	-6170.1
120 g	-7488.7	-7090.5	-9318.9	-9227.9
160 g	-9985.0	-9300.2	-12425	-12269
200 g	-12481	-11453	-15531	-15295
250 g	-15602	-14081	-19414	-19053
300 g	-18722	-16656	-23297	-22787
350 g	-21842	-19188	-27180	-26498
	$\Delta\rho_{pert.th.}$	$\Delta\rho_{fwd}$	$\Delta\rho_{pert.th.}$	$\Delta\rho_{fwd}$
Kr	[pcm]	[pcm]	[pcm]	[pcm]
2 kg	-23.5	-23.4	-29.2	-29.3
20 kg	-234.7	-233.5	-292.0	-290.8
200 kg	-2346.8	-2299.7	-2919.5	-2904.3
400 kg	-4693.5	-4521.2	-5839.0	-5796.5
600 kg	-7040.3	-6668.8	-8758.5	-8677.7
800 kg	-9387.1	-8752.1	-11678	-11548
1000 kg	-11734	-10783	-14597	-14407
1200 kg	-14081	-12771	-17517	-17256
1400 kg	-16427	-14726	-20436	-20094
1600 kg	-18774	-16655	-23356	-22922
	$\Delta\rho_{pert.th.}$	$\Delta\rho_{fwd}$	$\Delta\rho_{pert.th.}$	$\Delta\rho_{fwd}$
BF$_3$	[pcm]	[pcm]	[pcm]	[pcm]
20 g	-8.0	-8.2	-9.9	-9.9
200 g	-79.6	-79.5	-99.1	-98.8
2 kg	-796.1	-790.5	-990.6	-988.5
5 kg	-1990.2	-1959.5	-2476.5	-2467.5
10 kg	-3980.3	-3862.8	-4953.1	-4923.8
15 kg	-5970.5	-5711.9	-7429.6	-7368.3
20 kg	-7960.6	-7511.7	-9906.1	-9802.2
25 kg	-9950.8	-9268.4	-12383	-12226
30 kg	-11941	-10989	-14859	-14638
40 kg	-15921	-14344	-19812	-19433
50 kg	-19902	-17614	-24765	-24188

worth reduction increases up to 38.1% if large quantities of absorber gas are inserted.

Design implications

Obviously, the reactivity worths calculated by the inhomogeneous model with the forward calculations are closest to reality. It follows that 3705 kg of nitrogen needs to be added into the active core region for a reactivity worth of -15328 pcm. Theoretically, replacing all helium in the core by nitrogen, 2295 kg would fit in the active core region at 70 bar and 950 °C. This is a conservative estimate as 950 °C is a lot higher than the average core temperature. Still, for average core temperatures above 480 °C, it is not possible to insert the required amount of nitrogen. Krypton requires insertion of 1462 kg in the active core region, while 43.0 kg of BF_3 and 274.2 g of He-3 would suffice.

He-3 is clearly the most effective absorber as only a small amount is required for a sufficient reactivity worth, but it is also the most expensive and difficult to separate from the coolant (He-4). BF_3 is still quite effective, the required mass can still be reduced a factor five by enriching the amount of B-10, as compared to natural boron. BF_3 can be separated chemically from the helium coolant, it is widely available and a relatively low mass is required for a sufficient reactivity worth. Therefore, it can be considered the most practical candidate for an additional emergency shutdown system.

5.4. Conclusions

T HE neutronic design of the reactivity control system was analysed. Possible control rod positions, providing the required worth of over 15000 pcm for long-term cold shutdown, were investigated in the first part. Results from the two dimensional models show that the reactivity worth in the radial reflector of the thorium PBR is by far insufficient. With a 3D KENO-model it was demonstrated that 20 control rods can be positioned just outside the driver zone (R=105 cm) to allow for long-term cold shutdown, even if 2 out of the 20 rods fail to enter the core. During a DLOFC, the control rod temperature will rise above 900 °C, the limit for repeated use of Alloy 800H during scrams [12]. So, completely ceramic rods would be needed or replacement of the control rods is required, but only in case of a (D)LOFC. Alternatively, absorber balls can be used in guide channels just outside the driver zone to achieve long-term cold shutdown, while control rods with metallic parts on a more outward location provide reactor control and short-term hot shutdown only.

Secondly, the insertion of a neutron absorber gas into the primary circuit was investigated to achieve reactor shutdown. Perturbation theory was found to give a good estimate of the reactivity effect for this type of problem. BF_3 can be considered the most suitable absorber gas candidate due to its wide availability and the relatively low amount required to achieve a sufficient reactivity worth. 43.0 kg of BF_3 in the active core region is sufficient for natural boron and this can even be reduced with a factor of five by enriching the B-10 content. On the downside, BF_3 is highly corrosive [15] making the use of such a system undesirable for anything other than emergency situations. Furthermore, the absorber gas concentration becomes very low during a DLOFC, so it cannot replace regular shutdown systems, such as the control rods and absorber balls.

REFERENCES

[1] H. Reutler and G. H. Lohnert, *Advantages of going modular in HTRs,* Nuclear Engineering and Design **78**, 129–136 (1984).

[2] J. Sun, Y. Zheng, and F. Li, *Various Bypass Flow Paths and Bypass Flow Ratios in HTR-PM,* Energy Procedia **39**, 258–266 (2013).

[3] K. Yamashita, I. Murata, and R. Shindo, *Analysis of control rod reactivity worths for AVR power plant at cold and hot conditions,* Journal of Nuclear Science and Technology **31[5]**, 470–478 (1994).

[4] R. Bäumer and I. Kalinowski, *THTR commissioning and operating experience,* Energy **16**, 59–70 (1991).

[5] Y. Muto and Y. Kato, *A new pebble bed core concept with low pressure drop,* in *Transactions of the Global 2003 Conference* (New Orleans, LA, 2003) pp. 1202–1209.

[6] Y. Muto, Y. Kato, and R. Udagawa, *Improvement of fuel temperature characteristics in a pebble bed core with horizontal flow by means of fuel zoning,* in *Proceedings of ICAPP'05* (Seoul, Korea, 2005).

[7] B. Boer, D. Lathouwers, J. L. Kloosterman, T. H. J. J. van der Hagen, and G. Strydom, *Validation of the DALTON-THERMIX code system with transient analyses of the HTR-10 and application to the PBMR,* Nuclear Technology **170**, 306–321 (2010).

[8] Radiation Safety Information Computational Center, Oak Ridge National Laboratory, *"SCALE: A Modular Code System for Performing Standardized Computer Analyses for Licensing Evaluations", Vols. I-III, Version 6, CCC-750; ORNL/TM-2005/39* (2009).

[9] L. Massimo, *Physics of high-temperature reactors* (Pergamom Press, 1976).

[10] K. Kugeler and R. Schulten, *Hochtemperaturreaktortechnik* (Springer-Verlag, 1989).

[11] F. J. Wols, J. L. Kloosterman, D. Lathouwers, and T. H. J. J. van der Hagen, *Preliminary safety analysis of a thorium high-conversion pebble bed reactor,* in *PHYSOR-2014* (Kyoto, Japan, 2014).

[12] Y. Tachibana, H. Sawahata, T. Iyoku, and T. Nakazawa, *Reactivity control system of the high temperature engineering test reactor,* Nuclear Engineering and Design **233**, 89–101 (2004).

[13] K. O. Ott and R. J. Neuhold, *Nuclear Reactor Dynamics* (American Nuclear Society, 1985).

[14] J. W. Ryon and D. C. Schluderberg, *Ball-type control for a nuclear reactor, US Patent 3257286,* (1966).

[15] T. Overhoff, R. Schulten, J. Singh, G. Sylvester, and J. Witte, *Method of and apparatus for shutting down a gas-cooled nuclear reactor, US Patent 4279697,* (1981).

5

[16] A. R. Dastur, *Nuclear reactor control using neutron absorption fluid, US Patent 3498879,* (1970).

[17] R. L. Whitelaw, *Boron Trifluoride Regulating System, US Patent 3025228,* (1962).

[18] R. Schulten, W. Güth, A. Setzwein, H. Braun, and G. Berberich, *Heterogeneous nuclear reactor, US Patent 3089835,* (1963).

[19] T. O. Jeffries, E. Long, and R. W. Smyth, *Nuclear reactor control means, US Patent 3251746,* (1966).

[20] R. Bäumer, I. Kalinowski, E. Röhler, J. Schöning, and W. Wachholz, *Construction and operating experience with the 300-MW THTR nuclear power plant,* Nuclear Engineering and Design **121**, 155–166 (1990).

[21] Organization for Economic Co-operation and Development - Nuclear Energy Agency, *JANIS 4.0, User's Guide - Rev. 1* (2013).

[22] H. Petersen, *The Properties of Helium: Density, Specific Heats, Viscosity, and Thermal Conductivity at Pressures from 1 to 100 bar and from Room Temperature to about 1800K,* (1970).

5

6

ANALYSIS OF THE RUNNING-IN PHASE

This chapter analyses the running-in phase of the 100 MW$_{th}$ Passively Safe Thorium Breeder PBR, introduced in chapter 4. Since U-233 is not available in nature, an alternative fuel, e.g. U-235/U-238, is required to start the reactor. It is investigated how long it takes to converge to the equilibrium core composition and to achieve a net production of U-233, and how this can be accelerated.

A fast and flexible calculation scheme was developed to analyse these aspects of the running-in phase. Depletion equations with an axial fuel movement term are solved in MATLAB for the most relevant actinides (Th-232, Pa-233, U-233, U-234, U-235, U-236 and U-238) and the fission products are lumped into a fission product pair. A finite difference discretization is used for the axial coordinate in combination with an implicit Euler time discretization scheme.

Results show that a time-dependent adjustment scheme for the enrichment (in case of U-235/U-238 start-up fuel) or U-233 weight fraction of the feed driver fuel helps to restrict excess reactivity, to improve the fuel economy and to achieve a net production of U-233 faster. After using U-235/U-238 startup fuel for 1300 days, the system starts to breed U-233 within 7 years after start of reactor operation.

A basic safety analysis, which considers DLOFC with scram scenarios, uniform reactivity coefficients (and implications for a DLOFC without scram) and water ingress, shows that the same passive safety requirements as for the equilibrium core are fulfilled during every stage of the running-in phase.

I N section 4.4.2, the equilibrium core composition of the 100 MW$_{th}$ Passively Safe Tho-rium Breeder PBR was determined. However, U-233 is not available in nature, so an-other fuel is required to start the reactor. This chapter investigates the transition phase from the start-up core to the equilibrium core configuration, also called the running-in phase. Low enriched uranium will be considered as a start-up fuel in this chapter, but plutonium (and minor actinides) may also provide an alternative, its use has already been considered previously in combination with thorium inside PBRs [1–3]. The build-up of certain relevant actinides, e.g. U-234, U-235 and U-236, may take quite some time. There-fore, it is important to determine from which moment the reactor starts breeding, i.e. a net production of U-233, and how much time it takes to converge to the equilibrium core composition.

In addition to answering these questions, the running-in phase strategy should also be chosen carefully in order to minimize the additional U-235 fuel consumption, to achieve equilibrium quickly, to maintain a critical core configuration while restricting the amount of excess reactivity, and to maintain passive safety, at any time. In order to achieve this, the fresh fueled core composition and the enrichment of the U-235/U-238 feed fuel during the initial start-up phase and the U-233 weight fraction of the driver fuel in the remainder of the running-in phase should be chosen carefully over time.

To ensure that the thorium PBR is passively safe during the whole running-in phase, a basic safety analysis, i.e. calculation of the uniform reactivity coefficient, maximum power density, maximum fuel temperature during a Depressurized Loss of Forced Cool-ing (DLOFC) with scram and the maximum reactivity insertion due to water ingress, is performed at different moments of the chosen running-in phase strategy.

The most common code in literature for modelling the running-in phase of multi-pass PBRs is VSOP (Very Superior Old Programs) which was developed in Germany during the high temperature reactor program [4]. The VSOP code calculates the core depletion over the whole start-up phase until the equilibrium core, and was used for instance to model the running-phase of the HTR-10 [5]. Another code capable of modelling the start-up phase of a PBR is NRG's PANTHERMIX code [6, 7].

The calculation scheme used in chapter 4 for the design of the reactor only provides the option to calculate the equilibrium core composition directly. This code scheme could be extended to a full time-dependent version, but the calculations would become very time-consuming. The scheme also does not offer enough flexibility to vary the relevant fuel management parameters over time. In this scheme, a burnup calculation is performed and afterwards the fuel concentrations are shifted to a new lower grid position.

A new calculation scheme was developed to perform the running-in phase calcula-tions. This scheme solves the depletion equations in MATLAB for only the most relevant actinides (Th-232, Pa-233, U-233, U-234, U-235, U-236 and U-238), while the fission prod-ucts are lumped into a single fission product pair. Furthermore, several simplifications were made in the cross section generation scheme to reduce the computation time. The depletion equations are solved including an axial fuel movement term, so fuel movement and depletion are accounted for simultaneously, increasing the flexibility of the model. A finite difference discretization is used for the height term and an implicit Euler scheme to solve the time-dependent term. With this scheme, any of the relevant parameters can

easily be varied over time.

A detailed description of the scheme and the simplifications used is given in section 6.1, while section 6.2 demonstrates that the influence of the simplifications in the depletion equations and the cross section generation scheme is fairly small ($\approx$ 0.3%) for the conversion ratio (CR) of the equilibrium core configuration. Though the ratio between the fissile atom production and consumption rate may deviate a bit more during the running-in phase itself, this will not influence the trends observed in this chapter as the time-scales involved remain similar. Despite the simplifications used to reduce the computation time, the new running-in phase model provides a very useful and flexible tool to analyse and optimize the running-in phase strategy and to gain insight into the time-scales involved in the running-in phase.

The treatment of the running-in phase model and the equilibrium core calculation by the new model, precedes a discussion of the results of the running-in phase calculations, a basic safety analysis of the thorium PBR during the running-in phase and conclusions and recommendations.

6.1. RUNNING-IN PHASE MODEL

Fɪʀsᴛ, the calculational model for the running-in phase is discussed in section 6.1.1, followed by a discussion of the cross section preparation method in section 6.1.2, which also includes a discussion of a time-invariant version of the model to calculate the equilibrium core directly.

6.1.1. TIME-DEPENDENT FUEL DEPLETION MODEL

Assuming that the fuel moves only in the axial direction, the generalized burnup equation [8] of a nuclide k, with concentration N_k, is given by:

$$\frac{\partial N_k}{\partial t} + v_z \frac{\partial N_k}{\partial z} = \phi \sum_{i=l}^{m} N_i \sigma_{fi} y_{ik} + \phi \sum_{s=r}^{q} N_s \sigma_{as} y_{sk} + \sum_{j=n}^{p} N_j \lambda_j \alpha_{jk} - \lambda_k N_k - \phi N_k \sigma_{ak} \quad (6.1)$$

Here, v_z is the axial pebble velocity, ϕ the neutron flux, σ_{fi} is the microscopic fission cross section of isotope i and σ_{as} is the microscopic absorption cross section of isotope s, λ_j and λ_k are the decay constants of isotopes j and k, y_{ik} is the yield of isotope k due to fission in isotope i and y_{sk} is the yield of isotope k due to absorption in isotope s, while α_{jk} is the probability that isotope k is formed after decay of isotope j.

A simplified time-dependent core depletion model was developed for parametric studies of the running-in phase by numerically solving the burnup equations for the important actinides (i.e. Th-232, Pa-233 and the uranium isotopes), while the fission products are modelled by a single fission product pair for computational ease. The burnup equations will be solved as a function of height, using finite differences, and time, using an implicit Euler discretization scheme, for both driver and breeder zone. So, a single radially averaged concentration is obtained for each zone, in conjunction with the more extensive equilibrium core calculation scheme developed in chapters 3 and 4.

The advantage of the new model is that it allows for relatively fast calculations over the whole length of the running-in phase, while the code is flexible in varying several interesting time-dependent parameters, such as the enrichment of the feed fuel, pebble recycling

speeds, reactor power and initial core loading. The influence of these parameters on the progress of the running-in phase, i.e. k_{eff} over time, length of the running-in phase, U-233 mass inside and outside the core, can be evaluated with the model. Though possible, variations of the total driver pebble residence time and the reactor power over time are not considered in this chapter. Such variations are less desirable from an operational perspective and they were found unnecessary to achieve the goals of this chapter.

Due to the simplifications of the lumped fission product pair and not considering the build-up of actinides beyond uranium it is not possible to do waste characterization studies, but this is also not the goal of the model.

START-UP DRIVER FUEL

Since U-233 is not available in nature, an alternative has to be considered as a driver fuel for the start-up phase of the reactor. The most logical candidate and the one considered in this chapter is enriched uranium, but plutonium (and minor actinides) might also be considered. During this initial start-up phase, the burnup equations of U-235, U-238 and fission product pair, FP5, will be solved for the driver zone. This initial phase is referred to as the *'U-235 fueled phase'* in the remainder of this chapter.

It is assumed that the uranium content from the discarded enriched uranium driver pebbles will not be reprocessed, or at least that this uranium will not be mixed with the U-233 produced in the breeder pebbles. Therefore, the U-236 concentration is not considered as it takes a long time to reach a significant concentration, i.e. this will happen only with continuous reprocessing of U-233 later on. U-237 is also not considered since it has a very short half-life (6.75 d). In the later stage of the running-in phase, after switching to U-233 as a driver fuel the build-up of U-236 will be taken into consideration.

The burnup equations for U-235, U-238 and the lumped fission product pair (denoted by FP5, neglecting fast fission in U-238) are then given by:

$$\frac{\partial N_{U5}(z,t,p)}{\partial t} + v_z(t)\frac{\partial N_{U5}(z,t,p)}{\partial z} = -N_{U5}(z,t,p)\sigma_{a,U5}\phi(z,t) \tag{6.2}$$

$$\frac{\partial N_{U8}(z,t,p)}{\partial t} + v_z(t)\frac{\partial N_{U8}(z,t,p)}{\partial z} = -N_{U8}(z,t,p)\sigma_{a,U8}\phi(z,t) \tag{6.3}$$

$$\frac{\partial N_{FP5}(z,t,p)}{\partial t} + v_z(t)\frac{\partial N_{FP5}(z,t,p)}{\partial z} = N_{U5}(z,t,p)\sigma_{f,U5}\phi(z,t) - N_{FP5}(z,t,p)\sigma_{a,FP}\phi(z,t) \tag{6.4}$$

Here z refers to the axial position in the core, being 0 at the top and H at the bottom, t refers to the time and there is the pebble class p, which accounts for the actual passage number of the pebble. For all passages p, the initial condition of isotope x is given by:

$$N_x(z,0,p) = N_{fresh,x}(z), \tag{6.5}$$

while the boundary condition is:

$$N_x(0,t,p) = N_{feed,x}(t) \quad (p = 1), \tag{6.6}$$

$$N_x(0,t,p) = N_x(H,t,p-1) \quad (p > 1). \tag{6.7}$$

So, the concentration at the top of the core is given by the feed fuel for the first passage or the concentration at the bottom of the core in the previous passage. $N_{fresh,FP5}$ and $N_{feed,FP5}$ are obviously zero.

The balance equations are discretized using finite differences for the z-coordinate and Implicit Euler for the time variable. Time is denoted with index i, and k is used to index the axial coordinate. For U-235 and U-238, denoted by x, this results in:

$$\frac{N_{x,k}^{i+1} - N_{x,k}^{i}}{\Delta t} + v_z^{i+1} \frac{N_{x,k}^{i+1} - N_{x,k-1}^{i+1}}{\Delta z} = -N_{x,k}^{i+1} \sigma_{a,x} \phi_k^{i+1} \tag{6.8}$$

Which after collecting of terms results in:

$$N_{x,k}^{i+1} \left(\Delta z + \sigma_{a,x} \phi_k^{i+1} \Delta z \Delta t + v_z^{i+1} \Delta t \right) - v_z^{i+1} \Delta t N_{x,k-1}^{i+1} = N_{x,k}^{i} \Delta z \tag{6.9}$$

The resulting matrix-vector system ($\mathbf{A} N^{i+1} = N^i \Delta z$) is solved consecutively for each pebble passage p by MATLAB. Only the diagonal and lower diagonal elements of the matrix $\mathbf{A}$ are non-zero. For the fission product pair concentration (FP5) the discretization is similar, except for an additional production term, $N_{U5,k}^{i+1} \sigma_{f,U5} \phi_k^{i+1} \Delta z \Delta t$, appearing in the right hand side of the equation. The fission product pair concentration can be solved by MATLAB, after solving for the U-235 concentration.

THORIUM, U-233

After a while, a sufficient amount of U-233 has been produced to start using it for the driver fuel without ever supplying additional U-235/U-238 fuel afterwards. This will be referred to as the *'U-233 fueled phase'* in the remainder of this chapter. The breeder zone is fed with thorium pebbles directly from the start of reactor operation. For both the breeder zone and the U-233 fueled phase of the driver zone, the nuclide balance equations of Th-232, Pa-233 (assuming instantaneous decay of Th-233), U-233 till U-236 and the fission product pair concentrations, denoted by FP3, have to be solved. The nuclide balance equations for these nuclides are given in the following:

$$\frac{\partial N_{T2}(z,t,p)}{\partial t} + v_z(t) \frac{\partial N_{T2}(z,t,p)}{\partial z} = -N_{T2}(z,t,p) \sigma_{a,T2} \phi(z,t) \tag{6.10}$$

$$\frac{\partial N_{P3}(z,t,p)}{\partial t} + v_z(t) \frac{\partial N_{P3}(z,t,p)}{\partial z} = -N_{P3}(z,t,p) \left[\sigma_{a,P3} \phi(z,t) + \lambda_{P3} \right]$$
$$+ N_{T2}(z,t,p) \sigma_{c,T2} \phi(z,t) \tag{6.11}$$

$$\frac{\partial N_{U3}(z,t,p)}{\partial t} + v_z(t) \frac{\partial N_{U3}(z,t,p)}{\partial z} = -N_{U3}(z,t,p) \sigma_{a,U3} \phi(z,t) + \lambda_{P3} N_{P3}(z,t,p) \tag{6.12}$$

$$\frac{\partial N_{U4}(z,t,p)}{\partial t} + v_z(t) \frac{\partial N_{U4}(z,t,p)}{\partial z} = -N_{U4}(z,t,p) \sigma_{a,U4} \phi(z,t) + N_{U3}(z,t,p) \sigma_{c,U3} \phi(z,t) \tag{6.13}$$

$$\frac{\partial N_{U5}(z,t,p)}{\partial t} + v_z(t) \frac{\partial N_{U5}(z,t,p)}{\partial z} = -N_{U5}(z,t,p) \sigma_{a,U5} \phi(z,t) + N_{U4}(z,t,p) \sigma_{c,U4} \phi(z,t) \tag{6.14}$$

$$\frac{\partial N_{U6}(z,t,p)}{\partial t} + v_z(t)\frac{\partial N_{U6}(z,t,p)}{\partial z} = -N_{U6}(z,t,p)\sigma_{a,U6}\phi(z,t) + N_{U5}(z,t,p)\sigma_{c,U5}\phi(z,t)$$

(6.15)

$$\frac{\partial N_{FP3}(z,t,p)}{\partial t} + v_z(t)\frac{\partial N_{FP3}(z,t,p)}{\partial z} = -N_{FP3}(z,t,p)\sigma_{a,FP}\phi(z,t) + N_{U3}(z,t,p)\sigma_{f,U3}\phi(z,t)$$

(6.16)

These equations are solved by a similar matrix-vector system as for the U-235, U-238 and fission product pair concentrations in the previous subsection.

TIME-STEPS AND UPDATING THE NEUTRON FLUX

A time-step size, Δt, of 2.5 hours is used to solve the system of equations during the calculations in this chapter. In section 6.3, an 80.4 days total driver pebble residence time and 4 driver pebble passes are used, so it would take 4.4 hours to traverse a single grid cell of 10 cm height. So, a 2.5 hour time-step is used to obtain sufficiently accurate results.

The neutron flux $\phi(z,t)$ is obtained for both driver and breeder zone by performing a k_{eff} calculation of the core with DALTON, an inhouse developed neutron diffusion solver. The magnitude of the flux vector $\phi(z,t)$ is scaled to the desired power production during each time-step Δt, while the expensive update of the neutron flux by DALTON is performed only after multiple steps Δt. At the start of the U-235 fueled phase, the flux is updated by DALTON during every $5\Delta t$ steps. If the relative change in k_{eff} and the neutron flux shape becomes smaller than 0.02%, the flux update interval is doubled, but the flux is updated at least every 1000 time-steps Δt. At the start of the U-233 fueled phase, the flux update interval is reset again to every $5\Delta t$ steps, because significant changes in flux shape and k_{eff} can be anticipated again.

URANIUM AND PROTACTINIUM STOCKPILES

After each calculation step, the uranium (so U-233 till U-236) extracted from the breeder zone during the initial U-235 fueled phase and the uranium extracted from both breeder and driver zone during the U-233 fueled phase are added into a uranium stockpile. The Pa-233 content of the extracted pebbles is added to a protactinium stockpile. A schematic view of the use of the uranium and protactinium stockpiles in the different stages of the running-in phase is given in figure 6.1. It is assumed that reprocessing, i.e. the separation of uranium and protactinium, takes place instantaneously and that the uranium content in the stockpile is perfectly mixed. Obviously, in practice there would be some delay in the reprocessing and there will be multiple stockpiles, because a critical mass of U-233 should be avoided. These stockpiles will have a somewhat different composition depending on the extraction date of the uranium, which specifies the buildup of U-234 till U-236 that has taken place. Though such effects are relevant for more detailed fuel management studies in advanced stages of reactor design, they are not expected to have a significant influence on the trends observed during the more general studies in this chapter.

In the U-233 fueled phase, the concentrations of U-234, U-235 and U-236 in the driver fuel fed to the core, i.e. $N_{U4}(z=0,t,p=1)$, $N_{U5}(z=0,t,p=1)$ and $N_{U6}(z=0,t,p=1)$, are based on their mass ratios in the uranium stockpile. Obviously, the masses of the uranium isotopes inserted during the U-233 fueled phase are subtracted from the uranium stockpile.
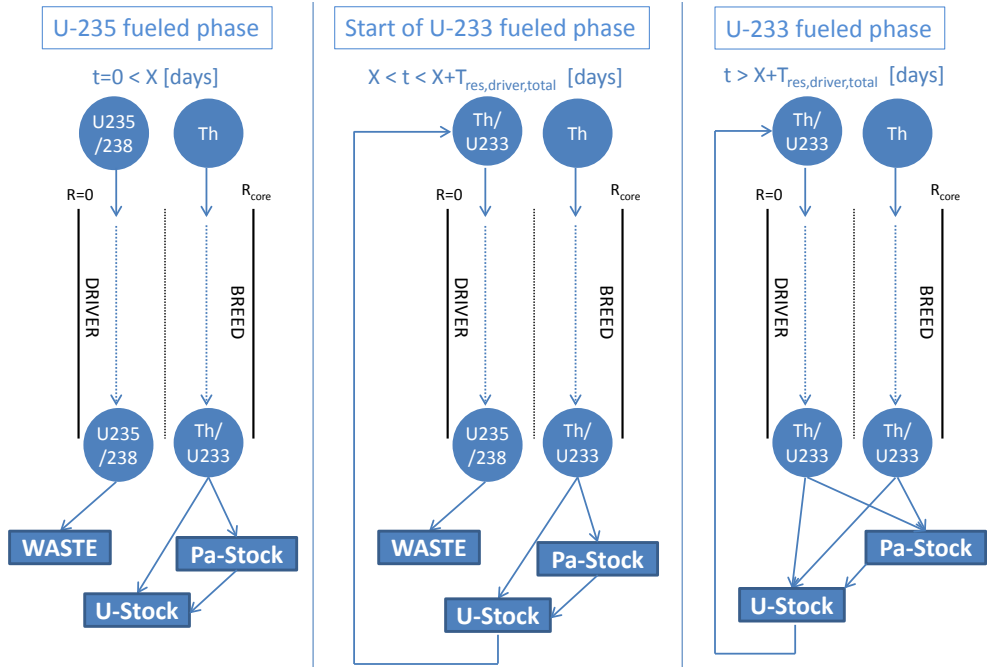
Figure 6.1: Schematic view of the use of the uranium and protactinium stockpile, after the final pebble passage, during the U-235 fueled phase and during, the start and remainder of, the U-233 fueled phase. X refers to the moment the U-233 fueled phase is started.

6

After each time-step of the calculation, the amount of Pa-233 decayed in the stockpile is transferred to the uranium stockpile. In reality, a longer timer interval before extracting the decayed U-233 from the protactinium stockpile may be more practical, but this won't affect the results significantly as the total amount of U-233 in both stockpiles remains the same.

6.1.2. CROSS SECTIONS

Obviously, the accuracy of the results obtained by the numerical scheme strongly depends on the reliability of the cross section data, i.e. the cross sections and neutron flux $\phi(z, t)$, used by the model. So, the cross sections should be collapsed with a neutron spectrum representative of the true operating conditions of the driver and the breeder zone. Microscopic cross sections have been determined using the average nuclide concentrations (and temperature) of the driver and the breeder zone in an equilibrium core composition calculation, which is discussed in more detail in the following. This way, cross sections only have to be generated for a single core slab using the CSAS and XSDRN modules included in SCALE6 [9], instead of at multiple heights. Furthermore, it only has to be performed for the equilibrium core calculation and not during the time-dependent calculation of the running-in phase. The influence of these approximations will be demonstrated to be fairly small for the equilibrium core configuration in section 6.2. During the running-in phase,

the ratio between fissile atom production and consumption may deviate somewhat more as the core composition deviates further from the equilibrium core, but this does not have a significant impact upon the time-scales involved and the trends observed in this chapter. To ensure the accuracy of the model, the cross sections are collapsed to five energy groups and the nuclide balance equations are solved using these five group cross sections and the five group fluxes obtained by DALTON, i.e. the reaction rates are determined by summing over five groups: $\sigma\phi(z,t) = \sum_{g=1}^{5} \sigma_g \phi_g(z,t)$.

A 2D(R,Z) macroscopic cross section set, to be used by DALTON, is generated by adding the microscopic cross sections multiplied with the nuclide concentrations obtained at the different heights of the driver and breeder zone using the ICE-module of SCALE6. Obviously, the macroscopic cross sections of the graphite and TRISO coating layers in the pebbles, and surrounding helium, as well as the graphite in the reflector regions are also included in the 2D cross section set.

EQUILIBRIUM CORE CALCULATION SCHEME AND CROSS SECTIONS

By setting the $\frac{\partial N_x(z,t)}{\partial t}$-terms in section 6.1.1 to zero, it is possible to calculate the equilibrium core composition by solving a similar matrix-vector system, but then without the Implicit Euler time discretization. The flux of the equilibrium core is not known a-priori, so an initial guess has to be made. The nuclide balance equations are solved using this flux guess and a new DALTON calculation is performed afterwards. This process is repeated until convergence is reached. However, the average nuclide concentrations of Th-232, Pa-233 and the uranium isotopes also require an initial guess. So, using the updated average nuclide concentrations, the microscopic cross sections can be updated and the equilibrium composition is calculated again. After a few cross section updates, this process has also converged and the equilibrium core is determined as well as the cross section set for the time-dependent calculation of the running-in phase. The U-235 and U-238 cross sections used in the driver zone during the U-235 fueled phase are collapsed after a 1D radial XSDRN-calculation using representative nuclide concentrations for the state of the reactor during this initial phase.

The equilibrium core composition obtained in section 4.4.2, with all relevant fission products included by ORIGEN, was used to determine the ratio between the different energy groups in $\sigma_{a,FP}$. The absolute value of $\sigma_{a,FP}$ was adjusted to approximate a critical core, i.e. $k_{eff} = 1.00086$, for the same operating conditions, e.g. a driver pebble residence time of 80.38 days, as the equilibrium core previously calculated in section 4.4.2. The fission product pair absorption cross sections used are shown in table 6.1.

Table 6.1: The five group fission product pair cross section

Group	Energy range	$\sigma_{a,FP}$ [b]
1	0.9 MeV - 20 MeV	0.034
2	30 eV - 0.9 MeV	2.158
3	0.625 eV - 30 eV	33.36
4	0.15 eV - 0.625 eV	60.14
5	10 meV - 0.15 eV	490.0

6.2. Equilibrium core results

T HE equilibrium core composition of the thorium PBR design, discussed in section 4.4, was calculated with the time-invariant version of the newly developed scheme, as discussed in section 6.1.2. This was done for three reasons. Firstly, the equilibrium core result of the new scheme will be used as a reference for the reactor configuration at the end of the running-in phase in order to analyse if, and how rapidly, the equilibrium core is approximated. Secondly, the microscopic cross section set obtained for the equilibrium core composition will be used for the driver fuel, during the U-233 fueled phase, and for the breeder zone throughout the whole running-in phase calculation, as explained in section 6.1.2. Thirdly, a comparison between the equilibrium core composition, calculated with the new simplified scheme (section 6.1.2) and the original equilibrium core calculation scheme from chapter 4, gives a proper estimate of the error introduced by the simplifications in the new running-in phase scheme.

A total driver pebble residence time of 80.38 days was used, as this was the result of the original equilibrium core calculation scheme. The mass flow rates calculated by the original equilibrium core calculation scheme and the new simplified method are shown in table 6.2.

Table 6.2: Comparison between equilibrium core results using the new and the original calculation scheme.

	Original equilibrium scheme	Running-in phase scheme
$T^{total}_{res,driver}$	80.38 d	80.38 d
$^{233}U_{in,driver}$	695.65 g/d	695.65 g/d
$^{233}U_{out,driver}$	605.81 g/d	605.61 g/d
$^{233}U_{out,breed}$	81.25 g/d	81.34 g/d
$^{233}Pa_{out,driver}$	7.68 g/d	7.88 g/d
$^{233}Pa_{out,breed}$	1.23 g/d	1.48 g/d
$^{233}U_{in-out}$	+8.58 g/d	+8.69 g/d
$^{233}Pa_{in-out}$	-8.91 g/d	-9.35 g/d
Net $^{233}U_{in-out}$	-0.33 g/d	-0.66 g/d
Power - Driver zone	95.67 MW$_{th}$	95.45 MW$_{th}$

The mass flow rates calculated by the different code schemes show a close agreement. The system is predicted to be a breeder by both codes, though the system's net balance of U-233, including Pa-233, is slightly more negative for the new scheme, -0.66 g/d compared to -0.33 g/d. Though this may be a large difference in relative terms, this deviation of 0.33 g/d is quite small in absolute terms considering that a bit more than 100 grams of uranium is fissioned in the system per day. For the purposes of this chapter, this deviation is acceptable. Furthermore, the fraction of the power produced in the driver zone deviates only 0.2% between the two codes.

6.3. Analysis of the running-in phase

T HIS section presents results of some initial running-in phase studies, followed by a separate analysis of the U-235 fueled phase and the U-233 fueled phase in sections

6.3.2 and 6.3.3. The k_{eff} values that will be shown in this section are of interest from a fuel management perspective, so the influence of control rods is neglected in this analysis. Obviously, a value of k_{eff} above unity in the following does not imply that the reactor will work in a supercritical state in reality. So, a k_{eff} of at least unity is desired in this analysis. On the other hand, large amounts of excess reactivity should also be avoided from a fuel economy perspective.

6.3.1. INITIAL STUDIES OF THE RUNNING-IN PHASE

First, results of some initial running-in phase studies will be presented for different feed fuel enrichments during the U-235 fueled phase. A uniform fresh driver fuel composition of 11 w% U-235 and 89 w% U-238 was used yielding an initial k_{eff} of 1.0075 for the fresh start-up core. For the feed driver fuel, three enrichments were investigated during the initial U-235 fueled phase, being 12 w%, 13 w% and 14 w% U-235. After 2000 days, the U-233 fueled phase starts and 10 w% U-233 fueled driver pebbles are added to the core, in consistence with the equilibrium core configuration introduced in section 4.4.2. The k_{eff} is shown on two time-scales for the different enrichments during the U-235 fueled phase in the top graphs of figure 6.2. The lower left graph shows the U-233 mass in the uranium stockpile over a time interval of 50 years, and the lower right graph shows the U-234, U-235 and U-236 fraction in the uranium stockpile over a time interval of 200 years.
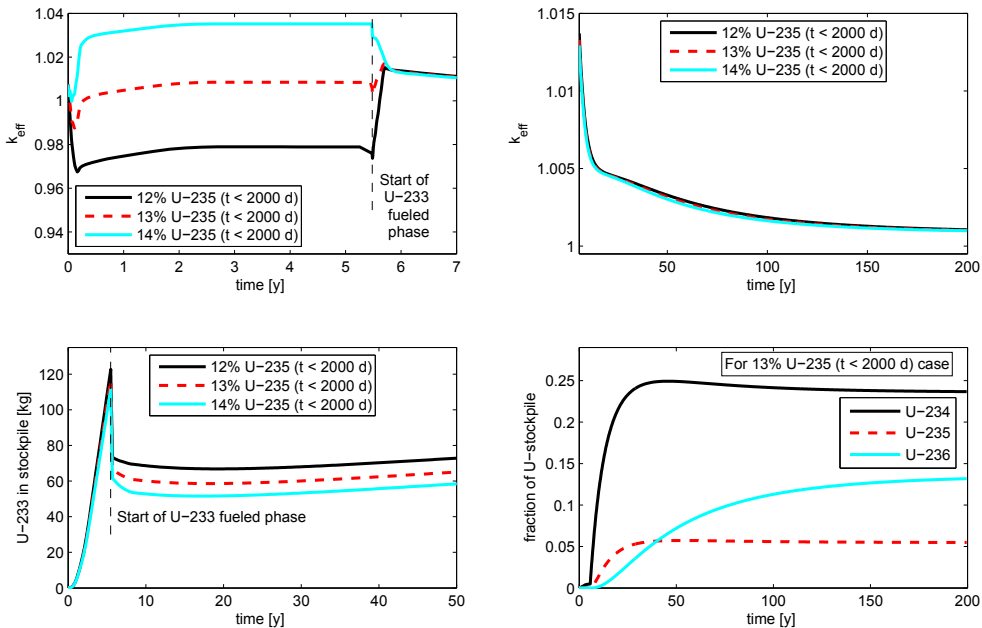
Figure 6.2: k_{eff} over short (*top left*) and longer time-scale (*top right*) and U-233 mass in stockpile over time (*bottom left*) using different U-235 enrichments during the initial U-235 fueled phase of 2000 days. The U-234, U-235 and U-236 fraction in the uranium stockpile are shown over time for a 13% U-235 feed fuel enrichment (*bottom right*).

The top left figure shows that the k_{eff} remains below unity over the whole U-235 fueled phase with a 12% enrichment during the U-235 fueled phase. For a 13% enrichment, k_{eff} is smaller than unity in the initial part of the U-235 fueled phase, but becomes larger than unity after 103 days and achieves a maximum value of 1.0085 in the U-235 fueled phase. For a 14% enrichment, the k_{eff} is generally larger than unity during the U-235 fueled phase, but it is 0.9998 for a very short moment. The maximum k_{eff} during the U-235 fueled phase is 1.0352, which is a lot higher than required. So, from a first view, an enrichment somewhat above 14% is required for the very initial stage ($t < 100$ days) of the U-235 fueled phase and a 13% enrichment afterwards. After starting the U-233 fueled phase, the k_{eff} rapidly approaches a similar value for the three different cases, because the same driver fuel is fed to the core for the three cases in the U-233 fueled phase.

For the long term behaviour (*top right graph*) it can be seen that k_{eff} remains above unity during the U-233 fueled phase. For all three cases, the k_{eff} drops quite rapidly, i.e. within 15 years, to a k_{eff} of 1.005 and than more gradually decreases to a value around 1.001, closely approximating the k_{eff} of 1.00086 in the equilibrium configuration.

The lower left graph shows that the U-233 mass in the stockpile increases rapidly in the U-235 fueled phase, since none of the U-233 extracted from the breeder zone is fed back to the core. After the start of the U-233 fueled phase, the amount of U-233 in the stockpile drops rapidly by approximately 50 kg, because U-233 is fed to the driver zone and not yet extracted, as shown in the middle scheme of figure 6.1. After the first U-233/Th driver fuel pebbles are extracted from the core, the amount of U-233 in the stockpile only reduces very slowly. Later on, the U-233 mass in the stockpile increases again after a net production of U-233 is achieved. It can also be seen that the build up of U-233 in the stockpile is a bit lower if the U-235 enrichment increases during the U-235 fueled phase. This is because a lower flux is needed to yield the same power production, which leads to a reduction of the neutron capture rate in Th-232, and because a larger fraction of the power is produced in the driver zone.

The lower right graph of figure 6.2 shows that the U-234, U-235 and especially U-236 fractions in the uranium stockpile take quite some time to reach equilibrium, which is still not fully achieved after 200 years, so multiple reactor lifetimes. However, one can also notice from the lower left graph that the minimum U-233 mass in the stockpile, after the start of the U-233 fueled phase, is quite a bit above zero. Firstly, this is undesirable from a fuel economy perspective. Secondly, the U-234, U-235 and U-236 concentrations extracted from the core are somewhat diluted after they are added to the uranium stockpile, which somewhat slows down reaching an equilibrium.

The start of the U-233 fueled phase should be timed in such a way that a sufficient amount of U-233 has been produced to feed the core without ever supplying additional U-235/U-238 fuel afterwards, while avoiding a significant excess amount of U-233. Therefore, the starting moment of the U-233 fueled phase was varied between 1300, 1500 and 2000 days in the following simulations. A 13% enrichment is used during the U-235 fueled phase, as this led to a k_{eff} close to one over the largest part of the U-235 fueled phase, as shown in the top left graph of figure 6.2. By shortening the length of the U-235 fueled phase, the excess of U-233 in the stockpile can be reduced, a net U-233 production may be achieved earlier and the U-234, U-235 and U-236 concentrations may approach equilibrium faster.

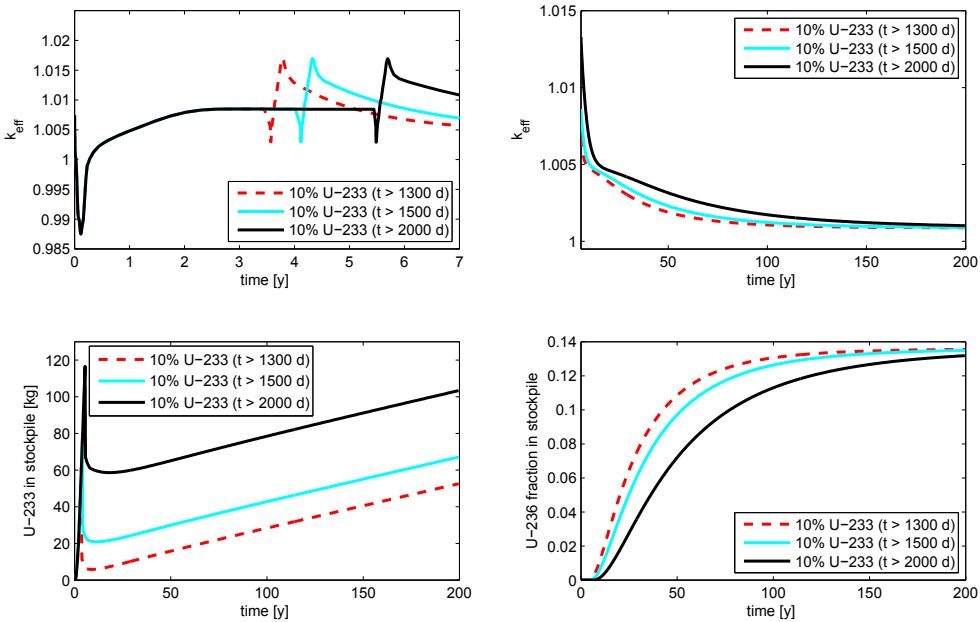Again, the k_{eff} is shown on a short and longer time-scale in figure 6.3.

Figure 6.3: k_{eff} over short (*top left*) and longer time-scale (*top right*), the U-233 mass in the stockpile over time (*bottom left*) and the U-236 fraction in the uranium stockpile over time (*bottom right*) using different starting moments for the U-233 fueled phase. A 13% enrichment was used during the U-235 fueled phase.

For practical application, the enrichment should be increased a bit during the first 100 days of the U-235 fueled phase to ensure a k_{eff} larger than unity over the whole 200 years (*top left graphs* of figure 6.2 and 6.3), which will be investigated in the next section. More importantly, an earlier start of the U-233 fueled phase (1300 days) leads to a smaller uranium stockpile (*lower left graph*) and consequently the U-234, U-235 and U-236 fractions also reach equilibrium values a lot faster (*lower right graph*). The upper right graph shows that this also influences k_{eff}, which seems to approach an equilibrium much faster if the U-233 fueled driver pebbles are added after 1300 days.

The left graph of figure 6.4 shows the system's net U-233 mass flow balance, i.e. inflow minus outflow, over time for a 1300 days U-235 fueled phase. The net balance becomes negative after 9.16 years and the system operates as a breeder. The U-233 net mass flow balance reaches an equilibrium after 200 years. The net U-233 mass flow balance, including Pa-233, of the equilibrium core (-0.6604 g/d) is closely approximated at the end of the simulation (-0.6619 g/d), as well as k_{eff} being only 1.7 pcm lower for the equilibrium core.

The right graph of figure 6.4 shows the U-234, U-235 and U-236 fractions in the uranium stockpile. The U-234 and U-235 fractions reach maxima after 25.6 and 29.3 years, followed by a slight decrease of their fraction, almost stabilizing after 200 years. The U-236 fraction slowly increases and is still slightly increasing after 200 years, but this does not have a significant influence on k_{eff} anymore.
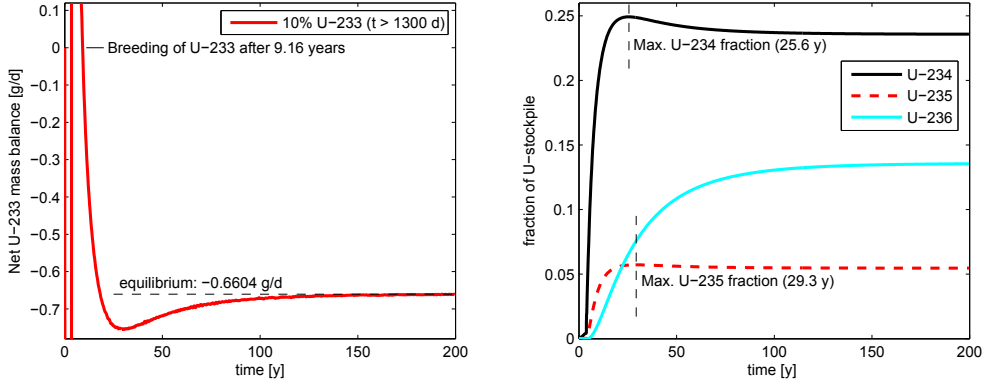
Figure 6.4: Net U-233 mass flow balance of the system (*left*) and U-234, U-235 and U-236 fraction in the uranium stockpile (*right*) over time. The U-233 fueled phase is started after 1300 days. A 13% enrichment was used during the U-235 fueled phase.

These initial studies have given a good insight in some of the characteristics and timescales of the running-in phase. There is still a shortage of reactivity in the initial stage of the U-235 fueled phase. Obviously, a higher enrichment of the driver fuel fed to the core is required in this initial stage to raise k_{eff} above unity. However, the enrichment should also be adjusted in a clever way to avoid large amounts of excess reactivity. Such studies can be performed, without analysing the U-233 fueled phase. After choosing a proper strategy for the U-235 fueled phase, the U-233 fueled phase will be analysed in order to reduce the excess reactivity during the U-233 fueled phase. Probably, this can help to achieve a net U-233 production at an earlier time. So, the following studies will be split up in an analysis of the U-235 fueled phase, followed by analysing the U-233 fueled phase.

6.3.2. FLATTENING k_{eff} IN THE U-235 FUELED PHASE

The k_{eff} changes quite a bit during the initial stage of the U-235 fueled phase. On the one hand, k_{eff} should be at least unity during the whole U-235 fueled phase, but one would also like to limit the maximum excess reactivity, for instance to 1%, to improve the fuel economy. Obviously, as the top left graph of figure 6.2 shows, this is not possible using a constant feed fuel enrichment. Therefore, a time-dependent adjustment scheme for the feed fuel enrichment is studied in this section to limit the excess reactivity during the U-235 fueled phase.

Different strategies can be considered to adjust the U-235 feed rate, η_{U5}, during the U-235 fueled phase. A relatively simple scheme is chosen for the following studies and is given by

$$\eta_{U5}^{i+1} = \eta_{U5}^i - \alpha \frac{\left(k_{eff}^i - k_{eff}^{i-1}\right)}{\Delta t} - \beta \left(k_{eff}^i - k_{eff}^{desired}\right). \tag{6.17}$$

So, the U-235 feed rate of the new time-step η_{U5}^{i+1} is determined by adding two terms to the feed rate of the previous time-step η_{U5}^i. The first term is a proportionality constant α

111

multiplied with the rate of change of k_{eff} and this term should stabilize k_{eff} on the shorter term. The constant α should be sufficiently large to ensure that rapid changes of k_{eff} can be sufficiently compensated by the feed fuel to ensure $k_{eff} > 1$. But a too large value of α will make the system unstable, because changing the feed fuel enrichment affects the reactivity over a long time-scale, i.e. proportional to the total driver pebble residence time.

The second term is a constant β multiplied by the difference between the actual k_{eff}^i and a desired final value: $k_{eff}^{desired}$. This term should ensure that the feed fuel enrichment is chosen in such a way that k_{eff} converges to the desired value of k_{eff} in the later stage of the U-235 fueled phase. The value of $k_{eff}^{desired}$ will be slightly larger than unity, e.g. 1.0002, to ensure the system is critical during any stage of the U-235 fueled phase.

Many other schemes might be considered to flatten k_{eff} by adjusting the feed fuel enrichment during the running-in phase. The advantage of this scheme is that it is rather simple and easy to implement. On the other hand, a disadvantage of this method is that the optimal values for α and β may differ among different reactor designs (and fuel management parameters). An interesting suggestion to resolve the latter problem would be an alternative scheme where the derivative of k_{eff} is minimized by adjusting the feed fuel enrichment within a first-order perturbation theory formulation. However, such a scheme is more cumbersome to implement and computationally more intensive due to the calculation of the adjoint fluxes, while the simple scheme of equation 6.17 will already prove to be quite effective for the current application.

Results

In the following, results will be shown for the U-235 fueled phase, using different values for α and β. Two goals should be achieved during the U-235 fueled phase. First, the k_{eff} should be above 1 during any stage of the running-in phase and preferably lower than 1.01, the latter value is in conjunction with the excess reactivity considered for the control rod positioning problem in section 5.1. Secondly, one would like the k_{eff} to stabilize quickly around the value of $k_{eff}^{desired}$.

Figure 6.5 shows k_{eff} as a function of time using different values of $\alpha/\Delta t$ (*left plot*) and β (*right plot*) to determine the enrichment of the feed fuel during the U-235 fueled phase. As the enrichment of the feed fuel is adjusted during each time-step in the calculation scheme, the flux shape is updated by DALTON at least every 20 Δt-steps during these calculations to ensure sufficient accuracy. The use of a larger coefficient $\alpha/\Delta t$ clearly reduces the maximum k_{eff}, but it takes longer to approach the desired k_{eff} of 1.0002. The use of a larger coefficient β can help to limit the maximum k_{eff} value and speed up approaching the desired k_{eff}. However, β should not be too high to avoid sub-criticality of the reactor and to avoid inducing oscillatory behaviour of the k_{eff}.

A few other combinations of $\alpha/\Delta t$ and β have been investigated in figure 6.6. From the two graphs in figure 6.6, it can also be seen that the k_{eff} (*top*) responds very closely to changes in enrichment (*bottom*). Using a combination of a relatively large coefficient $\alpha/\Delta t$ (=4.0) and β (=0.005) leads to a relatively fast approach of the desired k_{eff}, while the k_{eff} remains above unity for the whole U-235 fueled phase. Except for a few days of the initial stage ($k_{eff}^{max} = 1.0111$ after 9 days), the k_{eff} remains below 1.01 during the U-235 fueled phase. So, the enrichment over time prescribed by these coefficients is very suitable for the U-235 fueled phase.
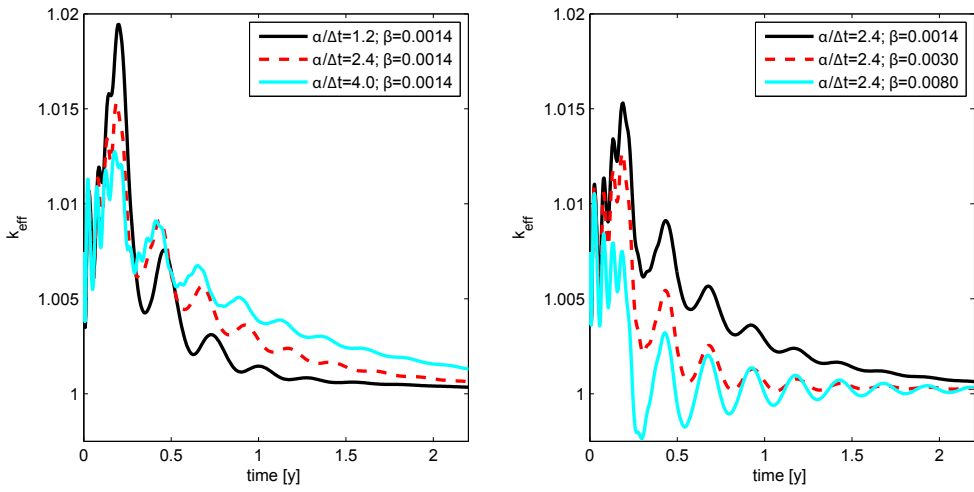
Figure 6.5: k_{eff} as a function of time using different values of $\alpha/\Delta t$ (*left*) and β (*right*) to adjust the enrichment of the driver fuel, according to equation 6.17.
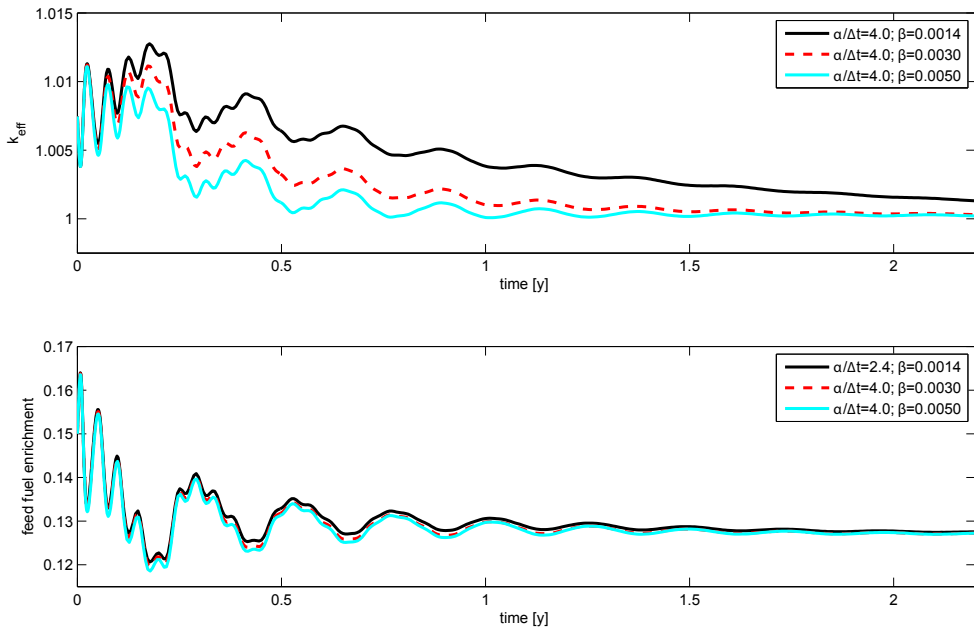

Figure 6.6: The upper graph shows k_{eff} as a function of time using different values of $\alpha/\Delta t$ and β to adjust the enrichment of the driver fuel, according to equation 6.17. The lower graph shows the feed driver fuel enrichment as a function of time.

However, the enrichment prescribed varies quite fast and quite a lot over time, i.e. between 11.9 w% and 16.3 w%. For practical application, it would be best to manufacture pebbles with a high enrichment, e.g. 17 w%, and pebbles with a low enrichment, e.g. 11 w% similar to the start-up core enrichment. To first order, the range of enrichments required during the U-235 fueled phase can then be attained by mixing of high enriched and lower enriched pebbles with the proper ratio. The difference in self shielding between a mixture with equal fractions of 11 w% and 17 w% enriched pebbles and the same amount of 14 w% pebbles is only a second order effect, which can also be compensated for by adjusting the fraction of higher enriched pebbles. Around 242 fresh driver fuel pebbles are added into the core per time-step of 2.5 hours. So, even on such a short time-scale, a relatively fine regulation of the feed driver fuel enrichment is possible.

After the start of the U-233 fueled phase, a drop in the k_{eff} occurs, as can be observed in the top left graph of figure 6.3. In order to avoid k_{eff} from dropping below unity, an increase of the U-235 enrichment to 15% is used in the following calculations during the final 80 time-steps (8.33 days) of the U-235 fueled phase. Due to the increase of the enrichment, the k_{eff} increases from 1.0002 to 1.0085 at the start of the U-233 fueled phase.

6.3.3. FLATTENING k_{eff} IN THE U-233 FUELED PHASE

The U-233 fueled phase is started after 1300 days, as this was shown to be the best option by the results in figure 6.3. For the first stage of the U-233 fueled phase, i.e. up to 25,000 time-steps or 7.13 years including the U-235 fueled phase, a similar scheme as in equation 6.17 is proposed to determine the U-233 weight fraction of the feed fuel. For a value of 4 for $\alpha/\Delta t$, the k_{eff} and the U-233 weight fraction of the feed driver fuel are shown as a function of time for β-values of 0.002, 0.003 and 0.004 in figure 6.7. A value of β of 0.005, like in the previous paragraph, led to k_{eff} values lower than unity. A value of β of 0.004 leads to a quick approach of the desired k_{eff} (of 1.0002), with little excess reactivity and without subcriticality.

Similar to the U-235 fueled phase, the flux shape profile was updated at least every 20 time-steps during the initial part of the U-233 fueled phase. Since a single five-group DALTON calculation takes around six minutes, a slightly different approach with larger flux update intervals, up to a maximum of 1000 time-steps per interval, should be chosen to avoid calculation times of several months for the remaining part of the U-233 fueled phase, from 25,000 up to 700,000 time-steps. It is also possible to lengthen the flux shape update interval, as figure 6.7 shows that k_{eff} is almost stable after 6 years, while the oscillations in the U-233 weight fraction have also damped out. There is still a slow increase of the U-233 weight fraction, associated with the long time-scale of saturation of the U-234, U-235 and U-236 fraction in the uranium stockpile, but this effect can also be described with a larger flux update interval. However, with a value of 4 for $\alpha/\Delta t$ and 0.004 for β, the scheme tends to become unstable and k_{eff} drops a bit below unity on such a longer flux update interval.

Different approaches are proposed to determine the U-233 weight fraction of the driver fuel during the remaining part of the U-233 fueled phase.

- Use a constant value of 10 w% U-233 in the fresh driver fuel pebbles after 25,000 time-steps. Only one pebble type is required for the remaining part of the U-233 fueled phase, at the price of some additional excess reactivity. Ideally, one could even use 10 w% U-233 driver pebbles from the start of the U-233 fueled phase, so
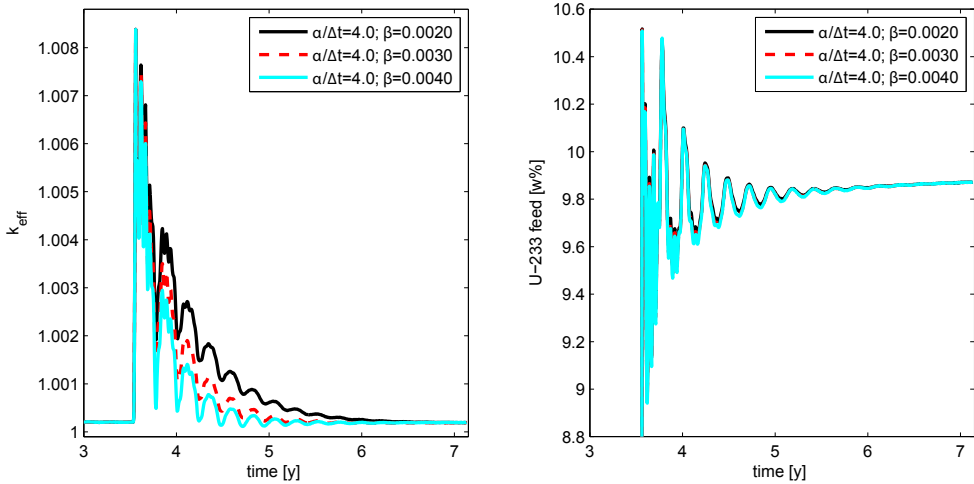
Figure 6.7: The left graph shows k_{eff} as a function of time for the initial part of the U-233 fueled phase, which starts after 1300 days, using different values of $\alpha/\Delta t$ and β to adjust the enrichment of the driver fuel, according to equation 6.17. The right graph shows the U-233 weight fraction of the feed driver fuel as a function of time.

that only one fuel pebble type has to be manufactured, which would significantly ease fuel fabrication and lower production costs. However, this leads to a relatively high maximum k_{eff} of 1.0229. Results for both approaches will be shown in the following.

- Use equation 6.17, but with smaller coefficients $\alpha/\Delta t = 1.0$ and $\beta = 0.002$ to enhance stability. The changes of k_{eff} that have to be compensated are also much smaller and on a long time-scale in this part of the running-in phase, so smaller coefficients $\alpha/\Delta t$ and β should also suffice. The thresholds before doubling the length of the neutron flux update interval, as mentioned in section 6.1.1, were increased to 10^{-7} for the flux shape change and 10^{-5} for the change of k_{eff}, to increase the stability of the calculation in combination with the U-233 weight fraction adjustment scheme.

The multiplication factor and the U-233 mass in the stockpile are shown as a function of time for these three approaches in figure 6.8. Clearly, the excess reactivity is rather large in case of using 10 w% U-233 driver fuel pebbles directly from the start of the U-233 fueled phase. Using a variable U-233 weight fraction for the fresh driver fuel pebbles limits the excess reactivity and criticality is approached rapidly. This also has a positive effect on the fuel economy of the system. The U-233 mass in the stockpile increases much quicker after breeding is achieved. Secondly, a net production of U-233 is already achieved after 6.3 years with a variable feed fuel U-233 weight fraction instead of after 9.3 years with a constant 10 w% U-233 weight fraction during the whole running-in phase. So, both in terms of limiting excess reactivity and improving the fuel economy, a variable U-233 weight fraction of the fresh driver fuel is preferred and this approach will also be used during the safety studies in the following section.
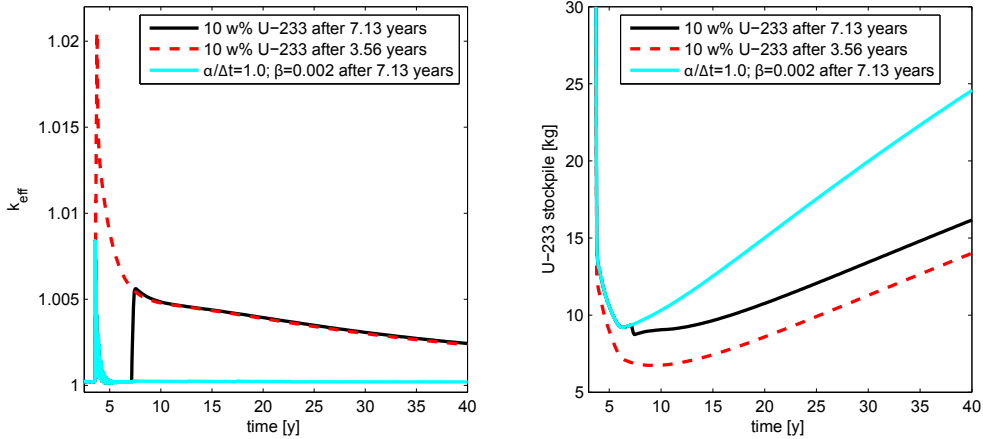
Figure 6.8: k_{eff} as a function of time using three approaches for the U-233 fueled phase: A variable U-233 weight fraction is fed to the driver zone using $\alpha/\Delta t = 4.0$ and $\beta = 0.004$ until 7.13 years and 10 w% U-233 is used afterwards (case 1), or 10 w% U-233 is fed in the driver zone directly after 3.56 years (case 2) or a variable U-233 weight fraction with $\alpha/\Delta t = 4.0$ and $\beta = 0.004$ is used until 7.13 years and $\alpha/\Delta t = 1.0$ and $\beta = 0.002$ afterwards (case 3). The right graphs shows the U-233 mass in the stockpile as a function of time.

6.4. PASSIVE SAFETY DURING THE RUNNING-IN PHASE

IN section 4.4, the 100 MW$_{th}$ thorium breeder PBR was demonstrated to be passively safe within the equilibrium state. Obviously, one would also like such a reactor to operate in a passively safe manner during all stages of the running in phase. Therefore, a basic safety analysis is performed in this section. First, the impact of a DLOFC with scram is studied for various stages of the chosen running-in phase strategy, followed by a study of the uniform reactivity coefficient over time and a study of the maximum reactivity insertion due to water ingress.

DLOFC without scram scenarios are not simulated in this chapter. The temperature feedback of U-235/U-238 fuel is generally stronger negative than for Th/U-233 fuel, as will also be demonstrated in section 6.4.2. Therefore, it can be anticipated that a failure to scram does not lead to a significant additional temperature increase during the initial part of the running-in phase, since the reactivity insertion by xenon decay can already be compensated by a much smaller increase of the average core temperature. Furthermore, fully coupled transient simulations of a DLOFC without scram are very time-consuming to perform.

6.4.1. DLOFC WITH SCRAM

A loss of pumping power and a depressurization of the core mark the beginning of a DLOFC transient, during which conduction and radiation are the main heat transfer mechanisms for decay heat removal. During the DLOFC transient, the maximum fuel temperature should remain below 1600 °C to ensure that radioactive fission products are retained within the coated fuel particles [10]. The maximum fuel temperature that occurs during a DLOFC with scram is strongly determined by the power density distribution over the core, espe-

cially the maximum power density, and the geometry of the core. Since the latter does not change over time, the change of the maximum power density (during normal operation) throughout the running-in phase is an important indication of how the maximum fuel temperature during a DLOFC with scram will be affected throughout the running-in phase, as compared to a DLOFC occurring in the equilibrium configuration. The evolution of the maximum power density (during normal operation) throughout the running-in phase is shown in the upper graphs of figure 6.9.
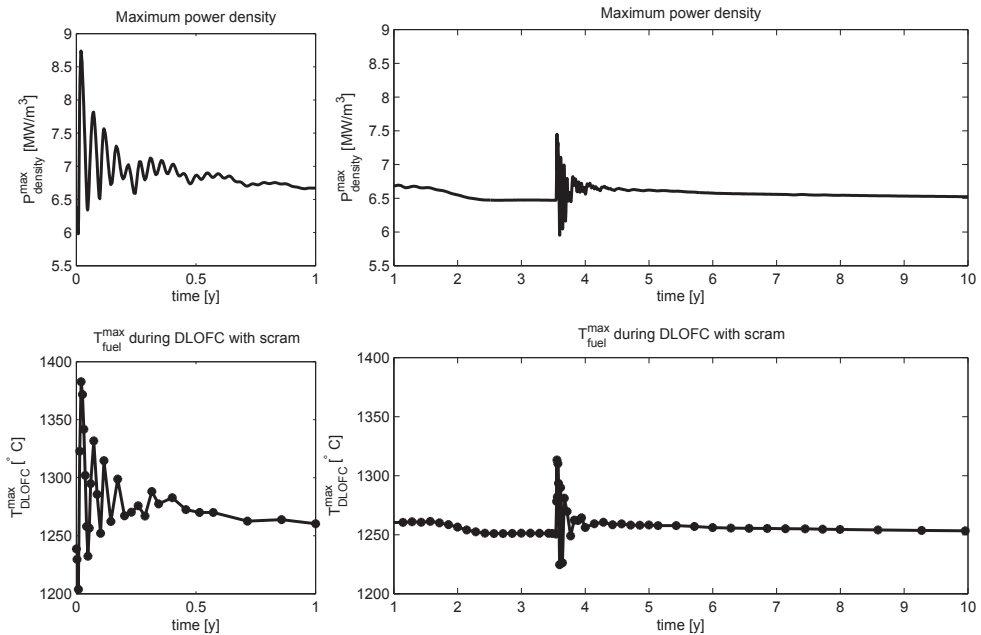
Figure 6.9: Evolution of the maximum power density during normal operation throughout the running-in phase (*top*) and evolution of the maximum fuel temperature that occurs during a DLOFC with scram throughout the running-in phase (*bottom*). The U-233 fueled phase starts after 1300 days.

The maximum power density during normal operation fluctuates quite a bit during the initial part of the U-235 fueled phase. These fluctuations are a consequence of the variations in the enrichment of the feed driver fuel. The maximum power density quickly reaches a peak value of 8.74 MW/m^3. The fluctuations in maximum power density disappear after around a year, as the fluctuations in the feed fuel enrichment also decrease in magnitude, as shown in figure 6.6. During the remainder of the U-235 fueled phase, the maximum power density during normal operation slowly reduces as the U-233 concentration builds up in the breeder zone, resulting in a decrease of the fraction of the power produced in the driver zone. At the start of the U-233 fueled phase, some fluctuations in the maximum power density occur again due to the variation of the U-233 weight fraction in the fresh driver fuel during the initial part of the U-233 fueled phase. However, the maximum power density peak (7.45 MW/m^3) is smaller than in the U-235 fueled phase. Later on, the maximum power density slowly decreases to reach a value of 6.52 MW/m^3 after

10 years, 6.46 MW/m^3 after 40 years, and stabilizes at a value of 6.45 MW/m^3 after 200 years. This is slightly lower than the value of 6.89 MW/m^3 calculated with the more detailed equilibrium core model in section 4.4.2, including all relevant fission products and thermal-hydraulic feedback.

The maximum fuel temperature during a DLOFC with scram was also calculated for various stages of the running-in phase using the THERMIX code scheme. The geometrical THERMIX-model used is equivalent to the model used in chapter 4. The power density determined by DALTON in the running-in phase calculation scheme is used in a single THERMIX calculation to approximate the steady-state temperature distribution in the core, i.e. no thermal-hydraulic feedback is taken into account as the cross sections were generated for a single driver and breeder zone temperature. The steady-state temperature profile is used as the initial condition for the THERMIX calculation of the DLOFC with scram, which is calculated in a similar way as in chapter 4. However, to save computation time, the transient calculation is performed without convection. This has only limited impact on the maximum fuel temperature, approximately +1 °C in comparison with a DLOFC calculation with convection, during the transient at atmospheric pressure and it is a conservative assumption, since the heat removal decreases slightly. The maximum fuel temperature during a DLOFC with scram is shown for various stages of the running-in phase in the lower graphs of figure 6.9.

The maximum fuel temperature after a DLOFC fluctuates quite a bit during the initial stages of the running-in phase, in a very similar manner as the maximum power density. Some small differences in these oscillations might be noticed because the maximum fuel temperature is simulated for less time-steps than the maximum power density. It reaches its maximum value (1383 °C) along with the maximum power density (8.74 MW/m^3). This maximum temperature is still quite a bit below the TRISO failure temperature of 1600 °C. At the start of the U-233 fueled phase, the maximum DLOFC temperature also fluctuates a bit, along with the U-233 weight fraction of the feed fuel and the maximum power density, but the peak temperature is much lower (1313 °C). At the end of the running-in phase, the maximum fuel temperature during a DLOFC with scram is 1250 °C, which is slightly lower than the value of 1280 °C calculated previously with the more detailed equilibrium core model in section 4.4.2. Such a difference could be expected due to the difference in the maximum power density, as discussed previously. Clearly, the maximum fuel temperature (+30 °C) predicted by the simplified scheme is not conservative for the equilibrium core, but the effect is fairly small compared to the remaining margin with respect to the TRISO failure temperature of 1600 °C.

6.4.2. UNIFORM REACTIVITY COEFFICIENT AND DLOFC WITHOUT SCRAM

The cross section generation methodology for the running-in phase model was explained in section 6.1.2. In addition to the cross section set generated using the average equilibrium core temperature per radial zone, a similar cross section set was generated with a 500 K temperature increase. The uniform reactivity coefficient is determined by comparing the k_{eff}-values calculated by DALTON using these two cross section sets. The uniform temperature reactivity coefficient is shown as a function of time during the running-in phase in figure 6.10.

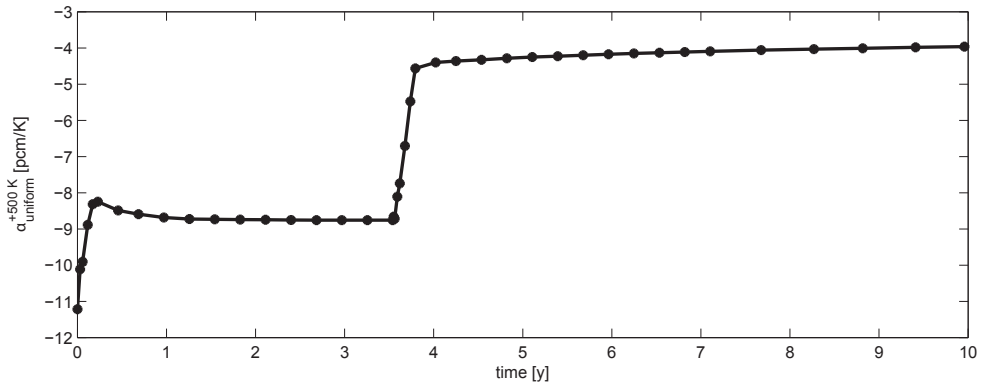The reactivity coefficient is strongly negative (-11.2 pcm/K) for the start-up configu-

Figure 6.10: Uniform temperature reactivity coefficient as a function of time during the running-in phase. These coefficients were calculated based on a uniform temperature increase of 500 K. The U-233 fueled phase starts after 1300 days.

ration with the uniform 11% enriched driver pebbles and rapidly weakens to a value of -8.2 pcm/K and then slowly becomes a bit stronger negative again. There is a rapid reduction of the reactivity coefficient's magnitude after starting the U-233 fueled phase (1300 days). Finally, a uniform reactivity coefficient of -3.68 pcm/K is achieved after 200 years. This value is very close to the value of -3.67 pcm/K calculated in section 4.4.2.

Since the reactivity coefficients are much stronger negative during the U-235 fueled phase, it can be expected that the reactivity insertion due to xenon decay during a DLOFC without scram can easily be compensated by the temperature feedback. Therefore, it can be expected that a DLOFC without scram leads to significantly lower maximum fuel temperatures after recriticality during the U-235 fueled phase than for the equilibrium core, which reaches a maximum temperature of 1481 °C during a DLOFC without scram due to the much weaker reactivity coefficient (section 4.4.2).

6.4.3. WATER INGRESS
In view of passive safety, the reactivity insertion caused by water ingress should be compensated by a temperature increase of the core without the maximum fuel temperature exceeding 1600 °C to ensure the retention of radioactive fission products.

Cross section sets were generated using different levels of water ingress according to the cross section processing method discussed in section 6.1.2, the water ingress itself was included in the cross section generation scheme in a similar way as in section 4.4.3. For different stages of the running-in phase, the reactivity insertion due to water ingress was calculated for water densities ranging from 4 to 40 kg/m^3 of the total core volume (so helium plus pebble), increasing in steps of 4 kg/m^3. The maximum possible reactivity insertion over time is shown in figure 6.11.

During the U-235 fueled phase, the reactivity insertion due to water ingress first increases rapidly after uranium with a higher enrichment is fed to the core. It slowly decreases later on as the amount of fissile U-233 in the breeder zone slowly starts to increase, causing a lower requirement on the enrichment of the feed driver fuel to main-
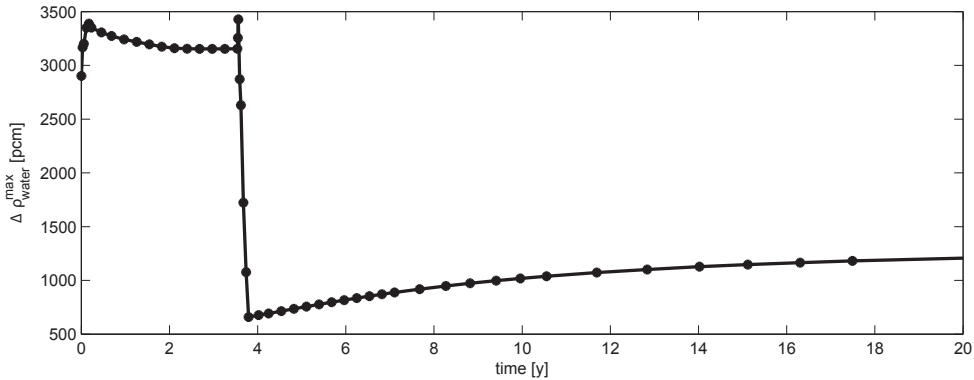
Figure 6.11: Maximum reactivity insertion due to water ingress as a function of time during the running-in phase. The U-233 fueled phase starts after 1300 days.

tain criticality, which results in a less undermoderated state of the driver zone. In the final 80 time-steps of the U-235 fueled phase, the maximum reactivity insertion due to water ingress increases a bit due to the slight increase of the U-235 feed fuel enrichment. After the start of the U-233 fueled phase (1300 days), the maximum reactivity insertion due to water ingress strongly decreases as the U-233 replaces the U-235 in the driver zone. Afterwards, it slightly increases again and has a value of +1345 pcm after 200 years, when the equilibrium configuration is closely approximated. This value is a bit lower than the maximum reactivity insertion of +1497 pcm calculated in section 4.4.3, but this calculation also included a large number of fission products, actinides and thermal-hydraulic feedback to determine the steady-state power profile.

Water ingress can clearly cause a more severe reactivity insertion during the U-235 fueled phase, since the driver zone is in a stronger undermoderated state. However, even in absence of a reactor scram, this is not a real safety concern since the reactivity coefficient of the core is also much stronger negative in the U-235 fueled phase. So, also for the U-235 fueled phase, any reactivity insertion caused by ingress of water can eventually be compensated by the temperature feedback without exceeding the TRISO failure temperature of 1600 °C. It should also be noticed that the strong decrease of the uniform reactivity coefficient after the start of the U-233 fueled phase occurs simultaneously with the decrease of the maximum reactivity insertion due to water ingress. There is no transition moment where weak reactivity coefficients can lead to a dangerous temperature increase in case of water ingress.

The passive safety of the equilibrium core of the 100 MW_{th} thorium breeder PBR has been demonstrated previously in section 4.4. After investigating several safety parameters related to the severest incidents that can occur in a Pebble Bed Reactor, it can be concluded that the thorium breeder PBR can also fulfill the same passive safety requirements during the running-in phase.

6.5. Conclusions and recommendations

THE studies presented in this chapter give an insight into the time-scales involved in the running-in phase of a passively safe thorium breeder PBR. After using U-235/U-238 startup fuel for 1300 days, the system starts to work as a breeder, i.e. the U-233 (and Pa-233) extraction rate exceeds the U-233 feed rate, within 7 years after start of reactor operation. Furthermore, the U-233 in the core at the end of reactor life can be used to start a new thorium PBR after reprocessing. So, the use of U-235/U-238 start-up fuel is only required for an extension of the fleet of thorium PBRs.

The studies also show that flattening the k_{eff} by a cleverly chosen time-dependent scheme for the U-233 weight fraction or enrichment of the feed driver fuel, leads to a significant improvement of the fuel economy of the system and contributes to achieving breeding of U-233 in a relatively short time (< 7 years).

Furthermore, a basic safety analysis was performed for the chosen running-in phase strategy. Results show that passive safety is also ensured during the running-in phase. The maximum fuel temperature during a DLOFC with scram remains far below the TRISO failure temperature of 1600 °C [10] during every stage of the running-in phase and the maximum temperatures are similar to a DLOFC occurring in the equilibrium core. Uniform reactivity coefficients are stronger negative for cores with U-235/U-238 driver fuel than in case of U-233/Th driver fuel. This ensures that water ingress, despite causing a stronger reactivity insertion for U-235/U-238 driver fuel, can be compensated by the temperature feedback. It should also ensure that the reactivity insertion due to xenon decay during a DLOFC without scram does not lead to a significant maximum fuel temperature increase in comparison with a DLOFC with scram during the initial stage of the running-in phase.

The calculations performed in this chapter involved some simplifications. For improved accuracy of the results, it would be good to investigate the running-in phase using more radial depletion zones with a realistic radial pebble velocity profile. Though results in section 4.4.5 show that the use of multiple radial depletion zones only has a limited impact upon the conversion ratio, it could somewhat delay the stabilization of the k_{eff} in the running-in phase [7], as well as the desired fuel management strategy. Furthermore, including all fission products and relevant minor actinides into the depletion calculation should yield more accurate results and allows for studying the radiotoxicity of the nuclear waste. Finally, results of the DLOFC calculation could be somewhat improved by including the thermal-hydraulic feedback into the calculation of the steady-state power profile.

However, these modelling refinements are not expected to have a great effect on the trends observed in this chapter, i.e. the slow build-up of the U-234, U-235 and U-236 concentrations, the relevance of optimizing the fuel management strategy with respect to the fuel economy and the main observation that a net U-233 production can be achieved after a limited time within a passively safe thorium PBR.

References

[1] H. J. Rütten and K. A. Haas, *Research on the incineration of plutonium in a modular HTR using thorium-based fuel,* Nuclear Engineering and Design **195**, 353–360 (2000).

[2] H. Chang, Y. Yang, X. Jing, and Y. Xu, *Thorium-based fuel cycles in the modular high temperature reactor,* Tsinghua Science and Technology **11**, 731–738 (2006).

[3] E. Mulder, D. Serfontein, W. van der Merwe, and E. Teuchert, *Thorium and uranium fuel cycle symbiosis in a pebble bed high temperature reactor,* in *High temperature Reactor Conference 2010* (Prague, Czech Republic, 2010).

[4] H. J. Rütten, K. A. Haas, and C. Pohl, *Computer Code System V.S.O.P. (99/11): Update 2011 of V.S.O.P(99)-Version 2009 CODE MANUAL,* Forschungszentrum Jülich (2012).

[5] B. Xia, F. Li, and Z. Wu, *The simulation of the running-in phase of the HTR-10,* in *ICONE-19* (Osaka, Japan, 2011) the 19th International Conference On Nuclear Engineering.

[6] J. Oppe, J. C. Kuijper, J. B. M. de Haas, E. C. Verkerk, and H. T. Klippel, *Modeling of continuous reload HTR systems by the PANTHERMIX code system,* in *M&C 2001* (Salt Lake City, Utah, USA, 2001).

[7] A. Marmier, M. A. Fütterer, K. Tucek, J. C. Kuijper, J. Oppe, B. Petrov, J. Jonnet, J. L. Kloosterman, and B. Boer, *Fuel cycle investigation for wallpaper-type HTR fuel,* Nuclear Technology **181**, 317–330 (2013).

[8] L. Massimo, *Physics of high-temperature reactors* (Pergamom Press, 1976).

[9] Radiation Safety Information Computational Center, Oak Ridge National Laboratory, *"SCALE: A Modular Code System for Performing Standardized Computer Analyses for Licensing Evaluations", Vols. I-III, Version 6, CCC-750; ORNL/TM-2005/39* (2009).

[10] W. Schenk, G. Pott, and H. Nabielek, *Fuel accident performance testing for small HTRs,* Journal of Nuclear Materials **171**, 19–30 (1990).

6

7

CONCLUSIONS AND RECOMMENDATIONS

A PPLYING a thorium fuel cycle within the pebble bed reactor (PBR) design, with its inherent safety features and high temperature applications, is a very interesting option for future energy supply. The use of thorium leads to an increased resource availability for nuclear power generation and can reduce the radiotoxicity and required storage time of nuclear waste. Combining breeding, passive safety and high temperature applications would result in a state-of-the art reactor design, capable of fulfilling the demands on nuclear power generation for the 21-st century. This thesis work has investigated whether it is possible to physically realize such a system and under which conditions.

7.1. CONCLUSIONS

T HE main conclusion of this thesis is that breeding, i.e. a net production rate of U-233, can be achieved within a passively safe thorium pebble bed reactor after a limited time (< 7 years). But the margins in terms of breeding, safety and practical constraints are rather small. Therefore, a passively safe thorium breeder PBR could only be achieved with a doubling of the fuel pebble handling speed as compared to the HTR-PM, as well as a high fuel pebble reprocessing rate. Alternative configurations with a lower pebble handling speed and reprocessing rate, but compromising either breeding (i.e. CR = 0.9660) or a passive safety feature (i.e. DLOFC without scram), are also possible. An overview of the most relevant conclusions drawn in this thesis work is given in the following:

- Fuel design studies show that the conversion of thorium into U-233 can be maximized for thorium pebbles with a large heavy metal loading of 30 g, using the standard fuel kernel radius of 0.025 cm, irradiated at low specific power. However, the use of a lower heavy metal loading, or the addition of moderator pebbles, is required to enhance fission. In neither case, criticality can be achieved for a system consisting of pebbles of a single metal loading, either high or low. So, breeding can only be achieved in a thorium PBR consisting of zones with different moderation ratios, either to enhance conversion or to enhance fission.

- Equilibrium core design and fuel management studies in chapter 3 show that breeding can only be achieved in a thorium PBR if the uranium content from all the pebbles extracted from the system is reprocessed and loaded into the fresh driver fuel pebbles.

- Coupled neutronics and thermal-hydraulics design studies, with inclusion of the spectral influence of the surrounding zones (driver, breeder and reflector) upon depletion of the fuel, show that high conversion ratios (CR > 0.96) and passive safety can be combined in a thorium PBR within a practical operating regime, in terms of thermal power, residence times and pebble handling speed.

- By increasing the U-233 content of the fresh driver fuel pebbles to 18 w%, breeding is already achieved for a relatively small 220 cm core radius. The decay heat removal is sufficient in this design, but the temperature feedback of the undermoderated driver pebbles is not strong enough to compensate the reactivity insertion due to the decay of Xe-135 during a DLOFC without scram.

- With a lower U-233 content per driver pebble (10 w%), it is possible to combine breeding and passive safety for a 300 cm core and 100 cm driver zone radius operating at a thermal power of 100 MW. However, the pebble handling speed needs to be doubled and a high reprocessing rate of the fuel pebbles is required. This design is passively safe with a maximum fuel temperature of 1481 °C during a DLOFC without scram and a maximum reactivity insertion of +1497 pcm due to water ingress.

- Using a more detailed core depletion model with eight radial depletion zones, instead of two, had only a small influence on the conversion ratio of the three designs, i.e. the two breeder designs remain breeders also for the eight-zone model. With eight radial depletion zones, the driver pebble residence time increases and the maximum power density reduces. So, results obtained with the two-zone model are accurate in terms of conversion ratio, while results are conservative in terms of fuel pebble handling speed and safety.

- For the passively safe thorium breeder design, the reactivity worth of rods inside the radial reflector was insufficient to achieve cold reactor shutdown, requiring a control rod worth of over 15000 pcm. Placing 20 control rods just outside the driver zone, between 100 cm and 110 cm radius, will provide the required reactivity worth, also if one or two control rods fail to insert. Furthermore, BF_3 can be inserted into the primary circuit as an additional emergency shutdown system to achieve a sufficient reactivity worth with a relatively small amount of gas.

- With a clever adjustment of the enrichment or U-233 weight fraction of the feed driver fuel over time, the thorium PBR starts to breed fuel within 7 years after starting reactor operation. A basic safety analysis for the various stages of the running-in phase, including uniform reactivity coefficients, maximum power density, maximum fuel temperature during a DLOFC with scram and water ingress, indicates that the thorium breeder PBR is also passively safe during every stage of the running-in phase.

7.2. Recommendations

Tшıs thesis work has clearly shown the advantages and possibilities of a passively safe thorium breeder PBR, but it should also be noticed that quite a few technical issues should still be addressed and that further modelling refinements are advisable for future design studies. First, recommendations for additional calculational refinements will be presented, followed by an overview of recommendations related to the design and fuel management of the passively safe thorium breeder PBR.

Calculational refinements

- The accuracy of the calculation schemes can still be improved further by the use of newer neutron cross section libraries (ENDF/B-VII). This is important as changes in cross section data could affect design choices because of the relatively small margins in terms of breeding, safety and practical constraints. However, a broad group library structure like the 44-group ENDF/B-V library is not available (yet), while the use of 238-group libraries would significantly increase computation times. Secondly,

the use of a specific decay heat profile for U-233 (instead of U-235) will influence the maximum temperature during a DLOFC, as well as a more accurate spatial decay heat profile, i.e. accounting for the power history, irradiation time and flow of different pebbles classes. However, the (average) irradiation time, t_0, of 365 days used in chapter 4 was also conservative for the cases considered, as all total driver pebble residence times in chapter 4 are smaller than two years. So, it should be noted that these modelling refinements might also have a positive influence upon the conversion ratio or passive safety.

- Results in section 4.4.5 indicate that more radially detailed models can be used to minimize the maximum power density, the fuel pebble handling speed and reprocessing rate, while preserving a similar conversion ratio. More realistic non-uniform radial pebble flow velocity profiles, under the influence of the conus region and defueling chute(s), can also be included in such more detailed studies.

- The accuracy of the running-in phase calculations can be improved by using more extensive models that include all fission products and the thermal-hydraulic feedback of the steady-state cores, which form the initial condition of the DLOFC calculations. However, this is not expected to have a huge impact on the trends observed in chapter 6. For example, the maximum DLOFC temperature was found to be 30 °C higher for the original equilibrium core calculation in chapter 4, which included these effects.

REACTOR DESIGN AND FUEL MANAGEMENT

- The total helium mass flow rate (480.2 kg/s) is very high for a 100 MW$_{th}$ core, as compared to 96 kg/s for the 250 MW$_{th}$ HTR-PM. This is due to the small fraction of the helium coolant flowing through the driver zone, a net mass transfer from the hot driver zone into the colder breeder zone and due to the relatively high inlet temperature of the helium (364.5 °C) after premixing with the helium flowing out of the breeder zone. The large mass flow rate may significantly reduce the efficiency of the reactor, from 40% to 28% as a rough estimate, due to the large pumping power requirement, which is around 7 times higher as for the HTR-PM. The pumping power could be reduced quadratically by increasing the system pressure, but this also increases the reactor's construction costs.

- One possible solution for the large helium mass flow rate is the use of a graphite layer to separate the driver from the breeder zone. This way, separate pebble flow speeds and helium mass flow rates can be applied for both driver and breeder zone. This graphite layer can also accommodate the control rods and absorber balls. However, this graphite layer may have to be relatively thick to ensure the structural integrity of the core. Furthermore, the influence of such a layer upon the conversion ratio should also be investigated. The increased moderation of neutrons entering the breeder zone and an increasing fraction of neutrons leaking from the driver zone without entering the breeder zone, i.e. at the top and bottom of the core, may slightly reduce the conversion ratio.

- An interesting alternative approach is the use of a radially cooled pebble bed [1–4]. The helium coolant will flow through both driver and breeder zone, so a lower helium mass flow rate is required. The pressure drop is much lower, further decreasing power losses to the coolant pump. Such a radially cooled reactor design requires the use of a central reflector, which is a very suitable location to position control rods with sufficient reactivity worth close to the driver zone. The impact upon the conversion ratio also has to be investigated for a radially cooled core design.

- To improve decay heat removal and to operate safely at higher powers, the use of a liquid salt coolant might be considered. This option was previously studied for regular uranium fueled Pebble Bed Reactors [5] and liquid salts are also used in the design of the Pebble Bed-Advanced High Temperature Reactor [6]. Another major advantage is that the system can operate at ambient pressure, which simplifies reactor operation and construction, e.g. no pressure vessel is required.

- Besides the engineering issues stated above, (the costs of) the fuel reprocessing [7] may also provide a challenge for practical application of a thorium breeder PBR. Fortunately, Fütterer et al. [8] recently reported relevant progress on the fragmentation of coated particle fuels by using high voltage discharges inside a water vessel, which cause shock waves that disintegrate the fuel pebble and/or protective TRISO layers of the fuel kernel. For further development of PBRs with a closed thorium fuel cycle, it is very important that such a technique is also demonstrated on an industrial scale. Furthermore, the required reprocessing rate is quite high for the passively safe thorium breeder design. It is advisable to perform further design studies of passively safe breeder designs with a lower reprocessing rate, as only a limited number of core design and fuel management parameters could be studied for this thesis work. On the other hand, the margins in terms of passive safety, breeding and practical constraints are also quite small, so reducing the reprocessing rate may not be easy.

- Alternative start-up fuels can be studied for the running-in phase, like plutonium, and further optimization can be performed, in conjunction with the use of more radially detailed burnup models and pebble flow velocity profiles. Finally, more practically applicable schemes to adjust the feed fuel enrichment or U-233 weight fraction over time can be developed, i.e. a scheme which describes the optimal enrichment to the operator for a certain state of the reactor, defined by a limited number of variables (or sensors). This is also an interesting research topic for the start-up phase of regular uranium fueled PBRs.

In conclusion, this thesis demonstrates that there is no fundamental limitation for the application of a thorium breeder fuel cycle in a passively safe PBR. Still, as indicated previously, there are quite a few technical difficulties that have to be addressed. However, in the author's opinion, these issues can and ought to be resolved as the design of a passively safe thorium breeder PBR, comes with a great reward, in terms of safety and sustainability, for future generations.

REFERENCES

[1] Y. Muto and Y. Kato, *A new pebble bed core concept with low pressure drop,* in *Transactions of the Global 2003 Conference* (New Orleans, LA, 2003) pp. 1202–1209.

[2] Y. Muto, Y. Kato, and R. Udagawa, *Improvement of fuel temperature characteristics in a pebble bed core with horizontal flow by means of fuel zoning,* in *Proceedings of ICAPP'05* (Seoul, Korea, 2005).

[3] B. Boer, D. Lathouwers, J. L. Kloosterman, T. H. J. J. van der Hagen, and H. van Dam, *Optimization of a radially cooled pebble bed reactor,* Nuclear Engineering and Design **240**, 2384–2391 (2010).

[4] J. de Jong, *Feasibility of a Radially Cooled Thorium Breeder Pebble Bed Type High Temperature Reactor*, Master's thesis, Delft University of Technology (2014).

[5] S. J. De Zwaan, B. Boer, D. Lathouwers, and J. Kloosterman, *Static design of a liquid-salt-cooled pebble bed reactor (LSPBR),* Annals of Nuclear Energy **34**, 83–92 (2007).

[6] M. Fratoni and E. Greenspan, *Neutronic feasibility assessment of liquid salt-cooled pebble bed reactors,* Nuclear Science and Engineering **168**, 1–22 (2011).

[7] M. Lung, *EUR 17771: A present review of the thorium nuclear fuel cycles (European Commission)*, Tech. Rep. ISSN 1018-5593 (1997).

[8] M. A. Fütterer, F. von der Weid, and P. Kilchmann, *A high voltage head-end process for waste minimization and reprocessing of coated particle fuel for high temperature reactors,* in *Proceedings of ICAPP'10* (San Diego, CA, USA, 2010).

7

APPENDIX A: NUMERICAL CALCULATION OF XENON CONCENTRATION OVER TIME

THIS appendix addresses the numerical implementation of the cross section variation due to the varying Xenon-135 concentration within the coupled code scheme introduced in section 4.2. The Iodine-135 and Xenon-135 concentrations, denoted by I and X, evolve over time according to [1, p. 569]:

$$\frac{\partial I}{\partial t} = \int_0^\infty \gamma_I \Sigma_f \phi(r, E, t) dE - \lambda_I I(r, t) \tag{A.1}$$

$$\frac{\partial X}{\partial t} = \int_0^\infty \gamma_X \Sigma_f \phi(r, E, t) dE + \lambda_I I(r, t) - \lambda_X X(r, t) - \int_0^\infty X(r, t) \sigma_a^{Xe} \phi(r, E, t) dE \tag{A.2}$$

Where γ_I and γ_X are the fission product yields, and λ_I and λ_X the decay constants of I-135 and Xe-135. Σ_f represent the fission cross section, $\phi(r, E, t)$ the scalar neutron flux and σ_a^{Xe} is the microscopic Xe-135 absorption cross section. The time-evolution of I-135 and Xe-135 can be described numerically using an implicit Euler scheme:

$$I^{j+1} = \frac{I^j + \sum_g \gamma_I \Sigma_{f,g}^{het} \phi_g^{j+1} \Delta t}{1 + \lambda_I \Delta t} \tag{A.3}$$

$$X^{j+1} = \frac{X^j + \sum_g \gamma_X \Sigma_{f,g}^{het} \phi_g^{j+1} \Delta t + \lambda_I I^{j+1} \Delta t}{1 + \lambda_X \Delta t + \sum_g \sigma_{a,g}^{Xe} \phi_g^{j+1} \Delta t} \tag{A.4}$$

With j being the time step number, g the neutron group number, $\sigma_{a,g}^{Xe}$ the microscopic Xe-135 absorption cross section and $\Sigma_{f,g}^{het}$ the fission cross section in the fuel kernel (so not homogenized with the moderator and helium). During a fully coupled run of the coupled code scheme ϕ^{j+1} is obtained using the DALTON diffusion code, while during the loosely coupled run a flux value of zero is applied. Using the ICE module of SCALE6 [2], a new xenon-adjusted cross section library is created. For each zone, this effectively results in

$$\Sigma^* = \Sigma + (X^{j+1} - X(0)) \frac{V_{fuel}}{V_{peb+He}} \sigma_X \tag{A.5}$$

Here Σ represents the cross section in the temperature interpolated library for all relevant processes, i.e. capture, elastic and inelastic scattering, fission and so on. This cross section Σ was obtained for the different core zones using the steady-state xenon concentration, and $X(0)$ is the xenon concentration of the steady state configuration. The volume

ratio between fuel and homogenized pebble material, V_{fuel}/V_{peb+He}, is included in the equation since the microscopic xenon cross section σ_X has to be smeared over the whole pebble (plus coolant) as Σ, used by the neutron diffusion solver DALTON, is a homogenized set of cross sections.

REFERENCES

[1] J. J. Duderstadt and L. J. Hamilton, *Nuclear Reactor Analysis* (John Wiley and Sons Inc., 1976).

[2] Radiation Safety Information Computational Center, Oak Ridge National Laboratory, *"SCALE: A Modular Code System for Performing Standardized Computer Analyses for Licensing Evaluations", Vols. I-III, Version 6, CCC-750; ORNL/TM-2005/39* (2009).

A

APPENDIX B: CONVERSION RATIO WITH A CENTRAL BREEDER ZONE

A POSSIBLE design variation is to switch the position of driver and breeder zone, so using a central breeder zone surrounded by a driver zone and radial reflector. Such a design is probably not ideal for the neutron economy due to increasing neutron leakage, but the idea is worth investigating. The third case of table 4.7 is taken as the starting point for these studies. First, some calculations are performed for a fresh fueled core, i.e. with uniform composition per zone, to choose a comparable reference case for the equilibrium core calculation with a central breeder zone.

B.1. FRESH FUELED CORE

THE U-233 weight fraction in the breeder zone of the fresh fueled core is chosen similar to the average concentration in the breeder zone of the third case of table 4.7. The U-233 weight fraction of the fresh fueled central driver zone with an 80 cm radius is changed until a critical core configuration is obtained, which requires 12.04 w% U-233. Using this U-233 weight fraction, the k_{eff} is calculated as a function of the ratio between the driver zone volume over the total core volume for cores with a central driver zone and cores with a central breeder zone. The results are shown in figure B.1.

Since $k_{eff} = k_\infty P_{NL}$, it can be concluded from the results in figure B.1 that neutron leakage increases dramatically with a central breeder zone. Such a strong increase of the neutron leakage is probably problematic to achieve breeding.

B.2. EQUILIBRIUM CORE CALCULATION

A CENTRAL driver zone with a uniform 12.04 w% U-233 weight fraction leads to a critical core configuration, while a 170 cm breeder zone radius brings the configuration with a central breeder zone closest to criticality ($k_{eff} = 0.98783$). Therefore, a core with a central breeder zone radius of 170 cm is a good starting point for the equilibrium core calculation. Slightly larger and smaller breeder zones are also evaluated. Table B.1 compares the conversion ratio and maximum power density of these designs with the configuration with a central driver zone (case III of table 4.7).

As could already be expected from the fresh core calculations, the results from equilibrium core calculations show that breeding can not be achieved by far with the driver zone on the outside of the reactor. A reduction of the breeder zone radius only decreases the conversion ratio, while criticality cannot be achieved anymore if the breeder zone radius is increased further, which leads to negative driver pebble residence time in the calculation scheme. So, a 170 cm breeder zone radius is optimal in terms of the conversion ratio for this configuration.
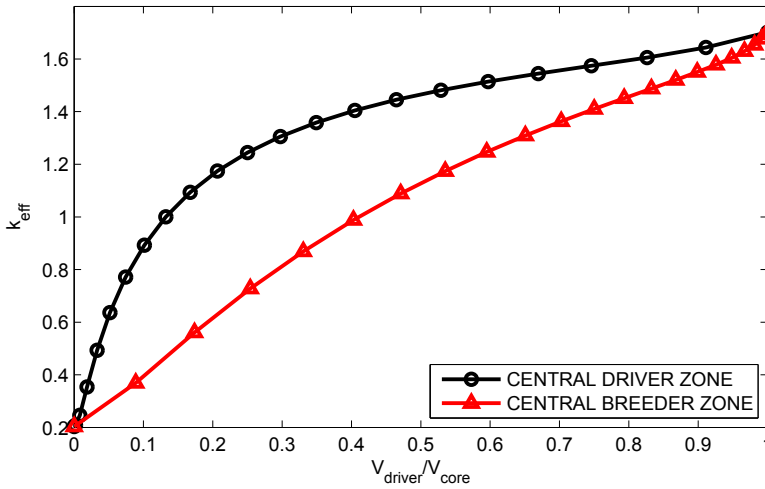
Figure B.1: Comparison between k_{eff} as a function of V_{driver}/V_{core} for 220 cm radius cores with a central driver zone and for cores with a central breeder zone. Fresh fuel pebbles with 12.04 w% U-233 (3 g HM) are used in the driver zone and 30 g HM breeder pebbles (0.2 w% U-233, 99.8 w% Th-232) are used in the breeder zone.

Table B.1: Comparison of driver pebble residence time, conversion ratio and maximum power density of core designs with different central breeder zone radii and the reference design with a central driver zone (table 4.7 - case III). (D=Driver and B=Breeder)

Inner zone	Outer zone	$T^{total}_{res,feed}$	Conversion ratio	$P^{max}_{density}$
D-80 cm	B-220 cm	170.6 d	1.0135	10.13 MW/m^3
B-150 cm	D-220 cm	1806.4 d	0.5964	3.29 MW/m^3
B-160 cm	D-220 cm	1230.0 d	0.6248	3.17 MW/m^3
B-170 cm	D-220 cm	522.6 d	0.6609	3.08 MW/m^3
B-180 cm	D-220 cm	< 0	-	-

B

Obviously, more extensive studies are required to discover what conversion ratio can ultimately be achieved with a central breeder zone in other configurations. However, the highest conversion ratio found in this study is so much smaller than one that it seems highly unlikely that breeding can ever be achieved with a central breeder zone. Still, such designs might be interesting from a safety perspective as the maximum power density is significantly reduced and it occurs next to the side reflector, which will improve decay heat removal during a DLOFC.

APPENDIX C: ANALYSIS OF THE TEMPERATURE FEEDBACK

THIS appendix presents a more detailed discussion of the temperature feedback of the passively safe thorium breeder PBR design (case II of table 4.8) to gain a better understanding of the factors contributing positively or negatively to the temperature feedback. The fuel, moderator and uniform temperature coefficients were recalculated for a 500 K temperature increase using the nuclide concentrations from the equilibrium core calculation. This time, a single volume-averaged temperature was used in the radial direction for the driver zone and a single volume-averaged temperature for the breeder zone, similar to the equilibrium core calculation scheme, to make it easier and computationally cheaper to analyse some parameter variations. This way, a uniform reactivity coefficient of -3.61 pcm/K was found, which slightly differs from the value of -3.67 pcm/K mentioned in table 4.8. A fuel temperature coefficient of -0.96 pcm/K and a moderator temperature coefficient of -2.62 pcm/K was found. The fuel temperature coefficient is negative because of increasing neutron capture by the resonance broadening of the Th-232 capture cross section with increasing fuel temperature. A moderator temperature increase leads to additional upscattering in the graphite which causes a spectrum shift towards higher neutron energies, as demonstrated in the lower graph of figure C.1. This spectrum shift causes an increase of neutron leakage from the core, which has a negative contribution to the moderator temperature coefficient, but it also affects capture rates in e.g. Th-232, Pa-233 and Xe-135 and the fission rate of U-233. The change of some of these reaction rates can have a positive impact on the moderator feedback, e.g. a reduction of capture in Xe-135 or an increase of fission in U-233, as will be demonstrated later on.

Table C.1 investigates the effects of different perturbations upon the reactivity, the moderator temperature feedback and the fuel temperature feedback. These values were calculated by performing forward calculations, with and without a 500 K temperature increase, and by comparing results for cases with and without a 10% increase of a certain parameter. Reductions of the core height by 50% and 75% were also considered to demonstrate the effect of neutron leakage on the moderator temperature feedback. Table C.1 also shows the relative change of the reactivity coefficients, i.e. the change in reactivity coefficient divided by the absolute value of the reactivity change due to the perturbation. This number provides a more objective comparison between the impact of different perturbations on the feedback coefficients.

The influence of the different perturbations upon α_{fuel} is generally quite small compared to its influence on $\alpha_{moderator}$, except for the addition of Th-232 in the driver zone. Adding U-233 in the driver zone has a positive effect on α_{fuel}, as the relative contribution of the Doppler feedback by the Th-232 resonance absorber to α_{fuel} reduces a bit and relatively more power is produced in the driver zone, which contains less Th-232. The

Table C.1: Change in reactivity, moderator temperature reactivity coefficient and fuel temperature reactivity coefficient (for a 500 K temperature increase) for different perturbations. Also included are the relative changes ($\Delta\alpha/|\Delta\rho|$) of the fuel and moderator coefficients as they provide a more objective comparison between the effects of the perturbations upon the temperature feedback.

Perturbation	$\Delta\rho$	$\Delta\alpha_{mod}$	Rel: $\frac{\Delta\alpha_{mod}}{|\Delta\rho|}$	$\Delta\alpha_{fuel}$	Rel: $\frac{\Delta\alpha_{fuel}}{|\Delta\rho|}$
	[pcm]	[pcm/K]	[K^{-1}]	[pcm/K]	[K^{-1}]
+10% U-233 in driver zone	+3340	+0.36	+1.07e-04	+0.033	+9.86e-06
+10% U-233 in breeder zone	+65	+0.018	+2.77e-04	-0.0026	-4.00e-05
+10% Th-232 in driver zone	-856	+0.050	+5.89e-05	-0.073	-8.53e-05
+10% Th-232 in breeder zone	-584	-0.20	-3.44e-04	-0.013	-2.30e-05
+10% Pa-233	-9	-0.0055	-5.82e-04	-0.00067	-7.09e-05
+10% Xe-135	-274	+0.13	+4.90e-04	-0.0031	-1.12e-05
+10% R_{driver}	+5784	+0.59	+1.03e-04	+0.12	+2.02e-05
+10% Driver pebble HM loading	+1774	+0.58	+3.28e-04	-0.049	-2.75e-05
+10% Breeder pebble HM loading	-592	-0.21	-3.57e-04	-0.014	-2.32e-05
-50% core height	-2147	-0.20	-9.48e-05	+0.001	+4.36e-07
-75% core height	-10646	-2.14	-2.01e-04	-0.069	-6.51e-06

addition of U-233 in the breeder zone has a negative effect[1] on α_{fuel}, because the relative power production in the breeder zone, with its large thorium content, increases. The contributions of adding Th-232 and Pa-233 on α_{fuel} are negative, since more resonance absorber material is added. Adding Xe-135 has a negative effect on α_{fuel}, since it causes a slight increase of the ratio between epithermal neutrons (in the resonance region) and thermal neutrons because of its large thermal absorption cross section. A large driver zone radius has a positive effect on α_{fuel}, because the relative importance of the driver zone, which has a much smaller content of the resonance absorber Th-232, increases. Adding heavy metal causes a hardening of the neutron spectrum, which increases the negative contribution of the Doppler resonance broadening. The impact of a smaller core height and increased neutron leakage on α_{fuel} is fairly small.

The top graph of figure C.1 shows the capture cross sections of Th-232, Pa-233 and Xe-135 and the fission cross section of U-233 as a function of neutron energy. For the driver zone at central core height, the neutron spectrum change induced by a moderator temperature increase of 500 K is shown in the lower graph of figure C.1.

An increase of the Pa-233 concentration[2] gives a negative contribution to $\alpha_{moderator}$, because the neutron spectrum peak (partly) shifts into the first resonance peaks of the Pa-233 capture cross section. So, adding more Pa-233 gives a relative increase of neutron capture by Pa-233 after the spectral shift caused by the moderator temperature increase. The positive contribution of adding Xe-135 to $\alpha_{moderator}$ can be understood from looking at the spectral shift and the Xe-135 cross section. The Xe-135 capture cross section decreases much stronger than other cross sections in the energy region of the spectral shift. Increasing the driver zone radius has a positive contribution to $\alpha_{moderator}$, because neutron leakage from the driver zone (with its large fissile content) decreases, which also results in a reduced change of neutron leakage due to the moderator temperature increase. A decrease of the core height results in an increase of (the change of) neutron leakage from

---

[1]i.e. making the value of the reactivity coefficient more negative.
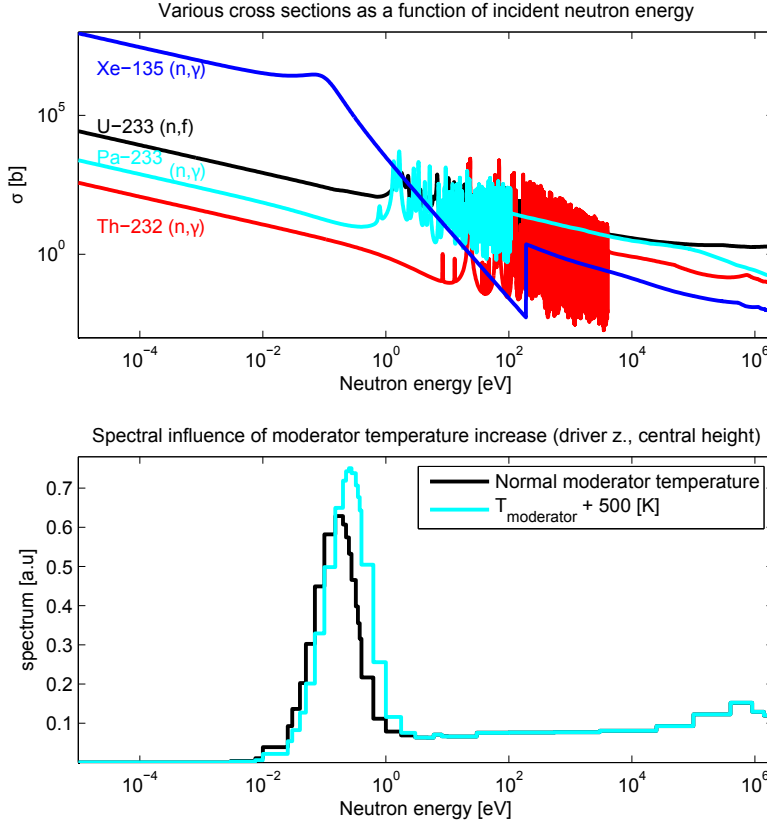[2]For example, as a consequence of a power increase of the core.

Figure C.1: Th-232, Pa-233 and Xe-135 capture cross sections and U-233 fission cross section as a function of neutron energy (*top*), and average neutron spectrum in the driver zone at central core height with and without a 500 K moderator temperature increase.

the core, which makes $\alpha_{moderator}$ more negative.

Adding U-233 gives a positive contribution to $\alpha_{moderator}$. The addition of Th-232, similar to adding heavy metal, has a positive effect on $\alpha_{moderator}$ in the driver zone and a negative effect in the breeder zone. However, these changes of the moderator coefficient are somewhat harder to assign mainly to one single effect. The addition of Th-232, U-233 or both changes the carbon to heavy metal ratio, resulting in a change of the neutron spectrum in driver or breeder zone (before the spectral shift occurs). This spectral change and its influence on the spectral shift due to the moderator temperature increase has an impact on both the (change of) U-233 fission rate and Th-232, Pa-233 and Xe-135 capture rates, as well as the (change of) neutron leakage from the driver zone and core and it also effects the ratio between the power production in the driver and the breeder zone. For example, a harder neutron spectrum increases leakage from the system and the associated change of neutron leakage due to the moderator temperature increase, but it also reduces the positive contribution of the change in neutron capture in Xe-135 to $\alpha_{moderator}$. Both these

effects can have a negative effect on $\alpha_{moderator}$, while a positive contribution can come from a reduced leakage rate due to increasing Th-232 concentrations or an increased fission rate of U-233 as the energy region of the spectral shift overlaps more with the first U-233 fission peaks.

C

SUMMARY

Nuclear power plants are expected to play an important role in the worldwide electricity production in the coming decades, since they provide an economically attractive, reliable and low-carbon source of electricity with plenty of resources available for at least the coming hundreds of years. However, the design of nuclear reactors can be improved significantly in terms of safety, by designing reactors with fully passive safety systems, and sustainability, by making more efficient use of natural resources in so-called breeder reactors, and by reducing the radiotoxicity and storage time of the waste produced by the reactor.

The application of a thorium breeder fuel cycle within a Pebble Bed High Temperature Reactor could provide such improvements. The core of a Pebble Bed Reactor (PBR) consists of a helium cooled random stacking of graphite spheres, which contain many small coated fuel particles retaining radioactive fission products for temperatures below 1600 °C. In case of a Depressurized Loss of Forced Cooling (DLOFC), the most serious accident that can occur in a PBR, decay heat can be removed from the core by passive means without the maximum fuel temperature exceeding 1600 °C. This is due to its relatively small core radius and low power density.

Thorium fuel cycles offer several interesting advantages. Thorium is three to four times more abundant in the earth's crust than uranium. In a closed breeder cycle, thorium can significantly reduce the radiotoxicity and storage time of nuclear waste, and all natural resources mined, i.e. Th-232 or U-235 and U-238, can be used for electricity production instead of roughly 1% of the natural uranium resources consumed by current light water reactors. Furthermore, the Th/U-233 fuel cycle has favourable nuclear properties, i.e. the neutron reproduction factor of U-233 and the relatively high thermal neutron capture cross section of Th-232, for use in thermal breeder reactors, like a PBR.

This thesis work investigates whether it is possible to achieve a thorium breeder fuel cycle in a pebble bed reactor within a practical operating regime and without compromising passive safety. Furthermore, the reactor should also achieve a net U-233 production within a limited time frame.

Neutronics studies of the fuel design show that the conversion of thorium into U-233 can be maximized for thorium pebbles with a large heavy metal loading of 30 g, a conservative maximum from a fuel fabrication perspective, and a standard fuel kernel radius of 0.025 cm, preferably irradiated at low specific power to improve k_∞[3]. Reprocessing or adding moderator pebbles is required to raise the k_∞ of these pebbles above unity.

Cylindrical cores, consisting of a central driver zone surrounded by a breeder zone and reflector regions, were investigated during equilibrium core design studies. 30 g thorium pebbles are inserted in the breeder zone, while a higher carbon to heavy metal ratio is used in the driver zone. Results obtained by an equilibrium core calculation scheme show

---

[3] k_∞: infinite multiplication factor

that the uranium content from both the discharged driver and uranium pebbles has to be reprocessed after their final passage to achieve breeding.

As a next step, coupled neutronic and thermal-hydraulic design studies using a coupled DALTON/THERMIX code scheme were performed to investigate whether it is possible to combine passive safety and breeding, within a practical operating regime, inside a thorium PBR. Additionally, the equilibrium core calculation scheme was extended to include the spectral influence of surrounding zones (driver, breeder and reflector) into the fuel depletion calculations.

High conversion ratios (CR > 0.96) and passive safety can be combined in a thorium PBR within a practical operating regime. Increasing the U-233 content of the fresh driver pebbles (18 w%), breeding (CR=1.0135) can already be achieved for a 220 cm core and 80 cm driver zone radius, but the temperature feedback is too weak to compensate the reactivity insertion due to decay of Xe-135 during a DLOFC without scram.

With a lower U-233 content per driver pebble (10 w%), breeding (CR=1.0036) and passive safety can be combined for a 300 cm core and 100 cm driver zone radius operating at a power of 100 MW$_{th}$, but this requires a doubling of the pebble handling speed and a high fuel pebble reprocessing rate, which may present a challenge from an engineering perspective. The maximum fuel temperature during a DLOFC without scram was 1481 °C, still quite a bit below the TRISO failure temperature. The maximum reactivity insertion due to water ingress is also limited (+1497 pcm).

For this 100 MW$_{th}$ passively safe thorium breeder PBR design, the total control rod worth is far insufficient in the radial reflector to achieve cold reactor shutdown, requiring a worth of over 15,000 pcm. 3D heterogeneous KENO calculations show that 20 control rods, positioned just outside the driver zone, can provide sufficient reactivity worth. Furthermore, the insertion of a neutron absorber gas, like BF$_3$, can be considered as an additional emergency shutdown system.

Finally, the running-in phase of the passively safe thorium breeder PBR was analysed using a simplified core depletion model, which solves the depletion equations with an axial fuel movement term for the most relevant actinides and a lumped fission product pair. Enriched uranium (U-235/U-238) is used during the first 1300 days of reactor operation and U-233/Th fuel is used afterwards. By clever adjustment of the enrichment or U-233 weight fraction of the feed driver fuel over time, the thorium PBR can start to breed U-233 within 7 years after starting reactor operation. Furthermore, a basic safety analysis for the various stages of the running-in phase indicates that passive safety is also ensured during any stage of the running-in phase.

This thesis work demonstrates that it is possible to achieve breeding within a passively safe thorium pebble bed reactor after a limited time (< 7 years), though the margins in terms of breeding, passive safety and practical constraints are rather small. Therefore, the passively safe thorium breeder PBR design presented requires a doubling of the fuel pebble handling speed, compared to the HTR-PM, and a high fuel pebble reprocessing rate, while also some other technical difficulties still have to be addressed, such as the large pumping power requirement and the modelling of the conus region and defueling chutes. However, these issues are no fundamental limitation for the application of a thorium breeder cycle within a passively safe PBR, which could offer a huge improvement in terms of safety and sustainability of nuclear power for future generations.

SAMENVATTING

K ERNENERGIE zal naar verwachting nog voor lange tijd een belangrijke rol blijven spelen
in de wereldwijde elektriciteitsproductie, omdat het een economisch aantrekkelijke,
betrouwbare en CO_2-arme energiebron is en de grondstoffen ruim voorradig zijn, voor in
elk geval de komende eeuwen. Het ontwerp van reactoren kan, in vergelijking met huidige
kerncentrales, echter significant verbeterd worden qua veiligheid, door reactoren met vol-
ledige passieve veiligheidssystemen te ontwerpen, en qua duurzaamheid, door efficiënter
gebruik te maken van natuurlijke grondstoffen in zogenaamde kweekreactoren en door de
radiotoxiciteit en levensduur van het radioactieve afval te reduceren.

Deze verbeteringen kunnen gerealiseerd worden door de toepassing van een thorium
kweekcyclus in een Hoge Temperatuur Reactor van het kogelbedtype. De kern van een
kogelbedreactor is een poreus bed van willekeurig gestapelde grafietkogels, welke elk dui-
zenden splijtstofdeeltjes bevatten, die worden omhuld door een coating van pyrolytische
carbon en siliciumcarbide. Deze coatings verzekeren de retentie van radioactieve splij-
tingsproducten voor temperaturen tot 1600 °C. Helium wordt onder hoge druk door het
poreuze kogelbed gepompt om de geproduceerde warmte aan de kern te onttrekken. Het
wegvallen van de actieve koeling en de systeemdruk is het ernstigste ongevalsscenario dat
in een kogelbedreactor kan optreden, maar zelfs in dat geval kan de vervalwarmte op vol-
ledig passieve wijze aan de kern onttrokken worden zonder dat de maximale splijtstoftem-
peratuur hoger wordt dan 1600 °C. Dit is mogelijk vanwege de kleine diameter van de kern
en de relatief lage vermogensdichtheid.

Thorium splijtstofcycli bieden een aantal interessante voordelen. Thorium komt drie
tot vier keer zo veel voor in de aardkorst als uranium. Thorium kan de radiotoxiciteit en op-
slagduur van nucleair afval significant reduceren binnen een gesloten kweekcyclus, waarin
verder al het gewonnen thorium (of U-235/U-238 in snelle kweekreactoren) kan worden
omgezet voor elektriciteitsproductie in plaats van ongeveer 1% van het gewonnen natuur-
lijke uranium in de huidige lichtwaterreactoren. Tenslotte beschikt de Th/U-233 splijt-
stofcyclus over voordelige nucleaire eigenschappen, nl. de neutron reproductie factor van
U-233 en de relatief grote werkzame doorsnede voor vangst van thermische neutronen van
Th-232, om daadwerkelijk een conversiefactor groter dan één te bereiken in een thermi-
sche reactor, zoals een kogelbedreactor.

Dit proefschrift onderzoekt of het mogelijk is om een kweekcyclus te bereiken in een
kogelbedreactor binnen praktische randvoorwaarden en met behoud van passieve veilig-
heid. Bovendien moet een netto U-233 productie bereikt kunnen worden na een beperkte
tijdsduur.

Neutronicaberekeningen aan het splijtstofontwerp tonen aan dat de conversie van tho-
rium naar U-233 maximaal is, binnen praktische randvoorwaarden, voor kogels die 30 g
thorium bevatten en voor splijtstofdeeltjes met een straal van 0.25 mm. Deze deeltjes wor-
den bij voorkeur bestraald bij een laag specifiek vermogen om k_∞ te vergroten. Opwerking

of de toevoeging van moderator kogels is noodzakelijk om een multiplicatiefactor groter dan één te realiseren.

Diverse SCALE6 modules, o.a. voor de generatie van werkzame doorsnedes en opbrandberekeningen, zijn gekoppeld aan DALTON, wat een diffusieberekening van de multiplicatiefactor en het fluxprofiel uitvoert, om de evenwichtssamenstelling te berekenen voor een cilindrische kern, bestaande uit een centrale splijtingszone omringd door een kweekzone. Kogels met 30 g thorium worden ingevoegd in de kweekzone, welke verhoudingsgewijs veel minder grafiet (of meer thorium) bevat dan de splijtingszone. Het uranium in alle uit de kern verwijderde kogels, dus zowel uit de splijtingszone als uit de kweekzone, moet na hun laatste passage worden opgewerkt en hergebruikt om een conversiefactor groter dan één te bereiken.

Vervolgens zijn gekoppelde reactorfysische en thermohydraulische ontwerpstudies uitgevoerd met DALTON en THERMIX. Hierbij is het schema voor de evenwichtskernberekening verder uitgebreid om ook de spectrale invloed van omringende zones (splijtingszone, kweekzone en reflector) in de opbrandberekeningen mee te nemen. Hoge conversiefactoren (> 0.96) en passieve veiligheid kunnen worden gecombineerd in een thorium kogelbedreactor binnen praktische randvoorwaarden. Een kweekreactor kan zelfs al gerealiseerd worden met een kernstraal van 220 cm en een splijtingszone van 80 cm, na een verder toename van de U-233 fractie in de verse kogels van de splijtingszone naar 18% (gewicht). De reactiviteitscoëfficiënt voor de uniforme kerntemperatuur is in dit geval echter te zwak om het verval van Xe-135 voldoende te compenseren tijdens een verlies van actieve koeling en systeemdruk.

Een passief veilige kweekreactor (100 MW$_{th}$) kan ook worden bereikt met een kernstraal van 300 cm en een splijtingszone van 100 cm met een lagere U-233 fractie in de verse kogels van de splijtingszone (10%), maar dit vereist wel een verdubbeling van de doorvoersnelheid van de kogels in de kern en een hoog opwerkingstempo. De splijtstoftemperatuur bereikt een maximum van 1481 °C na een verlies van actieve koeling en systeemdruk, zodat er nog een behoorlijke marge is tot aan de limiet van 1600 °C die de retentie van de splijtingsproducten verzekert. Het intreden van waterdamp leidt ook slechts tot een beperkte toename van de reactiviteit (+1497 pcm).

De totale reactiviteitswaarde van regelstaven in de radiële reflector is onvoldoende om een koude afschakeling te bewerkstelligen in deze 100 MW$_{th}$ passief veilige kweekreactor, hetgeen een negatieve reactiviteit van meer dan 15000 pcm vereist. Monte Carloberekeningen met KENO aan een heterogeen[4] 3-dimensionaal model tonen aan dat 20 regelstaven op een positie net buiten de splijtingszone voldoende negatieve reactiviteit kunnen bewerkstelligen. Daarnaast is de toevoeging van een neutronen absorberend gas, zoals BF$_3$, een reële optie als aanvullend afschakelsysteem tijdens noodgevallen.

Tenslotte is de inloopfase van de passief veilige kweekreactor bestudeerd aan de hand van een vereenvoudigd tijdafhankelijk opbrandmodel van de kern. Het model lost opbrandvergelijkingen met een axiale bewegingsterm op voor de belangrijkste nuclides, terwijl de splijtingsproducten worden samengevoegd tot een enkel kunstmatig splijtingsnuclide met representatieve doorsnede. Tijdens de eerste 1300 dagen wordt uranium (U-235/U-238) met een verrijking tussen 11% en 17% gebruikt in de splijtingszone om de reactor op gang te brengen. Vervolgens wordt U-233/Th gebruikt voor de verse splijtstof in

---

[4]d.w.z. met discrete regelstaven, dus zonder homogenisatie over de hoek

de splijtingszone. De thorium kogelbedreactor kan binnen 7 jaar een netto productie van U-233 bereiken door de verrijking of de U-233 fractie van de splijtstof in de splijtingszone telkens op een slimme manier aan te passen. Een veiligheidsanalyse toont verder aan dat de passieve veiligheid van de reactor ook gewaarborgd is gedurende elk moment van de inloopfase.

Dit proefschrift toont aan dat het mogelijk is om een netto productie van U-233 te bereiken in een passief veilige thorium kogelbedreactor na een beperkte tijdsduur (< 7 jaar). De marges op het gebied van conversie, passieve veiligheid en praktische randvoorwaarden zijn echter wel vrij beperkt met een conversiefactor net groter dan één en de maximale splijtstoftemperatuur van 1481 °C na een verlies van actieve koeling. Bovendien vereist het gepresenteerde ontwerp van een passief veilige kweekreactor een verdubbeling van de circulatiesnelheid van de kogels, vergeleken met de HTR-PM, evenals een hoog opwerkingstempo. Verder is er nog een aantal andere technische aspecten die aandacht vereisen, zoals het hoge vereiste pompvermogen en de modellering van de uitlaatkleppen en het stromingsprofiel van de splijtstofkogels. Dit alles levert echter geen fundamentele beperking op voor de toepassing van een thorium kweekcyclus in een passief veilige kogelbedreactor, hetgeen een enorme verbetering kan opleveren voor de veiligheid en de duurzaamheid van kernenergie voor komende generaties.

ACKNOWLEDGEMENTS

LIST OF PUBLICATIONS

JOURNAL ARTICLES

5. **F.J. Wols**, J.L. Kloosterman, D. Lathouwers and T.H.J.J. Van der Hagen, *Analysis of the Running-in Phase of a Passively Safe Thorium Breeder Pebble Bed Reactor*, *Accepted by* Annals of Nuclear Energy, 2015.

4. **F.J. Wols**, J.L. Kloosterman, D. Lathouwers and T.H.J.J. Van der Hagen, *Conceptual Design of a Passively Safe Thorium Breeder Pebble Bed Reactor*, Annals of Nuclear Energy **75**, pp. 542-558 (2015), doi:10.1016/j.anucene.2014.09.012.

3. **F.J. Wols**, J.L. Kloosterman, D. Lathouwers and T.H.J.J. Van der Hagen, *Reactivity Control System of a Passively Safe Thorium Breeder Pebble Bed Reactor*, Nuclear Engineering and Design **280**, pp. 598-607 (2014), doi:10.1016/j.nucengdes.2014.09.015.

2. B. Wolterbeek, J.L. Kloosterman, D. Lathouwers, M. Rohde, A. Winkelman, L. Frima and **F.J. Wols**, *What is wise in the production of ^{99}Mo? A comparison of eight possible production routes*, Journal of Radioanalytical Nuclear Chemistry, pp. 1-7 (May 2014), doi:10.1007/s10967-014-3188-9.

1. **F.J. Wols**, J.L. Kloosterman, D. Lathouwers and T.H.J.J. Van der Hagen, *Core Design and Fuel Management Studies of a Thorium-Breeder Pebble Bed High-Temperature Reactor*, Nuclear Technology **186-1**, pp. 1-16 (2014), doi:10.13182/NT13-14.

CONFERENCE PROCEEDINGS

6. H. Haoran, **F.J. Wols** and J.L. Kloosterman, *Modelling and transient studies of a liquid-salt-cooled pebble bedded reactor (LSPBR)*, Proceedings of the HTR 2014, Weihai (China), October 2014.

5. **F.J. Wols**, J.L. Kloosterman, D. Lathouwers and T.H.J.J. Van der Hagen, *Preliminary Safety Analysis of a Thorium High-Conversion Pebble Bed Reactor*, Proceedings of PHYSOR 2014 (Kyoto, Japan), September 2014.

4. **F.J. Wols**, J.L. Kloosterman and D. Lathouwers, *Fuel Pebble Design Studies of a High Temperature Reactor using Thorium*, Proceedings of the HTR 2012 (Tokyo, Japan), October 2012.

3. M. Ding, J.L. Kloosterman, **F.J. Wols**, *Thermal-Hydraulic Evaluations of the U-Battery for Loss of Forced-Cooling Conditions*, Proceedings of the HTR 2012 (Tokyo, Japan), October 2012.

2. W. Uyttenhove, G. van den Eynde, P. Baeten, A. Kochetkov, G. Vittiglio, J. Wagemans, D. Lathouwers, J.L. Kloosterman, T.H.J.J. van der Hagen, **F.J. Wols**, A. Billebaud, S. Chabod, H.E. Thybault, J.L. Lecouey, G. Ban, F.R. Lecolley, N. Marie, J.C. Steckmeyer, P. Dessagne, M. Kerveno and F. Mellier, *Detector Positioning for the Initial Subcriticality Level Determination in Accelerator-Driven Systems*, Proceedings of PHYSOR 2012 (Knoxville, USA), April 2012.

1. **F.J. Wols** and D. Lathouwers, *Transient analyses of accelerator driven systems using alpha mode expansions,* Proceedings of the M&C 2011 conference (Rio de Janeiro, Brazil), May 2011.

CURRICULUM VITÆ

Frank Jozef WOLS

E-mail: f.j.wols@tudelft.nl
Date of birth: 12-04-1985
Place of birth: Rotterdam, the Netherlands.

PROFESSIONAL EXPERIENCE

2014-....   Reactor development engineer at Reactor Institute Delft
2010-2014   PhD researcher at Reactor Institute Delft, Delft University of Technology

EDUCATION

1997-2003   Preparatory Scientific Education (VWO) at Marnix Gymnasium, Rotterdam

2003-2009   BSc. Applied Physics, Delft University of Technology

2007-2010   MSc. Applied Physics, Delft University of Technology
               Thesis: Transient analyses of accelerator driven systems using
                               modal expansion techniques